

# POLITECNICO DI TORINO

Master's Degree in  
Mechatronic Engineering

Master's Thesis

## Study and Development of a Laser Welding Robotic Cell with Seam Teaching and Seam Tracking Capabilities



**Academic Supervisor:**

Prof. Alessandro Rizzo

**Company Supervisor:**

Eng. Stefano Garino

**Candidate:**

Fabrizio Tirapelle - 253462

A.Y. 2018/2019

# Contents

<b>Introduction</b>	<b>2</b>
<b>1 Laser Welding</b>	<b>3</b>
1.1 The Welding Process . . . . .	3
1.2 Laser Principles . . . . .	11
1.3 Laser Welding Technologies . . . . .	17
<b>2 Visual Servoing</b>	<b>23</b>
2.1 General Concepts . . . . .	23
2.2 Position Based Visual Servoing . . . . .	28
2.3 Image Based Visual Servoing . . . . .	31
2.4 Discussion on Visual Servoing Systems . . . . .	33
<b>3 Seam Teaching and Seam Tracking</b>	<b>34</b>
3.1 Definitions . . . . .	34
3.2 Literature Review . . . . .	36
3.3 Industrial Applications . . . . .	54
<b>4 SM System S.r.l. Robotic Cell</b>	<b>57</b>
4.1 General Description . . . . .	57
4.2 Welding Requirements and Equipment . . . . .	60
4.3 Robot . . . . .	65
4.4 External Axes . . . . .	77
4.5 Vision and Algorithms . . . . .	84
<b>Conclusions</b>	<b>92</b>
<b>Acknowledgments</b>	<b>93</b>
<b>References</b>	<b>94</b>
<b>List of Figures</b>	<b>100</b>
<b>List of Tables</b>	<b>103</b>

## Introduction

This Master's Thesis deals with the study and development of a laser welding robotic cell. From March to September 2019 I had the chance to take part in the design of such cell at SM System S.r.l. [1], a company specialized in laser technology and industrial automation solutions. The project was commissioned by a customer in the sheet metal working field. The goal of the design was a robotic cell able to perform laser welding on small-to-medium quantities of different products; flexibility and reliability were the main objectives.

During the drafting of this Thesis, I was involved in several different stages of the development, from the initial conceiving of the cell to the simulation of high-level control algorithms, from the review of the scientific literature on the subject to the programming of the robot. In order to achieve the required performances, each subsystem of the cell was designed on the basis of the state of the art: laser welding technologies were investigated for finding the most suitable welding laser for the application; visual servoing algorithms were introduced to increase flexibility in following different seam trajectories; seam-teaching and seam-tracking concepts were extracted from the literature and applied to the concrete case; robot modeling was performed and simulations were carried out to test the robustness of the system.

The Thesis is structured to cover all these topics, providing the main theoretical concepts underlying the design choices made during the development of the cell at the SM System S.r.l. company. Chapter 1 provides an insight on the welding process, on laser concepts and on their combination: laser welding. Chapter 2 introduces the main ideas behind visual servoing, used in the cell to provide visual feedback to the robot during its operations. Chapter 3 deals with the problem of seam-teaching and seam-tracking, that was investigated starting from the extensive collection of literature existing on the topic. Eventually, Chapter 4 thoroughly analyzes the laser welding robotic cell by SM System S.r.l. in all its parts, explains how the previous concepts were applied to the practical application, and describes the various design, programming and testing phases that were carried out during the development process.

# 1 Laser Welding

Welding is the most common and versatile method of joining metallic components, applicable to the manufacturing of products in almost every industrial field. Among the innumerable welding techniques, during the last decades, laser welding has become more and more important, thanks to the different advantages that it can offer.

This Chapter deals with laser welding in general and it is organized as follows: Section 1.1 introduces the main concepts of welding, Section 1.2 briefly describes the physical phenomena and the technological solutions related to industrial lasers, Section 1.3 wraps up and analyzes more in depth the process of laser welding and its peculiarities.

## 1.1 The Welding Process

As defined in [2], welding is a material joining process in which two or more parts are coalesced at their contacting surface by a suitable application of heat and/or pressure. The American Welding Society [3] defines about 50 different types of welding operations, that can be divided into two broad categories:

- Fusion welding, in which heat is used to melt the base metals. This topic will be analyzed more in depth in the following.
- Solid-state welding, where coalescence results from the application of pressure alone or a combination of pressure and heat. Examples of this class are diffusion welding, friction welding and ultrasonic welding.

There are mainly five types of fusion welding:

- Arc welding. Heating of the materials is accomplished by an electric arc between an electrode and the workpiece.
- Resistance welding. Coalescence is achieved using heat from electrical resistance to the flow of a current passing through the faying surfaces of two parts held together under pressure.
- Oxyfuel welding. An oxyfuel gas is used to produce a hot flame for melting the base materials.

- Electron beam welding. The heat for welding is produced by a highly focused, high-intensity stream of electrons impinging against the work surface.
- Laser beam welding. Coalescence is achieved by the energy of a highly concentrated, coherent light beam focused on the joint to be welded.

Since this paper focuses on laser welding, it is now important to briefly analyze the physics behind the fusion welding process.

Fusion is accomplished by supplying a high-density heat energy to the faying surfaces, able to cause localized melting of the base metals. It is possible to define the power density as the power entering the surface divided by the corresponding area:

$$PD = \frac{P}{A} \quad (1)$$

- $PD$  = power density, [W/mm<sup>2</sup>]
- $P$  = power entering the surface, [W]
- $A$  = surface area over which the energy is entering, [mm<sup>2</sup>]

Two factors are not taken into account by equation (1): the power source is moving over the workpiece, which results in pre-heating ahead of the operation and post-heating behind it; and the power density is not uniformly spread throughout the affected surface, being instead a function of area.

On the other hand, it is important to quantify the amount of heat required to melt a given volume of metal: it can be seen as the sum of the heat required to raise the temperature of the solid metal to its melting point, which depends on the metal's volumetric specific heat, plus the latent heat of fusion of the material, that is the heat needed to transform the metal from solid to liquid phase at the melting point, dependent on the metal's heat of fusion.

The American Welding Society in [3] proposes the following equation to estimate, to a reasonable approximation, this quantity of heat:

$$U_m = KT_m^2 \quad (2)$$

- $U_m$  = unit energy for melting, starting from room temperature, [J/mm<sup>3</sup>]

- $K = 3.33 \cdot 10^{-6}$ , empiric constant
- $T_m$  = melting point absolute temperature, [K]

However, not all the input energy is used for melting the base metals, because of two additional heat transfer mechanisms, as depicted in Figure 1:

- the first one is the transfer of heat between the power source and the surface of the work. It is characterized by the heat factor  $f_1$ , that is the ratio between the actual heat received by the workpiece and the total heat generated by the source.  $f_1$  mainly depends on the welding process and the capacity to convert the power source into heat.
- the other one involves the dissipation of heat throughout the work metal and it is described by the melting factor  $f_2$ , defined as the proportion of the heat received at the work surface that can be used for melting.  $f_2$  also depends on the welding process, but is also influenced by the thermal properties of the metal, joint configuration, and workpiece thickness.

The numerical values of these coefficients, that vary between 0 and 1, can be found in the literature, for example in [4]. It is then possible to write an equation to compute the net heat available for welding:

$$H_w = f_1 f_2 H \tag{3}$$

- $H_w$  = net heat available for welding, [J]
- $f_1$  = heat transfer factor, [-]
- $f_2$  = melting factor, [-]
- $H$  = total energy generated by the source, [J]

The following energy balance equation can now be written:

$$H_w = U_m V \tag{4}$$

- $H_w$  = net heat used for welding, [J]
- $U_m$  = unit energy for melting, [J/mm<sup>3</sup>]

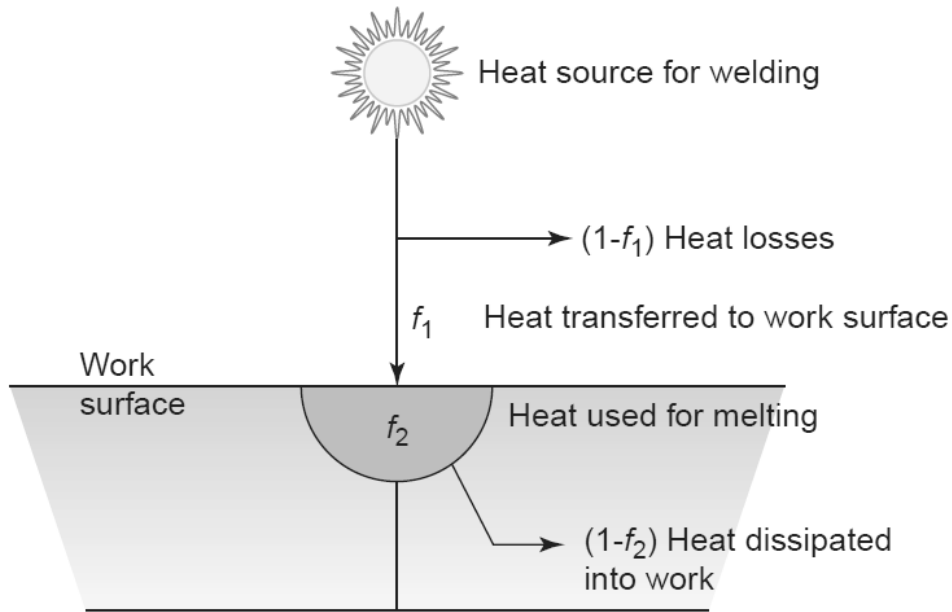


Figure 1 – The heat transfer mechanism in fusion welding. Picture from [2].

- $V$  = volume of metal melted, [mm<sup>3</sup>]

It is also convenient to represent the previous concept with a rate balance equation:

$$R_{Hw} = U_m R_W V \quad (5)$$

- $R_{Hw}$  = rate of heat used for welding, [J/s] = [W]
- $U_m$  = unit energy for melting, [J/mm<sup>3</sup>]
- $R_W V$  = volume rate of metal melted, [mm<sup>3</sup>/s]

Since most fusion welding operations involve the relative movement between the heat source and the workpiece, it is possible to express the volume rate of metal welded as the product of weld area  $A_w$  and travel velocity  $v$ . Substituting these terms and applying Equation (3), the above rate balance equation can be written as:

$$R_{Hw} = f_1 f_2 R_H = U_m A_w v \quad (6)$$

- $R_H$  = rate of input energy generated by the source, [W]

- $A$  = weld cross-sectional area, [mm<sup>2</sup>]
- $v$  = travel velocity of the welding operation, [mm/s]

These concepts, quantities and equations rule every fusion welding process, and will be useful in the next Sections to characterize laser welding and its advantages.

Now that the main phenomena involved in fusion welding are clear, it is time to analyze the five basic types of joint used to bring two parts together. As depicted in figure 2, they are:

- Butt joint, where the two parts lie in the same plane and are joined at their edges.
- Corner joint, where the joint is at the corner of the angle between two non-coplanar parts.
- Lap joint, where the two parts overlap.
- Tee joint, where the two parts are perpendicular each other.
- Edge joint, where the two parts are parallel with at least one edge in common.

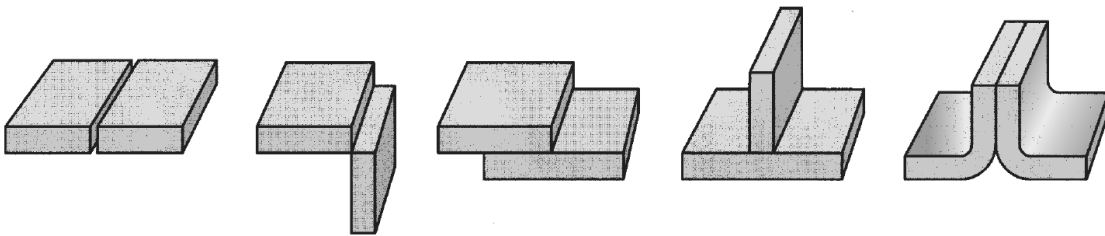


Figure 2 – *The main types of joints. Form left to right: butt, corner, lap, tee, edge. Picture from [2].*

Besides the joint configuration, it is important to analyze the properties of the welded joints, as they appear in a cross-sectional view like the one presented in Figure 3. A generic fusion-weld joint consists of several zones:

- Fusion zone. It is composed of the metal that have completely melted and then solidified.

- Weld interface. It is a narrow boundary of partially melted metal between the fusion zone and the heat affected zone.
- Heat-affected zone (HAZ). The metal here did not melt, but the high temperatures caused microstructural changes in its configuration. The HAZ is a critical part of any weld joint. In [2] it is asserted that “the amount of metallurgical damage in the HAZ depends on factors such as the amount of heat input and peak temperatures reached, distance from the fusion zone, length of time the metal has been subjected to the high temperatures, cooling rate, and the metal’s thermal properties”.
- Unaffected base metal zone, where no metallurgical change has occurred.

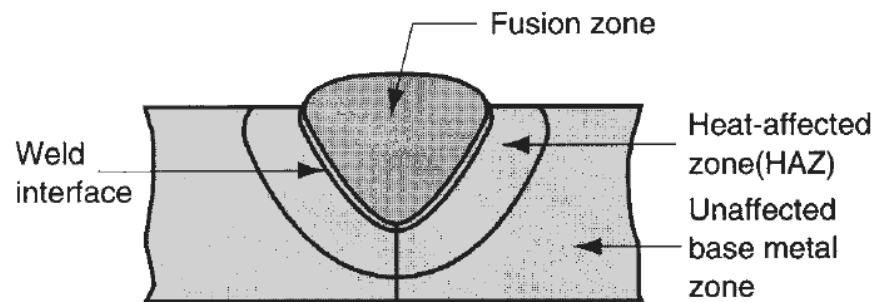


Figure 3 – *Typical cross-section of a fusion-welded joint. Picture from [2].*

Moreover, in order to obtain a good quality joint, many welding operations need the application of shield gas. At the high temperature required for fusion welding, the metals being joined are chemically reactive to oxygen, nitrogen and hydrogen in the air; these reactions, in particular oxidation, can seriously degrade the properties of the weld joint. Shielding is obtained by covering the molten weld pool with a blanket of gas, which inhibits exposure of the weld metal to air. The most common shielding gases are argon and helium, that are inert. Other gases are used in specific applications.

As a last point of this Section, it is worth discovering the main fields in which welding is applied and analyzing the ongoing process of its complete automation. The most common application areas of welding are automobile, manufacturing, ship-

building, construction and pipelines, but the technology advancements led to an increased use of welding also in more peculiar application fields, such as space vehicles, aircraft, and nuclear reactors. As complexity grows, many advantages for automating the welding operations arise. In [5], the authors list and discuss the main points in favor of industrial robotic welding:

- Safety aspects. Welding is inherently dangerous to human workers, due to the high temperatures and emitted radiations. Robots can work in hazardous environments, substituting manual labor.
- Severe shortage of skilled welding operators. In this sense, automation is imperative. In robotic welding, the operator is not in charge of welding, but just of overseeing the robot operations and, in some cases, loading/unloading the workpieces.
- Increased productivity. Industrial robots are capable of high duty cycles.
- Consistent and improved quality. Higher precision and accuracy lead to more uniform and controlled welds.
- Increased profit, determined by all the previous considerations.

In particular, the use of articulated robots has proven to be the best solution for automating the welding process. A meaningful data is that, according to the International Federation of Robotics [6], about 50 percent of all the world's robots are used for welding. The versatility of the robot arm allows the use of relatively simple fixtures for the workpiece, and the robot's capacity to be reprogrammed for new tasks makes this form of automation applicable to relatively low production quantities. If, once, automated welding was performed almost only for long-run, large lot applications, nowadays robotic welding cells are an increasing trend in the flexible automation field. This concept is well represented in Figure 4, where it is possible to notice that the use of robotic automation is mostly beneficial with medium production volumes.

On the other hand, there are still some concerns in using a robotic welder. One of the main issues is the fact that the workpiece needing to be welded has to be placed every time in the same exact position. Indeed, in most of the applications, the robot always

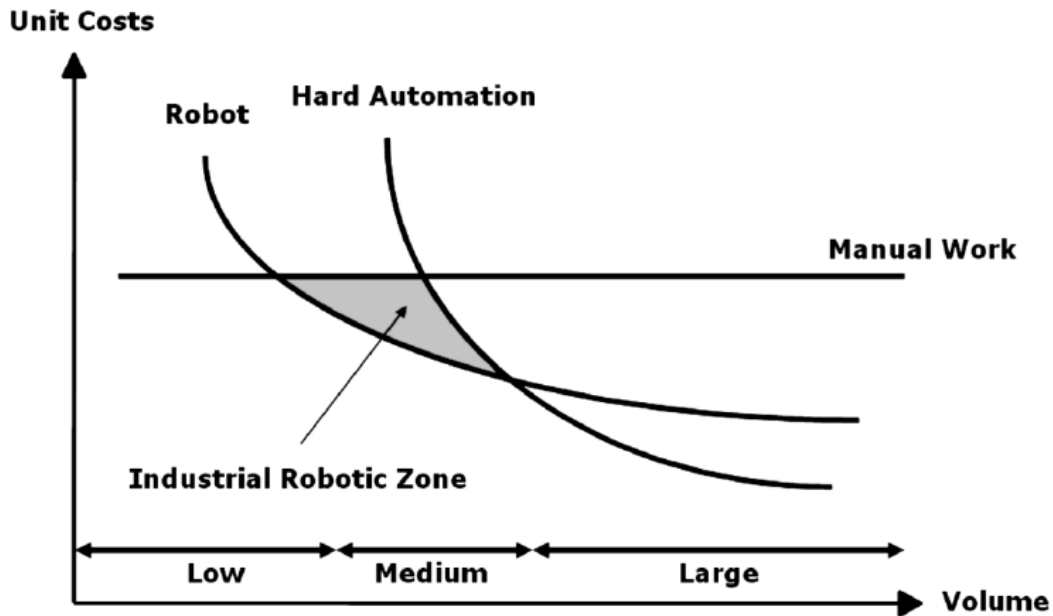


Figure 4 – *Application area of industrial robots in welding. Picture from [5].*

follows the same trajectory, programmed offline for the specific job. If the workpiece lays in a different position or it has an incorrect attitude, the welding operation will suffer from an error and the final welds will be located in the wrong place. Therefore, controlling the actual pose of the workpiece with respect to a predefined reference frame is often required in many automated welding cells. This operation can be expensive and time consuming, since an operator is usually needed, and specific fixtures and clamps may be required.

With the recent advancements of technology, this problem was tackled by introducing computer vision systems into the loop of the robot control algorithm. In particular, the application of some visual servoing concepts to the industrial world led to interesting results during the last decade. The details of visual servoing will be presented in Chapter 2, while its application to welding will be discussed in Chapter 3. The next Section, instead, deals with the main concepts of industrial lasers, that will be useful to characterize the laser welding process in its entirety.

## 1.2 Laser Principles

The word laser, that is an acronym for Light Amplification by Stimulated Emission of Radiation, indicates both the physical phenomenon and the technological device used to generate it.

The authors of [7] begin their deep analysis of the topic with a fundamental question: “What is the difference between a laser and a simple light bulb?” The answer immediately reveals the distinctive feature of lasers: spatial and temporal coherence of the emitted light waves. Lasers, indeed, produce a highly collimated and coherent beam of light, that have a much higher power density with respect to the light generated from a common light bulb, and that can be focused to a very small spot size.

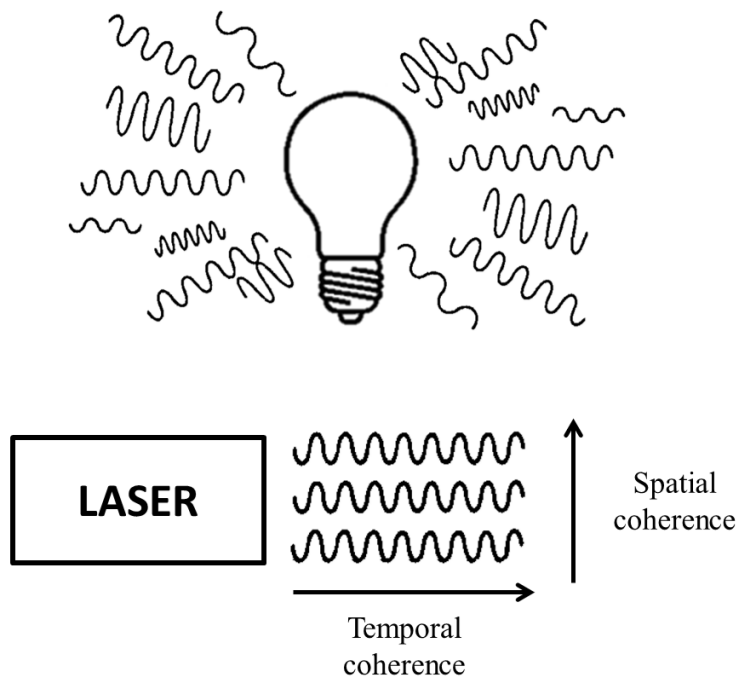


Figure 5 – *Radiations emitted by a light bulb versus radiations emitted by a laser.*

As regards the actual device, a laser is composed of the three parts depicted in figure 6 and listed below:

- an active medium, also called gain medium or laser medium. It is a gas, liquid or solid material that serves as a mean to amplify electromagnetic radiation;

- a pumping system, that is able to excite the active medium to the amplifying state;
- an optical resonator, that has the task of providing optical feedback.

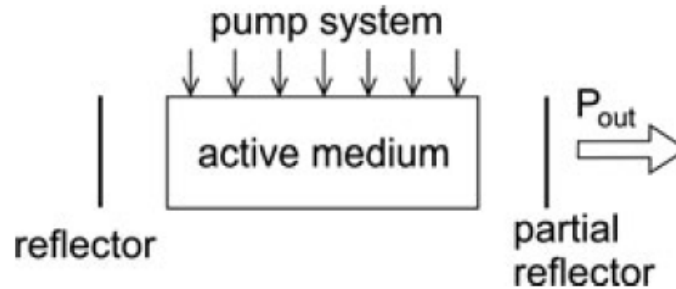


Figure 6 – *Generic scheme of a laser. Picture from [7].*

Instead, as regards the physical phenomena on which the laser is based, it is important to start from the atomic theory. Indeed, it is known that atomic systems can exist in certain discrete states, each of which is characterized by an energy level. When a transition between states of energy  $E_1$  and  $E_2$  happens, the system emits or absorbs a photon, with frequency:

$$\nu_{12} = \frac{|E_1 - E_2|}{h} \quad (7)$$

where  $h$  is Planck's constant.

As explained in [8], there are three main ways in which the atoms can interact with an electromagnetic field:

- **spontaneous emission.** An atom in level 2 decays spontaneously to level 1, emitting a photon. It comes out in a random direction, in the  $4\pi$  steradians.
- **absorption.** An atom in level 1 absorbs a photon from the field and jumps to level 2.
- **stimulated emission.** If a photon collides with an energized atom, it causes it to release its photon before spontaneous emission can happen, and the two photons will travel along in phase until the next collision. The added photon has the same

frequency, the same phase and the same sense of polarization, and propagates in the same direction as the wave that induced the stimulating photon.

Lasers are based on the stimulated emission phenomenon: they basically consist of two mirrors, placed parallel to each other to form an optical resonator, and an active medium between them, capable of amplifying the light thanks to stimulated emission, as described above. Therefore, it is possible to define the laser as a self-excited oscillator: it starts oscillations itself and maintains oscillation as long as pump energy is supplied by an external energy source. Output power is proportional to the power of the pumping source and to the amount of active medium, so power can be controlled by controlling either the pumping source or the active medium.

Invented in 1960, the laser was soon employed in many different branches of modern technology. It is possible to distinguish three broad areas of applications: optical uses, power uses, as in material processing, and ultrahigh power uses, as for atomic fusion. In the more specific field of material processing, the laser is employed for several tasks. The most common ones are:

- laser cutting, drilling and piercing
- laser welding
- laser surface treatment
- laser marking
- laser bending and forming
- laser cleaning

To perform these operations, it is required that the laser has certain features, that mainly depend on the material that composes the active medium. In this regard, lasers can be classified as follows [7]:

- Gas lasers. The active medium consists of atoms, ions, or molecules in gases. Gas lasers are available in the ultraviolet, visible, infrared, and microwave ranges. Two of the most important industrial lasers are gas lasers: the CO<sub>2</sub> laser and excimer lasers.

- Solid state lasers, except semiconductor lasers. They have the active medium held in an insulating dielectric crystal or amorphous glass. Solid state lasers, operated at room temperature, are available in the visible and the near infrared. The main types of solid-state lasers are ruby, neodymium glass, and neodymium yttrium aluminum garnet (Nd:YAG). In recent years, also fiber lasers are becoming more and more important.
- Semiconductor lasers. They make use of conduction electrons in semiconductors. Semiconductor lasers are available in the visible, near ultraviolet, and near infrared spectral ranges. Stimulated emissions are due to electronic transitions between the conduction and the valence band of the a semiconductor material.
- Free electron lasers. They are based on the emission of radiation by oscillating free electrons. The electrons are passing at a velocity near the speed of light through a spatially periodic magnetic field. Free-electron lasers are available in the visible and infrared spectrum.

Among these, the laser types that are most suited for material processing are Nd:YAG lasers, CO<sub>2</sub> lasers, and fiber lasers.

Nd:YAG lasers with average output power ranging from about 100 W to over 1 kW are commercially available. Figure 7 shows a schematic representation of a Nd:YAG laser. It is possible to notice that the resonator is composed of flash lamp, laser rod, reflector and mirrors. The laser rod is a yttrium aluminum garnet crystal (YAG), implanted with carefully distributed neodymium (Nd) atoms. The flash lamps excites the crystal, then the fully reflecting and partially transmitting mirrors are able to concentrate and collimate the light rays. The resonator is immersed in cooling water to avoid thermal distortion, which would degrade the laser performance. One of the most important features of the Nd:YAG laser is that the output wave length of 1.06  $\mu\text{m}$  of its beam can be transmitted through a fiber optic cable. This possibility makes the Nd:YAG laser a very popular choice for high speed welding production and automation.

CO<sub>2</sub> lasers are commercially available with higher average output powers, ranging from 0.5 W to 25 kW. Figure 8 shows a schematic layout of a CO<sub>2</sub> laser. The active

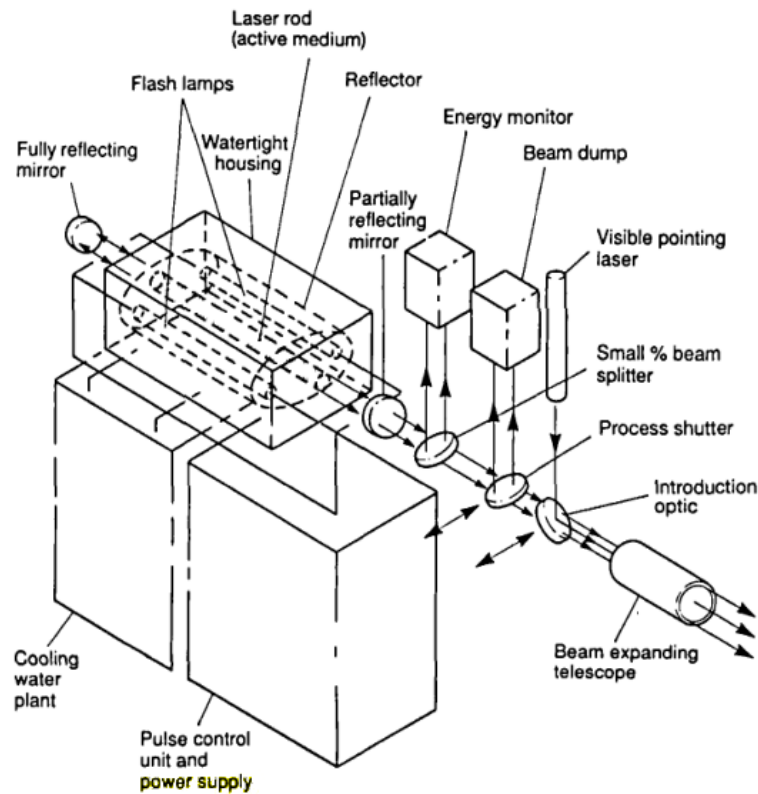


Figure 7 – Scheme of a Nd:YAG laser. Picture from [9].

medium is carbon dioxide ( $\text{CO}_2$ ), assisted in its lasing operations by the addition of helium (He) and nitrogen ( $\text{N}_2$ ). The gas is contained at a low pressure of about 50 mbar in the resonator housing. High voltage systems are used to excite the gas, that is driven in a continuous loop through the resonator. A heat exchanger system is employed to keep it cool.  $\text{CO}_2$  lasers can achieve much higher powers with respect to Nd:YAG lasers, but they are more complex and bulkier.

Fiber lasers are particular solid state lasers, in which the active gain medium is an optical fiber doped with rare earth ions. The main components of a fiber laser are shown in Figure 9. The glass fiber, doped with ions, is the active medium; the dichroitic mirror is highly reflecting for the laser radiation and transparent for the pump radiation; the output coupling mirror serves to collimate the light rays in order to reach maximum efficiency; the pump provides a continuous supply of energy. The main advantage of

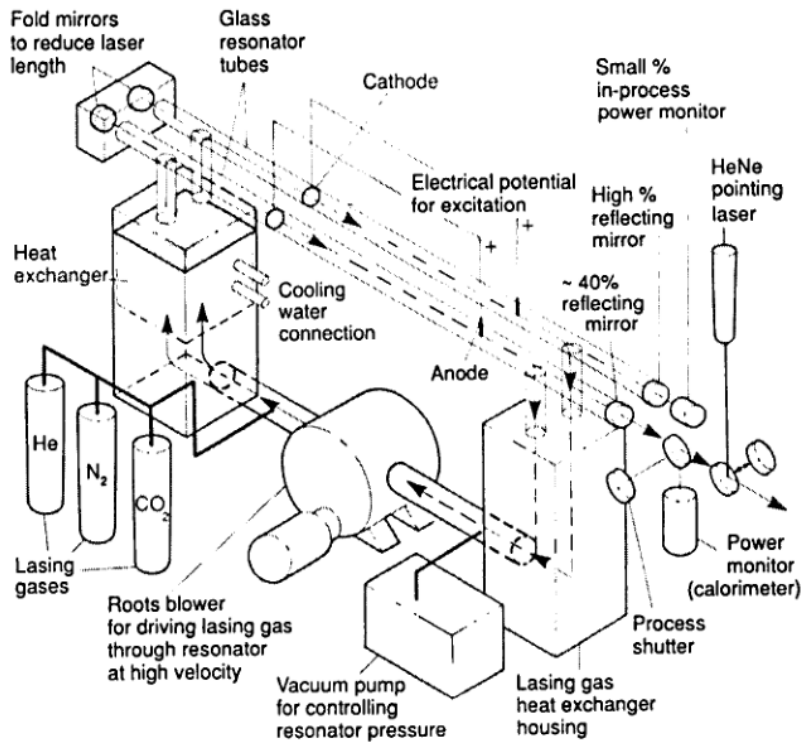


Figure 8 – Scheme of a CO<sub>2</sub> laser. Picture from [9].

fiber lasers is that the light is already coupled into a flexible fiber, so the power can be easily delivered to a movable focusing element, which is fundamental in laser cutting and welding.

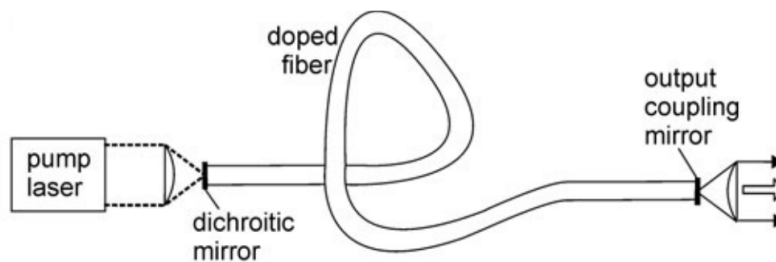


Figure 9 – Scheme of a fiber laser. Picture from [7].

### 1.3 Laser Welding Technologies

As defined by Groover in [2], laser-beam welding (LBW), or simply laser welding, is “a fusion-welding process in which coalescence is achieved by the energy of a highly concentrated, coherent light beam focused on the joint to be welded”.

To form a laser weld, the laser beam is focused on or very close to the surface of the workpieces to be joined. Since most metals are good reflectors, a large percentage of the incident light is reflected from the work surface. However, the small amount of energy that is absorbed by the workpieces quickly heats the material. The ionized metal vapor produced during this process accelerates the absorption phenomenon and much of the energy that previously would have been reflected is now delivered to the material.

At first, a small keyhole is initiated into the workpiece: it is a very small diameter cylindrical shaft caused by the rapid removal of metal by vaporization. According to [9], it is needed a focused power density in the order of  $10^3$  W/mm<sup>2</sup> for the keyholing process to start in steel components. At power densities in the order of  $10^4$  W/mm<sup>2</sup> –  $10^5$  W/mm<sup>2</sup> the welds are deep and narrow, and high speed welding is possible. At power densities greater than  $10^5$  W/mm<sup>2</sup> laser cutting and laser drilling regimes are reached.

The keyholing process is the main difference between laser welding and other types of fusion welding, such as arc welding or oxyfuel welding, described in Section 1.1. Indeed, the conventional fusion welding techniques are conduction-limited: that is, the provided power density is not enough to start a keyhole and penetration depth is achieved as heat is conducted into the work. The width of the weld is usually greater than its depth, and much heat is dissipated. The resulting weld characteristics are the ones discussed in Section 1.1 and presented in Figure 3. In laser welding, instead, during the keyholing process, the heat is transferred from the laser source into the material not to just a single point on the surface, but to a line extending through the material thickness. As a result, the cross-section of a laser weld joint is quite different with respect to the one obtained by means of conventional conduction-limited welding. Figure 10 shows a micrograph of the transverse section of a laser weld, where it is possible to notice the peculiar shape of the fusion zone and of the heat-affected zone (HAZ).

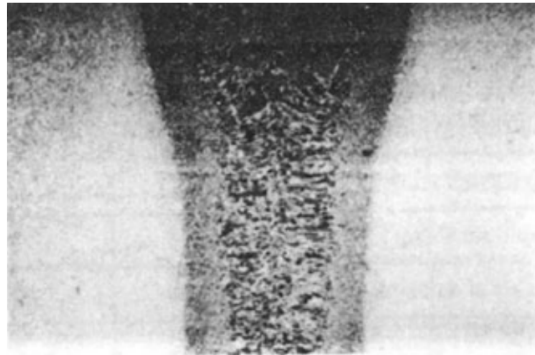


Figure 10 – *Micrograph of a joint obtained through laser welding. Picture from [8].*

Laser welding produces welds of high quality, deep penetration, and narrow heat-affected zone. High welding speeds are allowed and very little workpiece distortion is produced. The deep penetration capabilities lead to joints with high depth-to-width ratios, up to about 5:1, and several layers of material may be lap welded in a single pass.

On the other hand, laser welding presents one critical disadvantage with respect to other types of welding: the focused spot size of a laser beam, which is only a fraction of millimeter in diameter, requires close fitting joints, and great care has to be taken in aligning the laser beam with the joint line. Therefore, the accuracy requirements of the laser welding process are much stricter with respect to the ones of arc or oxyfuel welding. This issue is usually addressed by introducing vision sensors and specific algorithms in the control loop, as explained in the following sections of the present work.

In any case, the final quality of the weld, its shape and depth are determined by the manner in which the welding energy is applied to the joint. Several parameters are in play during the laser welding process. According to [8] they can be classified as follows:

- Laser beam properties. They depend on the nature of the laser employed to perform the welding operations and on how it is controlled.
- Transport properties. They are related to the movement of the welding head with

respect to the workpiece.

- Shroud gas properties. Laser welding is usually performed employing some sort of shielding gas to prevent the oxidation of the components. The characteristics of the chosen gas affect the final weld properties.
- Material properties. The material itself is a key element to be taken into account: its composition can enhance or deter the joining process.

Among the laser beam properties, the focused spot size, the depth of focus and focus position are three important parameters. They all depend on the optical equipment used in the system. As an example, here, a simple lens will be considered; please, refer to Figure 11. The following quantities can be measured:

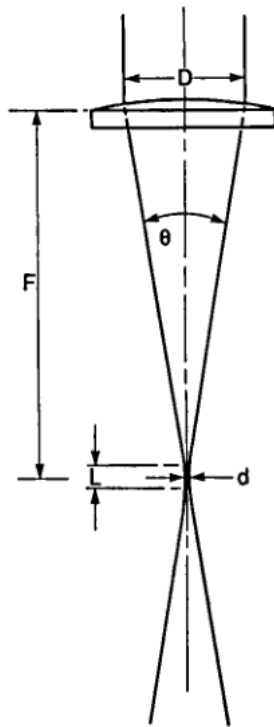


Figure 11 – *Laser beam focused by means of a lens. Picture from [9].*

- D: diameter of the beam incident on the optic
- $\theta$ : beam convergence angle

- F: focal length
- d: focus spot size, that is the minimum waist diameter
- L: depth of focus, that is the waist length

The focus spot size and the depth of focus depend on the characteristics of the optic. Their actual values are almost impossible to calculate accurately or physically measure. The choice of the right optic for the application is mainly based on experience. As regards the focus position, it should be where it gives the maximum penetration depth. Moving on, it is important to understand that the combination of laser power and welding speed is what determines the actual weld energy transmitted to the workpiece, and hence the weld properties and shape. Figure 12 shows how the welding penetration depth is affected by a change in welding speed, for different laser powers. As obvious, the highest depth is achieved when the laser power is higher and the speed is lower. By converse, low power lasers moving at high speed cannot achieve good penetration. Once again, the choice of the best speed-power combination is made on the basis of experimental results.

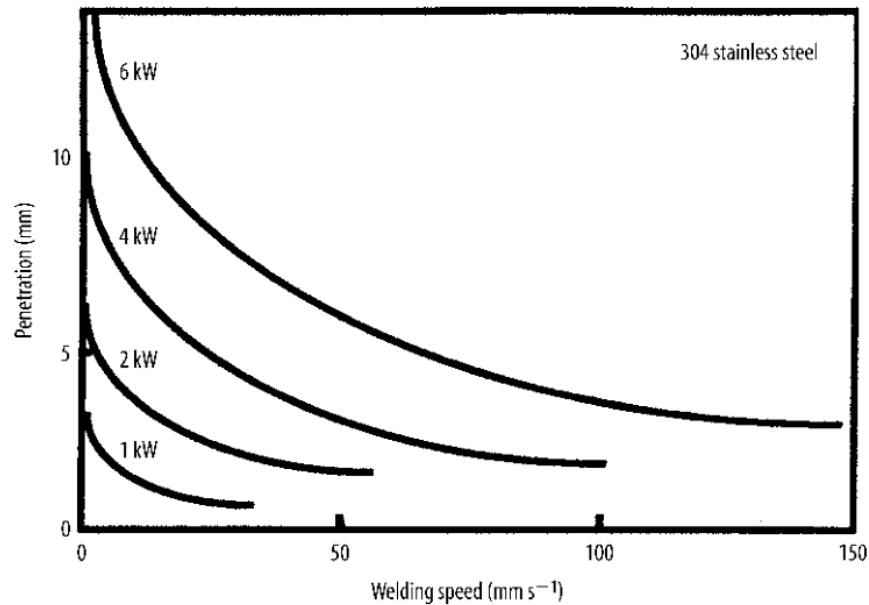


Figure 12 – Example of penetration vs speed graph for a CO2 laser. Picture from [8].

As regards the shielding gas, according to [9], in laser welding it has two main roles:

- to protect the molten and the cooling weld from oxidation;
- to protect the transmission of the laser beam when it focuses on the workpiece, since vapors, gases and plasma around the keyhole could modify the beam characteristics.

Some details on the first issue have been provided in Section 1.1, as this goal of the shielding gas is the same in laser welding and in other kind of welding, such as arc or oxyfuel welding. The second problem, instead, is more complicated and peculiar to laser beam welding. Actually, during welding, metal vapor ejected from the keyhole absorbs energy, ionizes and forms a plasma cloud above the welding zone. The plasma is only partially transparent to the laser beam and, if not controlled, it will expand and scatter the laser beam from its intended path, causing a reduction in weld penetration depth and, ultimately, in welding quality. The right provision of shielding gas can suppress plasma formation and grant maximum transmission of the laser power. Most common gases used for laser welding are argon, carbon dioxide, helium, and nitrogen. The necessary gas flow rate mainly depends on the laser power and on the welding speed, and it has to be tuned for each specific application. It is important to always provide it from the side opposite to the welding direction, so that the gas actually covers the cooling weld. An example of system utilized to carry the gas to the welding site is shown in Figure 13. It is a simple side tube gas shielding device, suitable for most applications.

Eventually, it is worth mentioning that the workpiece material itself has a significant impact on the results of the welding process. Table 1 show a list of common engineering alloys with some notes on their performance in laser welding. Anyway, this work is focused on carbon steel components, therefore no particular problems should arise.

Now that the main concepts of laser welding are established, it is possible to analyze how vision sensors and vision-based control can be employed in order to improve the welding performances. These are the topics covered in the next Chapter.

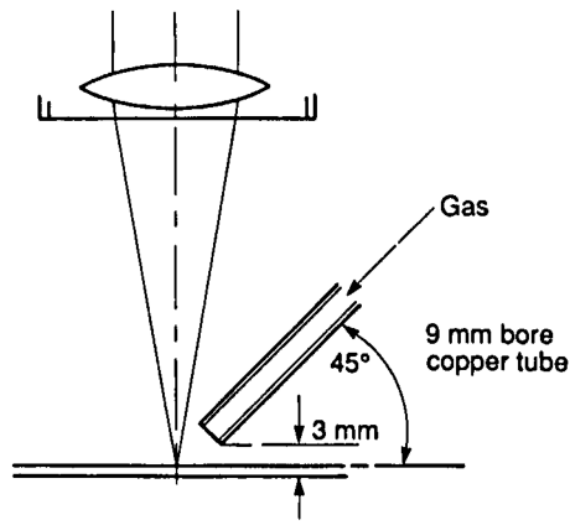


Figure 13 – *Example of side tube gas shielding device. Picture from [9].*

Alloy	Notes
Aluminium alloys	Problems with: <ol style="list-style-type: none"> <li>1. reflectivity – requires at least 1 kW;</li> <li>2. porosity; and</li> <li>3. excessive fluidity – leading to dropout.</li> </ol>
Steels	OK
Heat-resistant alloys, e.g., INCONEL <sup>®</sup> 718, Jeteht M152, HASTELLOY <sup>®</sup>	OK but: <ol style="list-style-type: none"> <li>1. weld is liable to brittle;</li> <li>2. segregation problems; and</li> <li>3. cracking.</li> </ol>
Titanium alloys	Better than slower processes owing to grain growth
Iridium alloys	Problem with hot cracking

Table 1 – *Laser welding performance for different alloys. Table from [8].*

## 2 Visual Servoing

This Chapter deals with the topic of Vision-Based Control, from the general problem formulation to the solutions developed throughout the years. In particular, it will be analyzed if and how these techniques can be applied to the specific field of automatic laser welding.

### 2.1 General Concepts

Robot control is a vast and complex world. In general, controlling an industrial manipulator means determining, instant by instant, the joint motor torques that need to be applied in order to perform a specific task. Many different techniques can be adopted for this purpose. The choice and the implementation of the right technique for the specific application is crucial for obtaining good performances.

The authors of [10] analyze in depth many control strategies, providing also a useful classification. The first distinction among the different algorithms is the following:

- Free space control, where the end effector moves without any contact with the workpiece.
- Interaction control, when the robot has to perform a manipulation task or it has to exchange forces with the environment. In these cases, it is crucial to keep under control the contact force between the end effector and the surrounding world.

Since laser welding does not require any contact between the manipulator and the workpiece, only the free space control techniques will be mentioned in this paper.

The free space control techniques are numerous. The mechanical structure of the robot and the joint actuation system vastly influence the choice of the control scheme. Moreover, it is important to underline that the motion characteristics are usually defined in the task space, while the control actions are directly applied to the joint space through the forces and torques generated by the actuators.

The task space is the one in which the pose of the end effector  $\mathbf{p}$  is defined, while the joint space is the one in which the vector of the joint variables  $\mathbf{q}$  is defined. The two

vectors are defined as:

$$\mathbf{p} = \begin{bmatrix} \mathbf{x} \\ \phi \end{bmatrix} \quad \mathbf{q} = \begin{bmatrix} q_1 \\ \vdots \\ q_n \end{bmatrix} \quad (8)$$

where  $\mathbf{x}$  is the end effector position,  $\phi$  its orientation, expressed for example using Euler angles, and  $q_i$  the  $i$ -th joint variable of the robot.

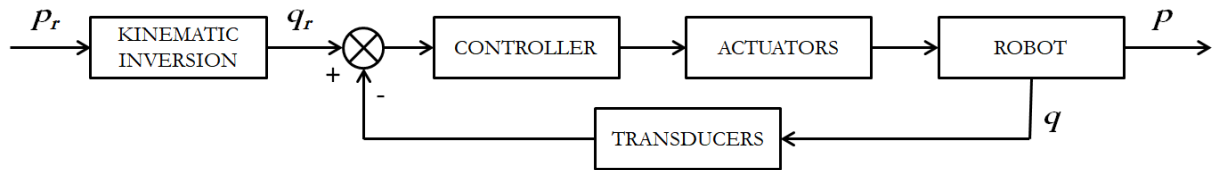


Figure 14 – *Joint space control general scheme.*

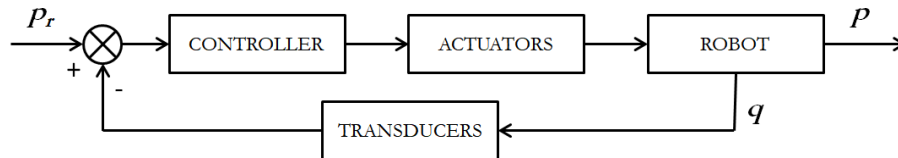


Figure 15 – *Task space control general scheme.*

The distinction between task space and joint space gives rise to the following classification of control techniques:

- Joint space control. Please refer to Figure 14. The control action is performed at joint level. Since the motion specifications are given in the task space, an intermediate step is needed, in which the inverse kinematic model of the robot is utilized to translate task space quantities into joint space quantities. Joint space control can be performed in two ways:
  - Decentralized control. Each joint is controlled independently from the others by a single-input single-output controller. All the coupling factors in the dynamics of the robot are treated as disturbances.

- Centralized control. A single multiple-input multiple-output controller is in charge of managing the whole system.
- Task space control. As shown in Figure 15, the control is performed directly in the task space. This global approach requires more complex algorithms, since the kinematic inversion step is implicitly performed inside the control loop.

During the last decades, several improvements were made in the field of robot control, so that nowadays it can be considered a mature technology. However, despite all the algorithms and enhancements, a fundamental problem has no solution using the previous control strategies: when the robot is commanded to move to an object, the robot actually only moves to a pose at which it expects the object to be. This happens because, in most of the cases, the robot cannot see what it is doing. The solution is to give the robot awareness of the surrounding environment by introducing computer vision into the control loop.

Vision is one of the most powerful sensing techniques, since it allows to acquire geometrical and qualitative information about the environment in which the robot operates, without direct contact with it. These data can be used by the control unit of the robot at various levels, just for the motion planning phase or also as a feedback for the control algorithm itself.

The first robotic systems that employed vision actually worked in open loop configuration: the extraction of data from the image and the control of the robot were two separate tasks. At first, image processing was performed, followed by the generation of a control sequence. In fewer words, the approach was “first look, then move”; the robot was still “blind” while moving, and it had to assume that the environment and the object to be reached remained static after the robot had started to move.

Actual visual servoing, instead, is utilizing visual information in a closed loop fashion: the vision system is used to close a feedback loop in order to increase the overall accuracy of the system. Two different methods can be adopted to achieve this goal. According to the taxonomy initially proposed by Sanderson and Weiss [11], then resumed by Hutchinson [12] it is possible to subdivide the visual servoing systems as follows:

- Dynamic Look-and-Move Systems. It consists of a hierarchical structure, with the

vision system providing set points as input to the robot's joint-level controller. The control of the robot is performed in two stages: the vision system provides input to the robot controller, then the robot controller itself uses joint feedback to internally stabilize the robot.

- Direct Visual Servoing Systems. The visual controller directly compute the joint-level inputs. The robot controller is eliminated from the loop.

For various reasons, nearly all implemented systems adopt the dynamic look and move approach. In particular, as pointed out by Hutchinson et al. in [12], the low sampling rate and the relatively high image processing time make the direct visual control a very challenging task. So true is it that Corke, in his more recent book [13], published in 2017, only analyzes the dynamic look and move approach, calling it with the general name of visual servoing. This is the approach implicitly assumed in the following of the whole Chapter.

Then, a second, more important classification can be made on the basis of the error signal definition. The error between the current location of the robot and its desired location, measured from the image information, can be defined:

- in the task space. This approach characterizes the Position Based Visual Servoing (PBVS) systems.
- in the image plane. This approach characterizes the Image Based Visual Servoing (IBVS) systems.

From a mathematical point of view, as in most of the control structures, the task of all vision based control schemes is to minimize an error vector  $e(t)$  between the current conditions and the desired conditions. The previous classification is based on the different ways in which the error vector is designed. For PBVS systems, vector  $e(t)$  is a pose error, and it depends on a set of task space parameters, which are estimated from image measurements. For IBVS systems, by converse, vector  $e(t)$  is a difference in the image itself, that depends on a set of features that are immediately available in the image data.

Position based visual servoing systems and image based visual servoing systems will be

analyzed in Section 2.2 and 2.3, respectively.

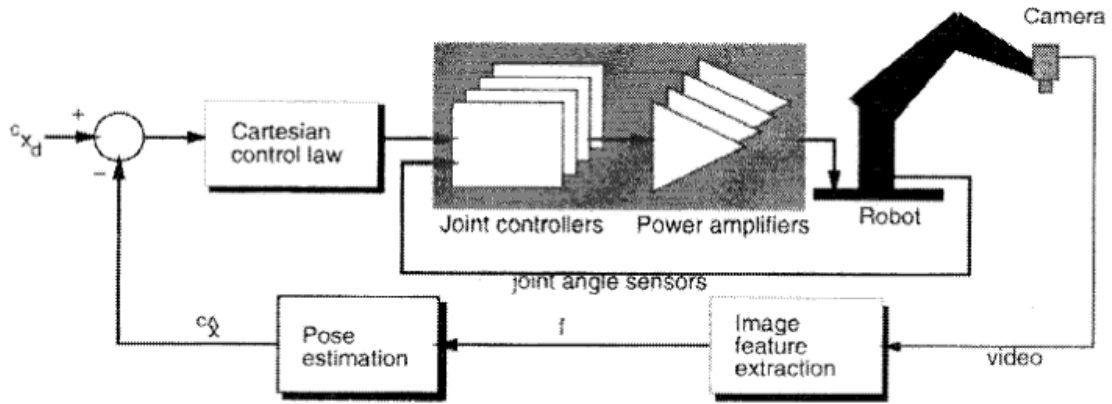


Figure 16 – *PBVS control scheme. Picture from [12].*

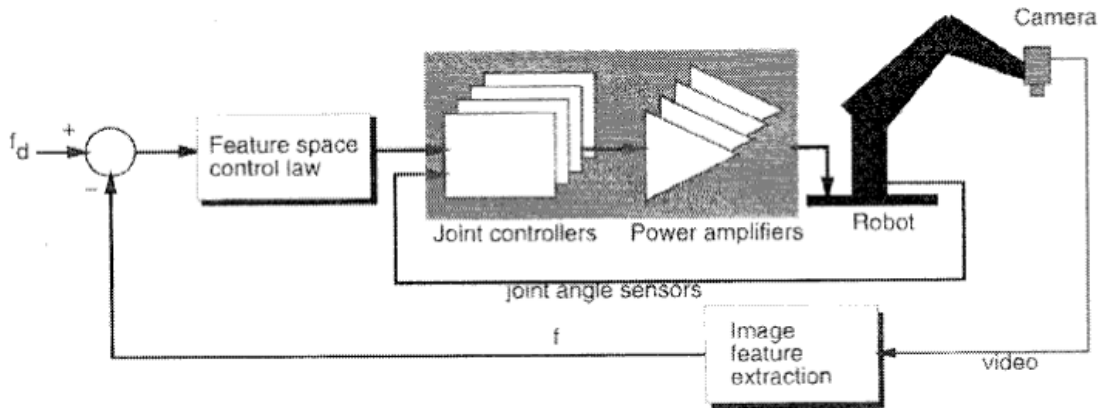


Figure 17 – *IBVS control scheme. Picture from [12].*

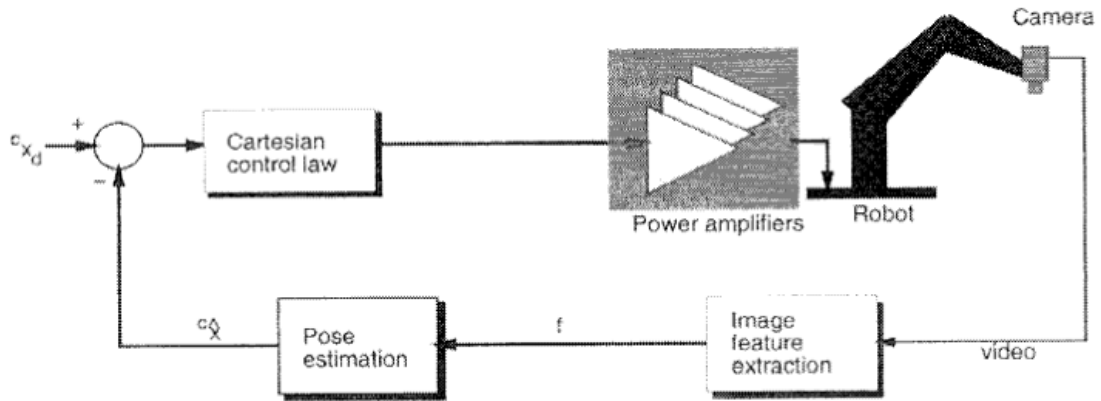


Figure 18 – *Direct PBVS control scheme. Picture from [12].*

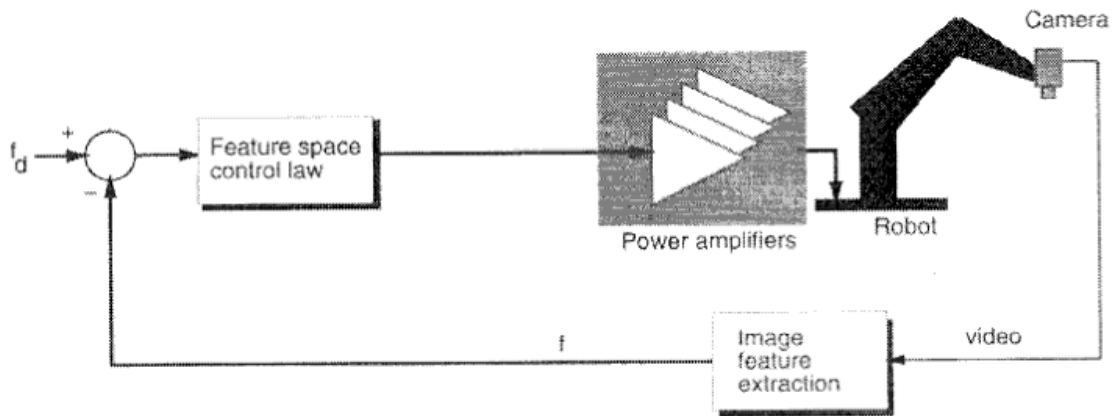


Figure 19 – *Direct IBVS control scheme. Picture from [12].*

## 2.2 Position Based Visual Servoing

Position based visual servoing systems use the visual measurements, in conjunction with the camera model and usually a geometric model of the environment, to estimate the pose of the target with respect to the camera coordinate system. Using these values, an error between the current and the desired pose of the robot is defined in the task space, as shown in Figure 20.

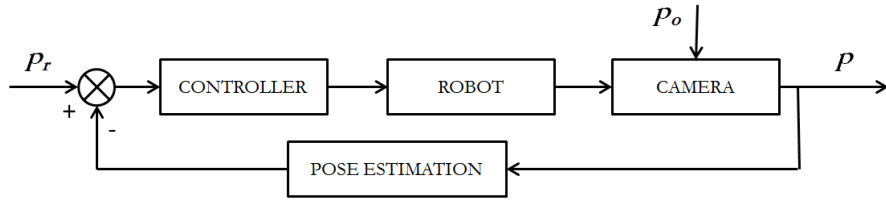


Figure 20 – *Position based visual servoing control general concept.*

From the conceptual point of view, the PBVS solution is similar to other task space control strategies. The key difference is that here the feedback loop is closed using real time data about the pose of the target object with respect to the camera, obtained by means of visual processing techniques. The advantage of PBVS over IBVS is that in PBVS the task space variables are directly controlled: this results in a simpler controller design and in good transient response of the end effector. As a drawback, however, since there is no control on the image plane, the target object can get out of the camera field of view during the operations; in this case, the feedback loop is broken and the overall stability of the system is lost.

The first objective in PBVS is to obtain from visual measurements the homogeneous transformation<sup>1</sup> matrix  $\mathbf{T}_o^c$ , that describes the position and the attitude of the object reference frame with respect to the camera reference frame.

The control strategy can then be formulated imposing that the pose of the object with respect to the camera reaches a desired value, represented by the homogeneous transformation  $\mathbf{T}_o^d$ , where apex  $d$  denotes the desired camera pose.

From  $\mathbf{T}_o^c$  and  $\mathbf{T}_o^d$  it is now possible to define the following homogeneous transformation matrix:

$$\mathbf{T}_c^d = \mathbf{T}_o^d \mathbf{T}_c^o = \mathbf{T}_o^d (\mathbf{T}_o^c)^{-1} = \begin{bmatrix} \mathbf{R}_c^d & \mathbf{t}_{d,c}^d \\ \mathbf{0}^T & 1 \end{bmatrix} \quad (9)$$

It represents the error between the current camera pose and the desired camera pose. It is also possible to associate this matrix to a vector, that represents the error in the

<sup>1</sup>Further details on homogeneous transformations and related topics can be found in numerous robotics books, for example [10] and [14].

task space:

$$\mathbf{e}_c^d = - \begin{bmatrix} \mathbf{t}_{d,c}^d \\ \boldsymbol{\alpha}_{d,c} \end{bmatrix} \quad (10)$$

where  $\mathbf{t}_{d,c}^d$  is the position error and  $\boldsymbol{\alpha}_{d,c}$  is the orientation error, expressed using the Euler angles extracted from rotation matrix  $\mathbf{R}_c^d$ . The final objective of the controller is to asymptotically drive the error  $\mathbf{e}_c^d$  to zero.

As suggested by Siciliano et al. in [10], it is possible to realize a PBVS controller using a proportional-derivative (PD) law with gravity compensation in the task space.

Making the derivative of Equation (10) with respect to time and assuming that the desired pose is constant in time, it is possible to show that:

$$\begin{aligned} \dot{\mathbf{t}}_{d,c}^d &= \dot{\mathbf{t}}_c^d - \dot{\mathbf{t}}_d^d = \mathbf{R}_d^T \dot{\mathbf{t}}_c \\ \dot{\boldsymbol{\alpha}}_{d,c} &= \mathbf{T}^{-1}(\boldsymbol{\alpha}_{d,c}) \boldsymbol{\omega}_{d,c}^d = \mathbf{T}^{-1}(\boldsymbol{\alpha}_{d,c}) \mathbf{R}_d^T \boldsymbol{\omega}_c \end{aligned}$$

The first expression is related to the derivative of the position, the second to the derivative of the attitude; it was taken into account that  $\dot{\mathbf{t}}_d^d = \mathbf{0}$  and  $\boldsymbol{\omega}_d^d = \mathbf{0}$ , since  $\mathbf{t}_d$  and  $\mathbf{R}_d$  are constant in time. Therefore, it is possible to write the derivative of the error:

$$\dot{\mathbf{e}}_{d,c} = -\mathbf{T}_A^{-1}(\boldsymbol{\alpha}_{d,c}) \begin{bmatrix} \mathbf{R}_d^T & \mathbf{0} \\ \mathbf{0} & \mathbf{R}_d^T \end{bmatrix} \mathbf{v}_c$$

being  $\mathbf{v}_c = \begin{bmatrix} \dot{\mathbf{t}}_c^T & \boldsymbol{\omega}_c^T \end{bmatrix}$ . Assuming that the camera reference frame is coincident with the end effector reference frame,  $\dot{\mathbf{e}}_{d,c}$  can be rewritten as:

$$\dot{\mathbf{e}}_{d,c} = -\mathbf{J}_A(\mathbf{q}, \mathbf{e}_{d,c}) \dot{\mathbf{q}}$$

where  $\mathbf{J}_A$  is the analytical Jacobian of the robot in the task space.

It is then possible to build the control law as:

$$\mathbf{u} = \mathbf{g}(\mathbf{q}) + \mathbf{J}_A^T(\mathbf{q}, \mathbf{e}_{d,c}) \mathbf{K}_P \mathbf{e}_{d,c} - \mathbf{J}_A^T(\mathbf{q}, \mathbf{e}_{d,c}) \mathbf{K}_D \mathbf{J}_A(\mathbf{q}, \mathbf{e}_{d,c}) \dot{\mathbf{q}} \quad (11)$$

in which  $\mathbf{K}_P$  and  $\mathbf{K}_D$  are the gain matrices of the PD controller. If they are symmetrical and positive-definite, it is possible to demonstrate the asymptotic stability of the system

for the equilibrium pose corresponding to  $e_{d,c} = \mathbf{0}$ , as shown in [10]. The corresponding controller block scheme is shown in Figure 21.

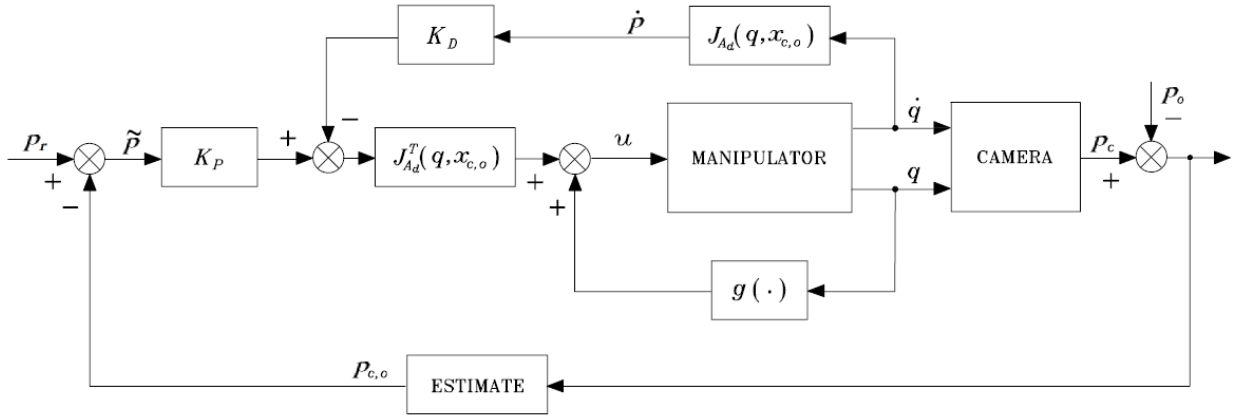


Figure 21 – Implementation example of a position based visual servoing controller.

### 2.3 Image Based Visual Servoing

Position based visual servoing systems directly use 2D image measurements to estimate the desired movement of the robot. Usually, the controller is built to reduce the image distance error between a set of current and desired image features in the image plane, as schematically illustrated by Figure 22.

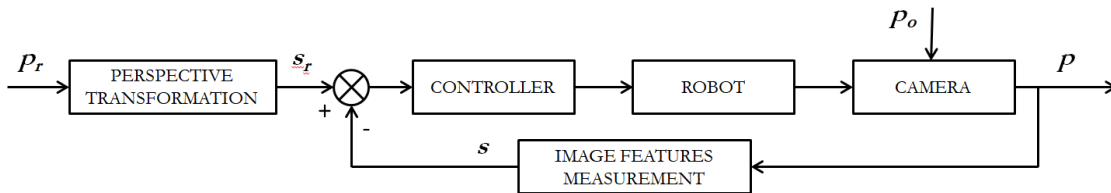


Figure 22 – Position based visual servoing control general concept.

The main advantage of IBVS over PBVS is that the pose estimation of the target object with respect to the camera is not required. Moreover, since the control action is directly performed on the characteristic features of the image, it is possible to avoid that during the operations the object gets out of the camera field of view. As a drawback,

the nonlinear nature of the relationship between the image parameters and the task space variables implies a more complex controller design and an unpredictable behavior of the robot end effector, that may follow unwanted trajectories.

The IBVS control strategy is usually performed by reducing the image distance error between a set of current and desired image features in the  $(u, v)$  image plane. The error is defined in the image plane as follows:

$$\mathbf{e}(u, v) = \mathbf{s}(u, v) - \mathbf{s}_d(u, v)$$

where  $\mathbf{s}$  is the vector of the current image features and  $\mathbf{s}_d$  the vector of the desired image features. They both implicitly correspond to a certain pose of the target object with respect to the camera:

$$\mathbf{s} = \mathbf{s}(\mathbf{p}_{c,o})$$

$$\mathbf{s}_d = \mathbf{s}(\mathbf{p}_{d,o})$$

As described in [15], the IBVS control involves the computation of the interaction matrix, or image Jacobian matrix, that sums up the relationship between world coordinates, image coordinates and camera spatial velocity:

$$\mathbf{J}(\mathbf{q}) = \left[ \frac{\partial \mathbf{s}}{\partial \mathbf{q}} \right] = \begin{bmatrix} \frac{\partial s_1(\mathbf{q})}{\partial q_1} & \cdots & \frac{\partial s_1(\mathbf{q})}{\partial q_m} \\ \vdots & \ddots & \vdots \\ \frac{\partial s_k(\mathbf{q})}{\partial q_1} & \cdots & \frac{\partial s_k(\mathbf{q})}{\partial q_m} \end{bmatrix}$$

where  $\mathbf{q}$  is the configuration vector of the end effector and  $\mathbf{s}$  is the vector of the image features. The following equation holds:

$$\dot{\mathbf{s}} = \mathbf{J} \dot{\mathbf{q}}$$

The simplest approach to design an IBVS controller is to use a simple proportional (P) controller that aims at minimizing the error:

$$\mathbf{u} = \mathbf{K} \mathbf{J}^\dagger \mathbf{e}(s) \tag{12}$$

where  $\mathbf{J}^\dagger$  is the pseudo-inverse of the image Jacobian and  $\mathbf{K}$  is a constant gain matrix.

Obviously, more complex control schemes can be implemented, as shown for example in [16], [10], and [13].

## 2.4 Discussion on Visual Servoing Systems

In the previous sections, the main theoretical concepts about visual servoing, both PBVS and IBVS, were introduced. However, their application in real world contexts is not straightforward.

A first issue is the cost and the complexity of vision-based systems: many different expensive components have to interact with each other in real time, and the control algorithms have to grant optimal performances. Luckily, the availability and the quality of key components such as cameras, image processing hardware and computers in general have exponentially increased during the last decades.

Anyway, the development of visual servoing systems in industrial fields is still subject to some other limitations: the unstructured environment in which the robots usually operate and the different light conditions that can be present in the working environment make the use of vision quite limited.

Moreover, there are issues for what concerns the need of a 3D model of the target object in PBVS control schemes, and the requirement of an accurate camera calibration in IBVS approaches, as explained more in depth for example in [10].

One solution to some of these problems is what is generally called hybrid visual servoing: as described in [15], “this approach is halfway between the classical position based and image based approaches”. In this way, the advantages of each solution are summed up, while the drawbacks are mitigated.

However, for the specific field of autonomous welding, other solutions were investigated, where application-specific algorithms were implemented over the visual servoing foundations. These concepts, namely seam teaching and seam tracking, are the main topic of the next Chapter.

## 3 Seam Teaching and Seam Tracking

This Chapter shows how the issues about visual servoing presented in the previous Section were solved during the last decades by different research teams. The concepts of seam teaching and seam tracking will be introduced in Section 3.1, the related scientific literature will be analyzed in Section 3.2, and eventually some industrial applications of these concepts will be presented in Section 3.3.

### 3.1 Definitions

During the '80s, thanks to the advancements in vision sensors and computing power, new efforts were put into improving the performance of automatic arc welding equipment. In this context, the concepts of seam teaching and seam tracking were initially introduced.

In the most common case, robotic welding is performed in two steps: in a first passage, the robot acquires the welding trajectory and saves it in its memory. In a second passage, it actually welds the workpiece by blindly reproducing the recorded path. This approach is usually adopted when the objects to be welded are all the same and production quantity is somewhat high: the robot is programmed once for every batch of products on a reference workpiece, then it confidently assumes that all the following objects are exactly the same and in the same position.

The first passage of two-step welding is called seam teaching. It can be performed in different ways:

- Manual teaching. The actual programming method depends on the particular model of the robot. Usually, a teaching-by-showing method is used, where the robot operator moves the robot by means of the teach-pendant and saves the points that compose the welding path.
- Offline programming using a CAD/CAM software. The welding trajectory is communicated to the robot by a specific software that has in its memory a 3D model of the workpiece.

- Automatic teaching. By means of a specific set of sensors, the robot is able to detect the seam on its own.

Two problems are evident in the two-step welding approach: first, it is difficult to have an entire batch of identical workpieces, especially if the required welding accuracy is high; second, it is common to have clamping inaccuracies. In both these cases, even if the reference nominal trajectory is perfect, the robot could incorrectly weld some elements of the batch, and quality is not granted. Moreover, if the batches are composed of few elements, the first step of the procedure, where the robot moves without welding, has to be repeated more frequently, causing a waste of precious time.

The ideal solution to all these issues is single-step welding, in which the robot directly welds the workpiece, without needing previous information. Of course, it is not an easy task, since specific sensors are needed and robustness has to be granted. Initially proposed for arc welding, where the accuracy requirements are less stringent, this approach was investigated by many research teams throughout the years. Its core part is seam tracking: in real-time, while welding, the robot adjusts the trajectory following the seam.

For both automatic seam teaching and seam tracking, two alternative exists for what concerns the sensing technology:

- Active sensing: a CCD or CMOS camera records the seam area, while a structured light pattern is projected onto it under a certain angle. The triangulation principle is applied to calculate the needed range data.
- Passive sensing: a CCD or CMOS camera records the seam area under environmental light only. In this case, more specific vision processing and segmenting algorithms have to be applied.

The two sensing techniques are illustrated in Figure 23.

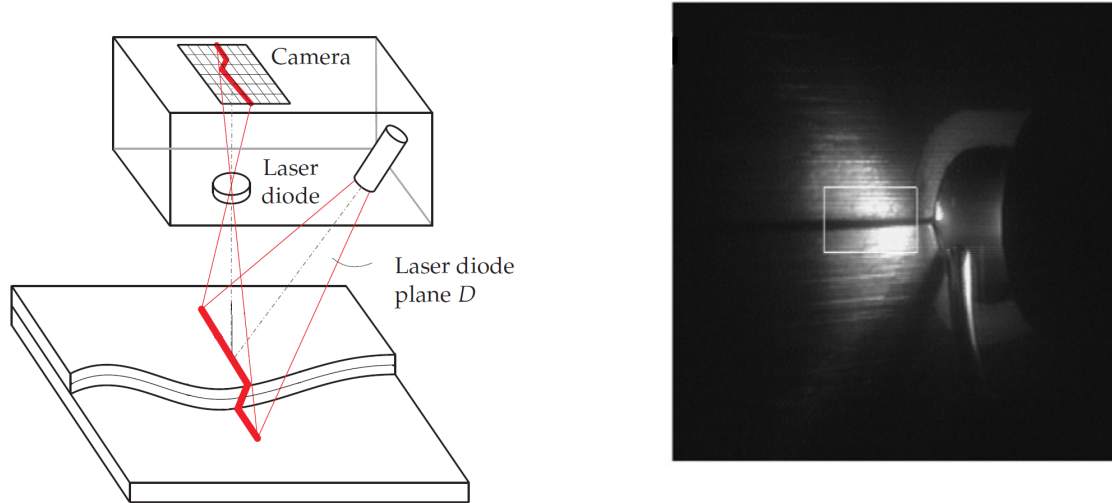


Figure 23 – *Sensing techniques. Active, on the left, and passive, on the right. Pictures from [17] and [18].*

### 3.2 Literature Review

In this Section, the main available literature on the subject of seam-teaching and seam-tracking is analyzed. The various articles and documents are presented in chronological order, focusing on the aspects relevant to the application discussed in this thesis.

One of the first papers on seam teaching and seam tracking is the one published by Clocksin et al. in 1985, [19]. Here, the authors investigate the problem of performing MIG welding of thin sheet steel pressings by means of a robot. In order to comply with the permitted dimensional variation of  $\pm 0.5\text{ mm}$ , the robot is equipped with sensors able to find corrected starting and ending points of the weld seam and to track its location as it is welded.

Clocksin et al. propose an enhancement of the conventional two-step welding approach by adding “a middle step called *vision teach*, in which the robot automatically inspects the workpiece, generating a model that is used in subsequent production”. Therefore, the three steps are as follows:

- manual teaching of the weld seam. The operator manually programs the path of

the desired welds.

- vision teach: automatic visual survey of the assembly. This is a sort of automatic re-teaching step, in which a model of the seam is constructed and the ideal location of the torch relative to the seam is derived.
- actual welding, repeated for each workpiece presented to the robot. Visual feedback is provided during each run. Torch positioning errors are detected and corrected.

The vision sensor used in this solution is composed of a CCD camera paired with a low power laser line. They operate on the principle of active triangulation ranging.

The algorithm proposed by Clocksin et al. is able to extract the segments of the weld seam from the images captured by the CCD camera. More in depth, a finite impulse response transversal filter is applied to the image, by means of a specifically designed hardware processor, whose analysis is beyond the scope of this thesis. Nowadays, thanks to the increased availability of computing power, the hardware implementation would be easily replaced by a software filter running on a microprocessor.

After the extraction of the weld seam from the image, during the vision teach phase a higher level algorithm is in charge of determining the joint type. A rule-based decision procedure is able to discriminate between butt joint, lap joint and T joint.

The model of the seam built in this phase is an expectation of what to find while actually welding the different workpieces. During the welding phase, the errors between the model and the actual seam are detected and compensated.

The results of the approach proposed by Clocksin et al. are compliant with the initial requirements: errors up to  $\pm 3$  mm are corrected to within  $\pm 0.1$  mm. The real limitation of this approach is its circumscribed application field: the algorithm is able to recognize and to track only a very specific number of joint types in very simple configurations.

Some years later, in 1992, Nayak and Ray [20] provide a thorough analysis of the available seam teaching and seam tracking techniques for arc welding.

They make a distinction between different generations of laser welding, namely:

- first generation, that is the classical two-pass welding, with a first step of manual teaching and a second step of repeated welding;

- second generation, in which the two steps are condensed into a single one: the weld is tracked in real time and no prior learning phase is present. However, these systems are capable of operating only in well-defined structured environments;
- third generation, only theoretical, where the welding system is required to operate within unstructured environments, while learning rapidly changing seam geometries.

In their monograph, Nayak and Ray, analyze the first and second generations, then lay the theoretical basis for the third generation, also depicted as “Adaptive, Real-Time, Intelligent Seam Tracker” (ARTIST).

As regards the sensing techniques, they introduce two different approaches:

- Through-the-arc sensing. It “uses the functional relationship between the variations in the Contact-Tip to Work Distance (CTWD) and the electrical arc signals, i.e. arc current and arc voltage”.
- Vision sensing. It is based on the techniques presented in Section 2.

For the purposes of this paper, only vision sensing is relevant, since through-the-arc-sensing, obviously, cannot be applied to laser welding. Moreover, the authors make a distinction between direct vision measurements, that result in range data of the surface points being measured, and indirect measurements, where the range data have to be inferred from monocular images. The former are achieved by means of stereo vision of structured lights, and are based on the triangulation or time of flight principles; the latter are achieved through several analysis methods of monocular images.

As regards the actual algorithms, Nayak and Ray briefly describe the two-pass approach, then propose the so called *tractrix* algorithm for performing the real time seam tracking. Eventually, they introduce the properties that a third generation system is required to have:

- the system should track a seam that may change in all three dimensions
- the system should track a seam along non-preprogrammed weld paths
- the system should be able to work in real time

- the system should operate in unstructured environments, with minimal external guidance

The following chapters of the paper by Nayak and Ray describe in depth different feature extraction and seam recognition techniques that can be applied in seam tracking systems, then discuss a case study with V-groove joints. The experiments are performed using a prototype system, composed of a microcomputer, a laser range sensor, a robot controller with a six DOF manipulator, and the equipment for welding. The results are encouraging, but they are limited to a very specific set of test cases and are subject to noise, due to welding spatters, arc glares, and smoke.

In order to achieve more robustness and generality, in 1995, J. S. Kim et al. in [21] return to study a sort of two-step adaptive robotic arc welding system, where two separate vision processing algorithms are implemented.

As usual, the system comprises a 6-DOF articulated robot, the welding torch and a vision sensor, that is again composed of a CCD camera and a laser light beam. The sensor operates using the active triangulation ranging principle.

A flow chart depicting the main steps of the algorithm is presented in Figure 24.

Before welding, when the noise is limited and no real time constraints arise, a first algorithm is in charge of determining the seam characteristics, of identifying the type of the joint, and of modeling the joint geometry. These operations are performed by different programs, whose detailed explanation can be found in the original paper. In any case, it is worth mentioning that the procedure dedicated to joint type identification is based on syntactic analysis, a particular class of artificial intelligence algorithms, quite popular at the time of that publication.

During welding, the processing of the images is far less favorable, because of the noise generated by the welding operations. Also, the vision algorithms now have to run in real time, in order for the feedback to be useful to the robot controller. To solve these problems, Kim et al. perform the image analysis only on a windowed image surrounding the expected laser stripe location, and employ a template matching algorithm that makes use of the joint models generated in the previous step.

Several tests are then carried out to investigate the performance of the system. Fillet, lap and V joints are used for the experiments. Results show that “a reasonable accuracy

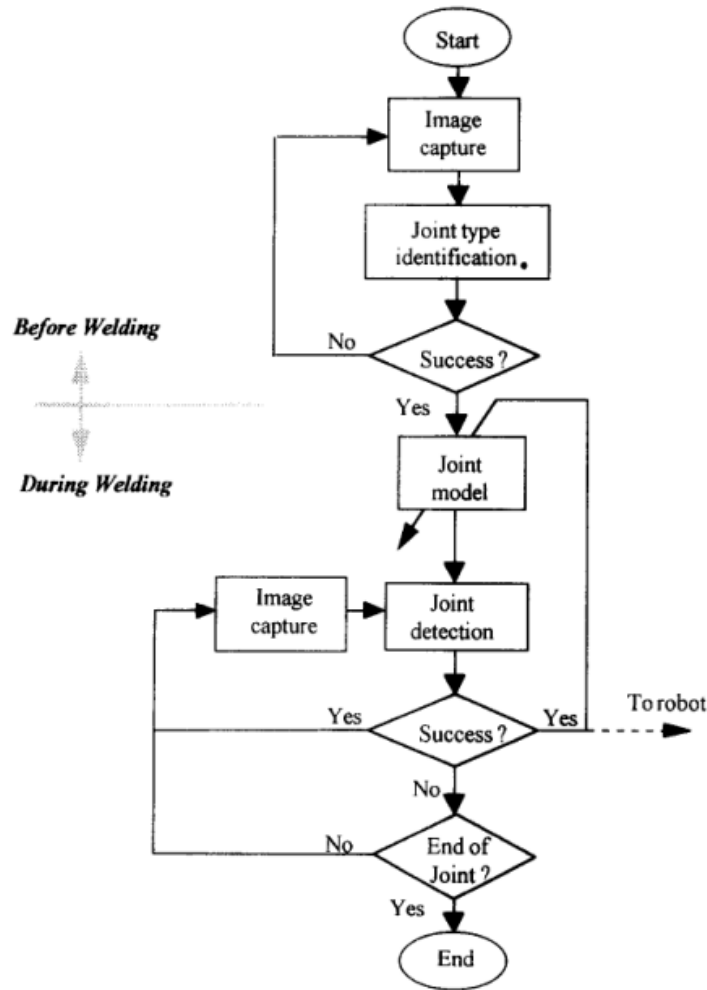


Figure 24 – Flow chart of the algorithm proposed by Kim et al. Picture from [21]

in the measurement of three-dimensional location of joint features and in seam tracking by a welding robot can be obtained. Seam tracking ability of the developed system was measured to be consistently better than  $\pm 0.5$  mm, which is more than adequate for most GMA welding processes”.

Even if during the early ‘90s the technology seemed ready to improve towards the so “intelligent third generation” of real time seam tracking systems, most of the prototypes have been proved to have limited functionality and flexibility for practical use. The limitations include their restricted use to only some very specific joint types, and

high sensitivity to image noise (arc glares, welding spatters and smoke) but also to variations in torch orientation and workpiece surface finish

With the advance of technology, in particular in the field of computer hardware and software, the first CAD-CAM programs were integrated into the manufacturing environment. This was a game changer for the seam teaching and seam tracking research progress: the CAD model of the workpiece could be used to provide a nominal trajectory to the visual based control algorithm. Such an approach was commonly adopted since the late '90s until today.

For example, in 1999, P. Kim et al. publish a paper [22] in which the CAD data and the range data acquired by the laser vision sensor are combined and used together to drive the robot.

This automatic welding system comprises a 6-axis articulated robot, the welding machine, the host computer and the vision sensor, composed of a laser diode and a CCD camera.

The authors propose a simple but efficient procedure, able to load a nominal trajectory from the CAD data of the workpiece, check and correct it by means of the vision system, then perform automatic welding. The various steps are depicted in Figure 25. It

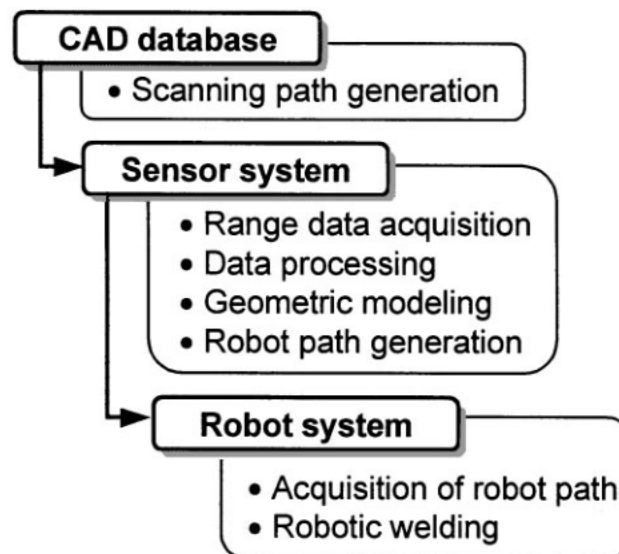


Figure 25 – Flow chart of the algorithm proposed by P. Kim et al. Picture from [22]

is clear that, in this case, the authors are not proposing a single-step real time seam tracking system, but a sort of seam re-teaching algorithm able to enhance the performances of a two-step welding machine. In a first step, the robot performs a scanning run along the nominal trajectory of the seam suggested by the CAD data of the workpiece. Range data are collected during this motion. After filtering the noise, feature extraction and joint modeling are performed. Eventually, the whole seam is modeled by means of a cubic spline connecting the various data acquisition points. The position and the orientation of the welding robot are then extracted from the geometric model of the seam. From these data, the robot path for actual welding can be generated.

In the first decade of the present century, many different authors try to address the various aspects of seam teaching and seam tracking that still have critical issues.

In 2003, Fridenfalk et Bolmsjo give their contribution by publishing a paper [23] on the development of a full 6D sensor guided control system for seam tracking, that is able to correct the tool center point (TCP) in the x, y and z direction and around roll, pitch and yaw.

Once again, the application area is automated arc welding, and the vision sensor relies on a laser scanner. The key points of the paper are the proposal of a control approach using differential vector interpolation, and the development of a simulation environment called FUSE, based on the robot simulator Envision and Matlab.

The following year, Xu D. et al. publish an article [24] on a real time arc welding robot visual control system.

The peculiarity of their approach is the use of two CCD camera plus the usual laser stripe. Combining structured light and stereovision, they propose a “*structured light stereovision*, which employs redundancy information to improve the precision and robustness of welding systems”.

After the analysis of the image feature extraction process, the hybrid visual servoing (see Section 2) control scheme reported in Figure 26 is proposed. It is composed of four parts:

- a position based control part makes the robot move along the direction of the

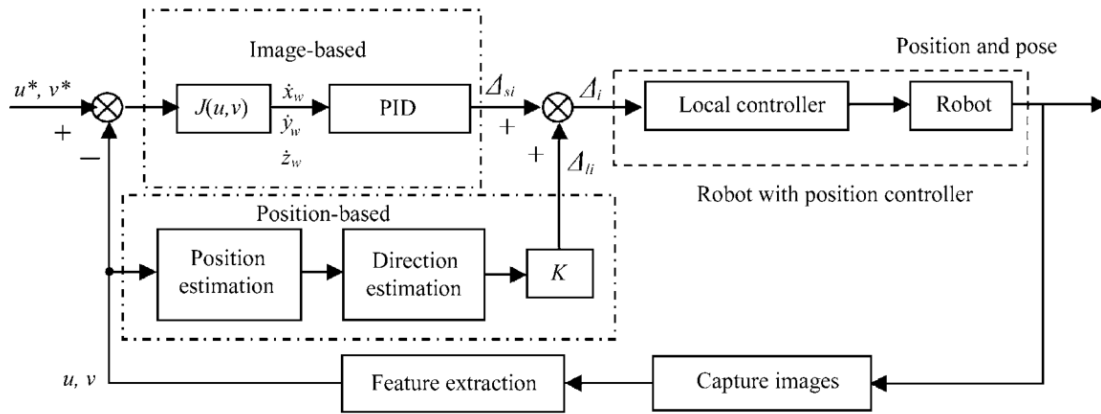


Figure 26 – Hybrid visual servoing control scheme proposed by Xu et al. Picture from [24]

weld seam

- an image based control part adjusts the robot pose and minimizes the pose error
- the image capturing and processing part provides real time feedback to the controller
- the robot controller performs the low-level control tasks

A couple of years later, the same authors publish a new paper [25] in which they improve the previous implementation.

The main difference is the renounce to stereovision, probably too computationally demanding. The seam tracking algorithm is then improved to face this change, and it is once again based on hybrid visual servoing: a position control inner-loop in the Cartesian space is supported by two outer-loops; one is a position based visual servoing loop in the Cartesian space, employed to control the movement along the seam, the other is an image based visual servoing loop in the image space, used to adjust the trajectory and to perform actual tracking.

The experimental results show the effectiveness of this hybrid visual servoing control system for robotic arc welding, but the application field remains limited to very structured cases.

It is now time to analyze the publications of one of the most influential authors on seam teaching and seam tracking: the Dutch researcher M. De Graaf, who, during the period from 2005 to 2013, published a PhD thesis [17] and several articles [26] [17] [27] [28] [29] [30] on the topic. His work is very relevant to the present discussion, since De Graaf is among the first to apply the concepts of seam teaching and seam tracking to laser welding, where the requirements are more stringent and the tolerances smaller.

It is worth analyzing in depth his papers since they deal exactly with the problem of automated laser welding, performed by a 6-axis anthropomorphic robot. The objective of the author's PhD thesis is the "Development of a sensor-guided robotic laser welding system that is suitable for 3D seam welding in small product series".

De Graaf builds a prototype using industrial 6-axis robots from the Stäubli RX series, in particular a Stäubli RX90 and a Stäubli RX130, controlled by a Stäubli CS8 controller. The welding laser is generated using a 4kW lamp-pumped Nd:YAG laser (Trumpf HL4006D) and transported to the welding head through an optical fiber. The seam tracking sensor is composed of a CMOS camera coupled with a laser diode; it works on optical triangulation using structured light; it is important to notice that the sensor measures ahead of the welding spot.

The author addresses both the seam teaching and the seam tracking problem. As regards the former, it is performed using point-to-point movements. That is, the robot moves in a discrete way to a certain number of points along the seam, where it stops and allows the sensor to take a measurement. The sensor only measures when the robot is at rest, therefore the influence of dynamic effects is reduced.

More in depth, two different phases in the teaching process can be distinguished: the actual teaching phase and the re-teaching phase. In the first case, no prior information on the seam trajectory is available, so an estimation for the next seam location has to be computed at each step by the algorithm; in the case of re-teaching, instead, this is not necessary, since a nominal seam trajectory is already known from manual programming, CAD data of the workpiece or a previous teaching phase. Figure 27 and 28 show the two phases, respectively. The Sensor Measurement Buffer contains all the measurements taken by the system, and it is paired with the Sensor Trajectory Buffer, that contains the location along the seam in which that measurement was actually taken. As regards the teaching algorithm, the author proposes as alternatives an adaptation

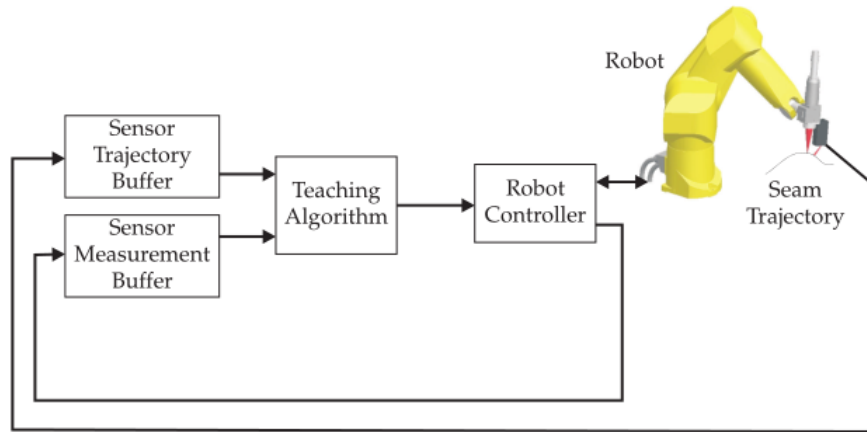


Figure 27 – *Teaching control scheme proposed by De Graaf. Picture from [17]*

of the *tractrix* algorithm developed by Nayak and Ray in [20] and a *polyfit* algorithm, more advanced. Their complete description can be found in [17].

The next part of De Graaf's thesis deals with real time seam tracking. The main difference with respect to seam teaching or re-teaching is that “the sensor now measures simultaneously with the robot motion instead of measuring only when the robot is at rest, requiring the robot joint measurement and sensor image acquisition to be synchronized”. Due to the high processing speeds and the 3D nature of the seam trajectories, the standard visual servoing techniques described in Section 2 present some shortcomings if applied to seam tracking. Therefore, De Graaf proposes a new approach: a trajectory-based control strategy. The control scheme, reported in Figure 29, is composed of a top branch and a bottom branch. The former contains the robot trajectory generation, the latter contains the sensor integration part. The main blocks are:

- Tool trajectory buffer: it contains a list of locations (positions and orientations) that the robot tool has to pass through during the robot motion.
- Real-time setpoint generator: it interpolates the locations in the tool trajectory buffer and computes the setpoints for every  $k$ -th fixed time interval.
- Motion descriptor: it specifies the maximum acceleration, velocity and deceleration to the setpoint generator.

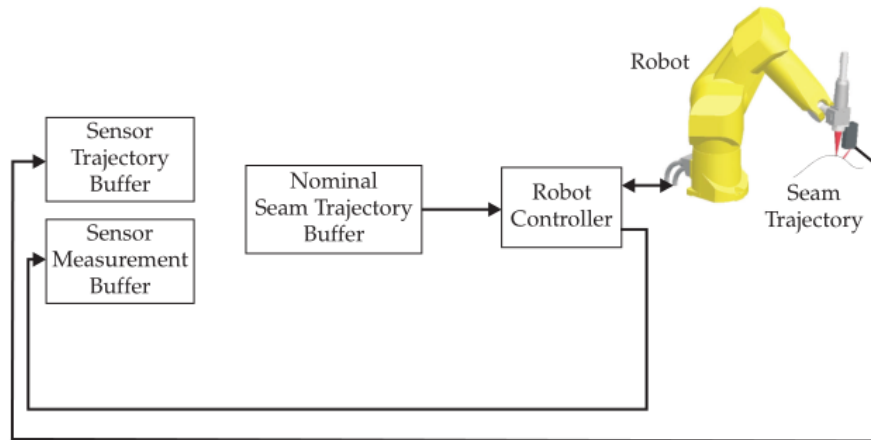


Figure 28 – *Re-teaching control scheme proposed by De Graaf. Picture from [17]*

- Inverse geometric model: it computes the robot joint angle setpoints starting from the task space setpoints.
- Joint motion controller: it is proprietary to the robot builder, in this case Stäubli; it receives the robot joint angle setpoints and tracks the joint measurements in such a way that the tracking error on the specified path remains small.
- Image processing block: it measures the position of the seam from the images obtained by the vision sensor. If properly synchronized, each measurement can be correlated to a specific position along the seam.
- Direct geometric model: it computes the tool pose in the task space starting from the measured joint angles.
- Synchronization block: it synchronizes the measurements performed by the vision sensor with the computation of the actual pose of the end effector.
- Seam trajectory buffer: it collects the results of the previous synchronization. Each measurement performed by the vision sensor is correlated to a specific position along the seam. “ By moving the sensor tool along the seam trajectory and storing the obtained seam locations into the seam trajectory buffer, the complete geometry of the seam trajectory is obtained”.

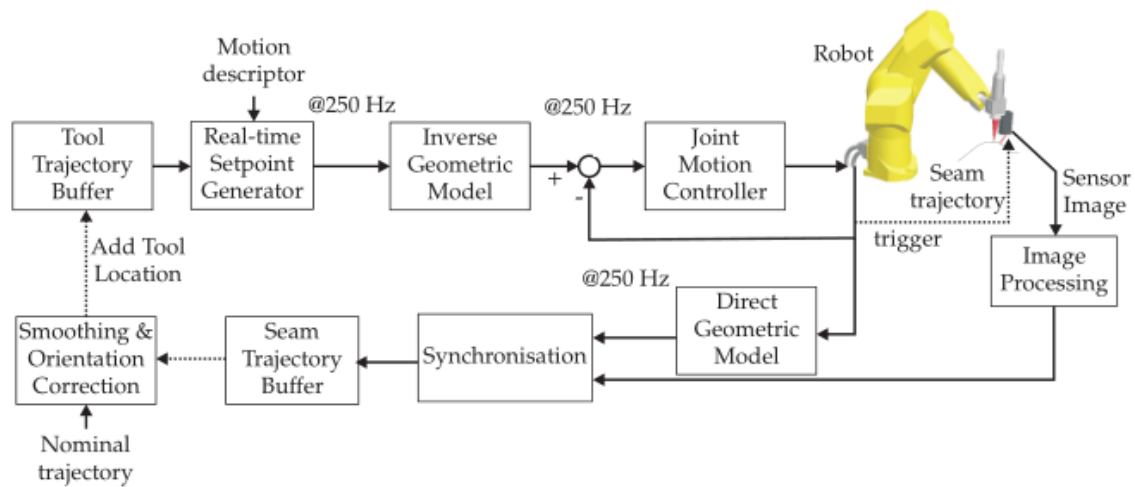


Figure 29 – *Trajectory-based control scheme proposed by De Graaf. Picture from [17]*

- Smoothing and orientation correction block: it is used for filtering and fixing the trajectory in real time seam tracking.

According to the author, the trajectory-based control approach can be used in different contexts:

- teaching an unknown seam trajectory
- re-teaching a seam trajectory, with prior knowledge of its geometry, from manual teaching or offline programming
- real time tracking a previously known seam trajectory
- real time tracking an unknown seam trajectory

For the differences in the control scheme among these applications and for the details about the actual algorithm, please refer to section 6.6 of [17]. The experimental results reported by De Graaf show that this system is applicable with good results, at least for what concerns line, corner and curved seam trajectories.

In the same years and up to the present day, other authors conduct studies on alternative ways of performing seam teaching and seam tracking.

In 2008 Regaard et al. write a paper [31] in which they propose other possible sensors for seam teaching and tracking in laser welding applications.

In particular, instead of a scanning triangulation sensor, they suggest to use a passive sensor, a simple camera coupled with a gray-scaling image processing algorithm. With this configuration, “the joint position is recognized not by discontinuity of the laser line but by separating areas of different reflectivity (or brightness) within the camera image. Moreover, the authors experiment with a coaxial camera setup, in which the sensor is integrated within the welding head and the camera is coaxial with the welding laser beam. Please refer to Figure 30. This setup is hardly applicable to real time seam tracking, since in this case the sensor cannot measure ahead of the welding spot, but is useful for accurate seam teaching and for reducing the size of the end effector.

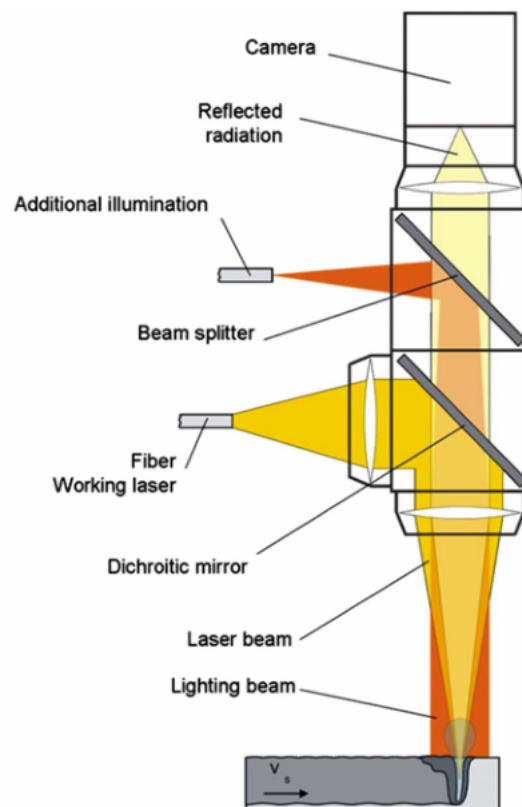


Figure 30 – *Optical setup of the coaxial vision sensor proposed by Regaard et al. Picture from [31]*

On the other hand, in 2009, Sung et al. in [32] propose an enhancement of the structured light sensor for seam teaching and seam tracking.

They build an test a prototype of a multiline laser vision sensor (MLVS), able to improve the tracking capability and reliability of conventional systems so as to apply high-speed joint tracking.

The prototype is based on a single CCD camera, a laser source and an aspheric lens, used to generate five laser strips. A more complex algorithm is needed to process multiple range data concurrently.

The results show a good tracking capability, with errors less than 0.3 mm in average.

In 2011, Shen et al. in [33] address the problem of tracking butt welds without groove, a difficult task for seam detection algorithms due to the narrow gap in the workpiece.

In particular, the authors focus on the weld center identification phase. They propose a new seam tracking image processing algorithm based on twice edge detection, one for the laser stripe identification, the other for weld seam centerline extraction.

In a certain sense, this approach combines again an active technique, where the structured light is employed, and a passive technique, where the simple CCD camera and image processing techniques are used to detect the seam trace.

The results presented by Shen et al. show that the algorithm is very rapid and efficient, but it needs additional refinements “for better anti-interference capacity in complicated ambient light”.

Y. Xu et al., in the years from 2012 to 2017, publish several documents [18] [34] [35] on the use of passive vision sensors for seam tracking in arc welding.

The main reasons of employing passive sensors instead of active triangulation systems are reduced costs and the presence of a minor number of critical components in the system. Figure 31 shows the procedure of image processing adopted by the authors to detect the seam center starting from a single CCD camera. It is possible to notice that several filters and algorithms were applied.

The approach employing only passive vision sensors was proposed also by Dinham

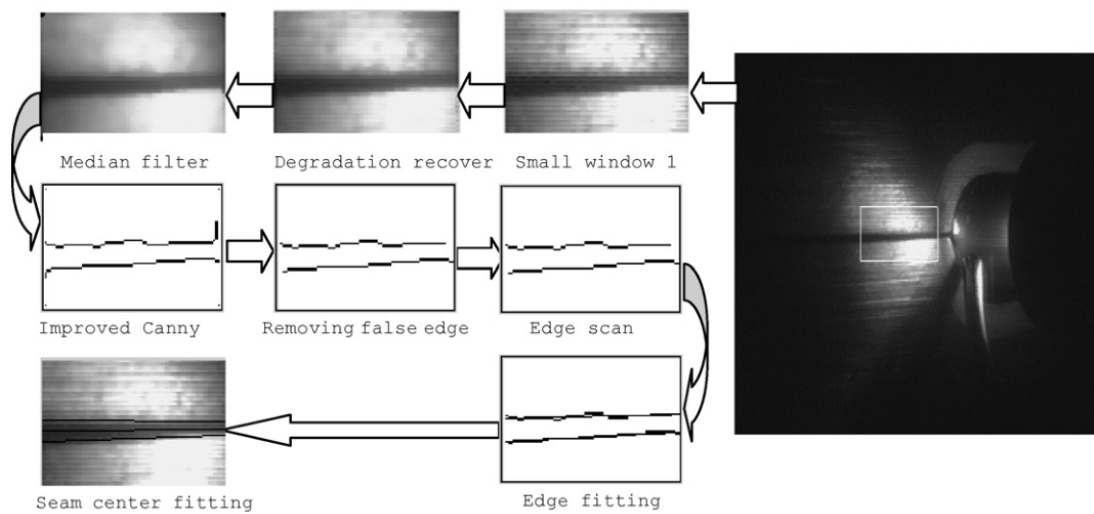


Figure 31 – *Image processing procedure proposed by Xu Y. et al. Picture from [18]*

et al. in 2014. In their paper [36], the authors introduce a new weld detection method, “capable of adaptively detecting fillet weld joints of any shape without prior knowledge of the shape or position of the joint in the image”.

The system is based on two cameras, that produce stereo images of the joint; the images are then converted to binary edge images; eventually, a line growing method developed by the authors is able to find the seam. The algorithm analyzes the entire image from a global perspective, then it is able to detect the welding joint on the basis of the assumption that the seam is darker than the surface of the workpieces.

Figure 32 shows a test example, in which the system is able to correctly identify the joint. The results presented by the authors highlight that the average localization errors are within  $\pm 1$  mm, which is acceptable in most arc welding applications but not good enough for laser welding.

In 2015, Lahdenoja et al. in [37] address the problem of tracking very narrow seams in laser welding.

As previously underlined, for very small seam width, structured light does not work. In this case, the authors employ a smart camera based on a CMOS sensor chip and an FPGA processor. The algorithm for image processing comprises segmentation, several filters and transforms. Figure 33 shows the seam identification process in a very chal-

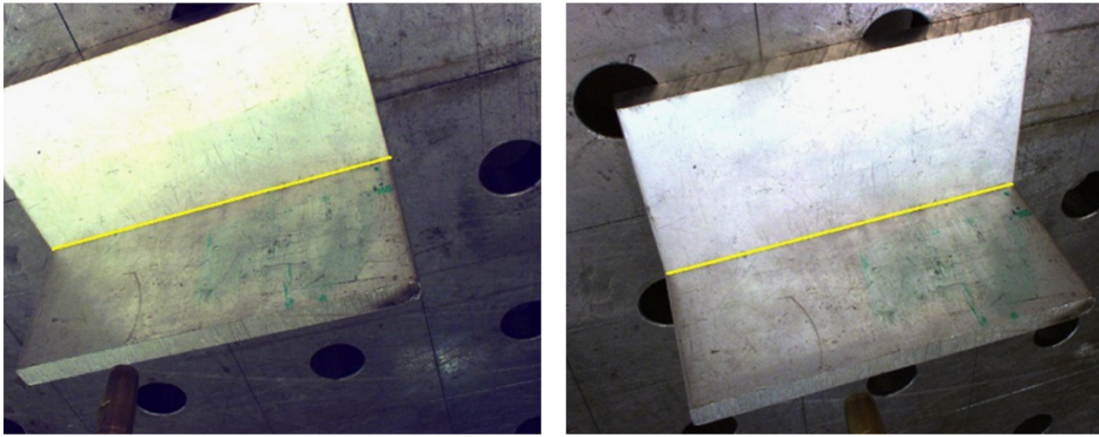


Figure 32 – *Stereo images and seam identification using Dinham's algorithm. Picture from [36]*

lenging scenario. The results are positive, but the system would require more testing.

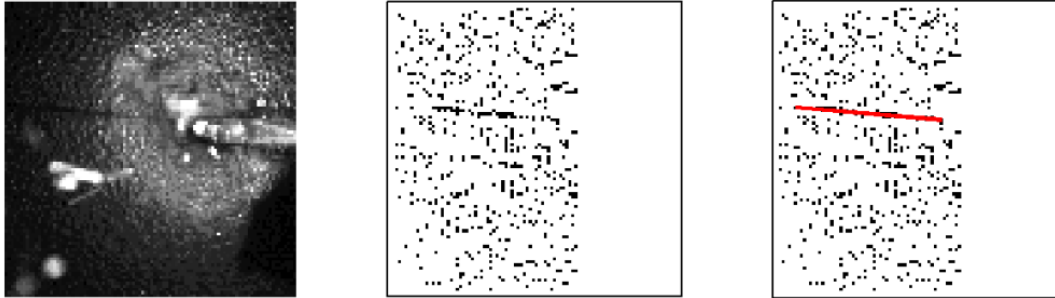


Figure 33 – *Seam identification in Lahdenoja's work. Picture from [37]*

On the contrary, in 2016, Ding et al. keep studying laser-based machine vision system for seam teaching and seam tracking.

In [38], the authors employ a CCD camera and a diode laser to obtain data about the seam by means of the triangulation principle, then they use an on-line shape-matching algorithm for determining the features of the weld joint. in particular:

- the CCD camera acquires a gray scale image of the seam, with a resolution of 640 x 480 pixels

- a median filter with a kernel size of  $3 \times 3$  is applied
- the image is made binary by setting an appropriate threshold
- the laser stripe is extracted from the original image

Then, the last groove shape is used as a template to locate the next one: the shape-matching algorithm proposed by Ding et al. calculates the similarity of the laser stripe profiles of the two adjacent images by shifting image ( $t$ ) to match image ( $t + 1$ ), as shown in Figure 34. The seam tracking system takes advantage of this algorithm and is able to track seams with an accuracy of  $\pm 0.5$  mm.

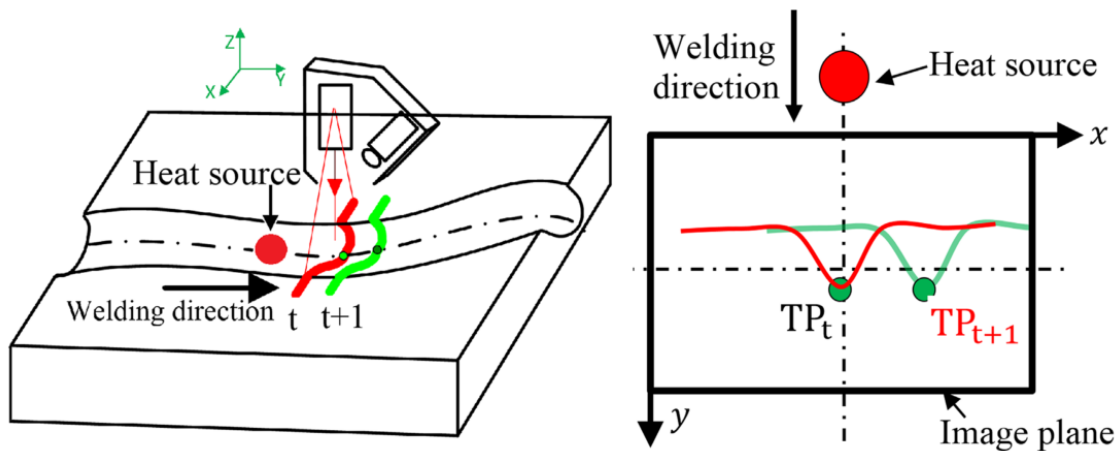


Figure 34 – *Shape matching algorithm proposed by Ding et al. Picture from [38]*

In 2018, Shao et al. in [39] investigate the problem of detecting weld seams whose width is less than 0.1 mm.

The problem is relevant in the field of laser welding, where the accuracy requirements are very stringent, but conventional sensors do not ensure an exact retrieval of the seam features.

First of all, the authors analyze the two available sensing techniques. On one hand, active sensors based on structured light and the triangulation principle are a good choice for detecting butt joints with V-shaped or T-shaped grooves, because the projected laser line gets bent in the weld joint and it can be easily detected; on the other hand,

passive sensors have better performances in measuring of narrow butt joints, but they are very sensitive to variations in the environmental light.

Therefore, Shao et al. propose “a novel seam measurement system, which effectively combines the superiority of passive light sensor and active light sensor”, that “can detect narrow butt joint with seam gap less than 0.1 mm” and can measure weld seam width, center, and normal vector.

The vision sensor proposed by the authors consists of a CCD camera and four laser stripe projectors, two red and two green. The red stripes are used to determine the region of interest (ROI) in which the analysis will be performed, then the green stripes, overlapped, are used to extract the features of the seam. Figure 35 shows an image of

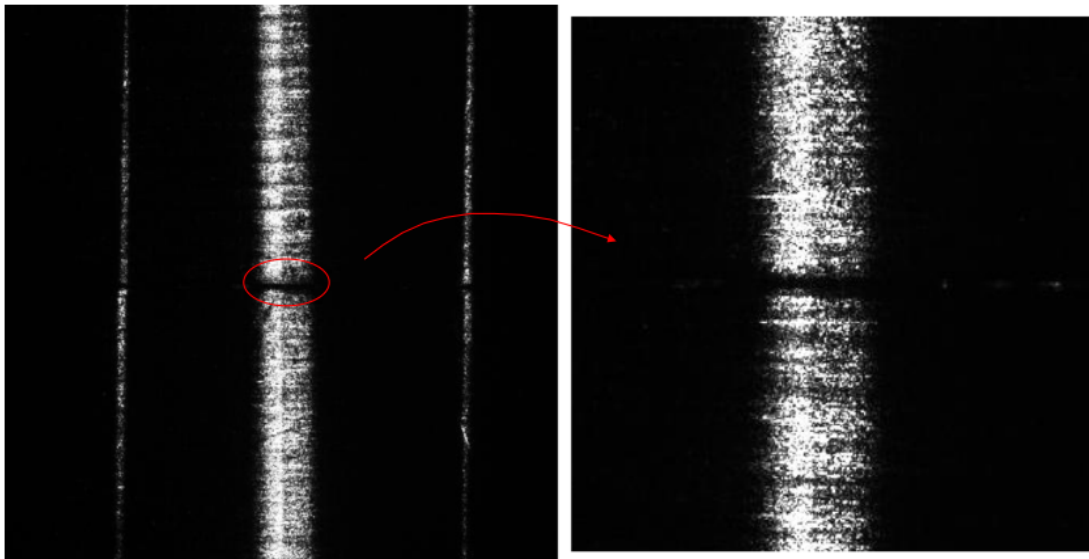


Figure 35 – *Image of the seam as detected by the algorithm proposed by Shao et al. Picture from [39]*

the weld seam taken by said vision sensor. The lateral bands are given by the red lasers and they identify the ROI; the bold central stripe, where the seam is visible, is given by the green lasers. The image is then processed by a specific algorithm and “the three dimensional coordinates of the points in seam edge and seam center can be obtained”, with an average deviation of about 0.005 mm. Unfortunately, the authors do not show results of this kind of vision sensor applied to a real seam-tracking welding system.

More recently, in 2019, Fan et al. publish an article [40], where they propose a similar but simpler method for addressing the problem of detecting narrow butt joints. Once again, the system relies both on an active and on a passive vision sensor; the

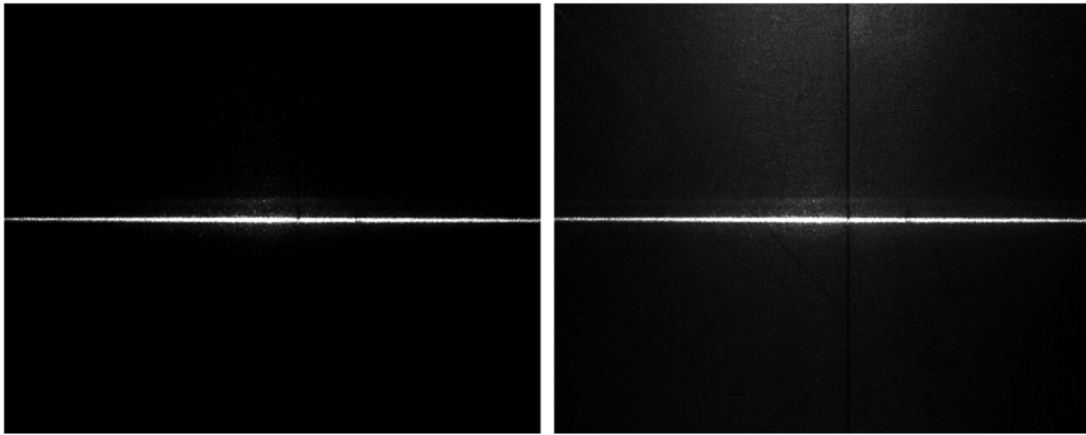


Figure 36 – *Images of the seam under different illumination conditions, as analyzed by Fan et al. Picture from [40]*

former is composed of the combination of a CCD camera and a laser stripe, the latter by the same camera and an additional LED light source. Figure 36 shows on the left the image of a seam captured by the camera when only the laser diode is active, while on the right the image of the seam when both the laser stripe and the LED are active. In this way, when both light sources are on, a proper algorithm is able to detect as feature point of the weld joint the intersection of the laser line and the seam itself. The details of the procedure are discussed more in depth in the paper by Fan et al. The results of the proposed seam tracking algorithm show an accuracy of about  $\pm 0.3$  mm.

### 3.3 Industrial Applications

In the previous Section, the main papers and documents on seam teaching and seam tracking for automatic welding were analyzed. Most of the presented welding cells, however, are merely prototypes, with little practical use.

When moving from the academic research field to the industrial field, even if the technology is available, the main actors in the scene of automatic laser welding still prefer to

stick to the traditional two-step welding. The industrial reality, in fact, presents more challenges with respect to the controlled situations tested in the research laboratories: the environment is largely unstructured, the weld joints may assume very diverse configurations, the seams usually follow complex, non-coplanar, 3D paths and so on.

Therefore, in most of the cases, especially when dealing with small to medium production quantities of highly customizable products, fully automated welding is rarely performed. The human operator still has a crucial importance during the process: he loads the workpiece, he locks and checks it, then he manually program or at least controls the welding trajectory, and eventually he oversees the robot operations. The fully automated system would provide more flexibility, but today it does not provide enough robustness, yet: for safety reasons, the human operator is still in the loop.

Moving to the specific kind of laser welding cell developed during the work of this thesis, it is possible to identify three main companies that put on the market similar products: Amada, Trumpf, and IPG Photonics. The following is a brief analysis of their proposals, in the limits of what it is available online:

- Amada FLW Welder Series [41]. The Japanese company Amada proposes a 3000 W fiber laser welding cell, offering automated robotic welding. It is based on a FANUC 6-axis robot, mounted on a linear 3 m tracking axis, coupled with a 2-axis positioning table. The robot accuracy is  $\pm 0.07$  mm, the tracking axis accuracy  $\pm 0.1$  mm. The seam trajectory is taught by a CAD-CAM program. No details on automatic seam teaching or seam tracking are provided.
- Trumpf TruLaser Weld 5000 [42]. Trumpf, the German leading company in hi-tech manufacturing, sells “a turn-key system for automatic laser welding”. Once again based on a 6-axis anthropomorphic robot, it achieves a repeatability of  $\pm 0.05$  mm. It also presents two additional positioning table: a rotate-and-tilt positioner and a rotary table. Several different laser configurations can be adopted; the FusionLine technology allows to close gaps up to 1 mm wide, while the TeachLine technology is able to perform automatic seam teaching and seam tracking; the initial trajectory of the robot is programmed using the TruTops Weld offline programming system.

- IPG Photonics Laser Welding Cells [43]. The American leader of fiber laser production, IPG Photonics, besides actual laser equipment, proposes also several laser welding cells, all based on 6-axis robots. Lasers of different power can be selected, from 1 kW to 6 kW; the typical repeatability is  $\pm 0.06$  mm; the workpiece is moved by means of an actuated table base. As regards seam teaching and seam tracking, a weld joint guidance system is mentioned, but no further details are provided.

The laser welding cells produced by the competitors, in combination with a good understanding of visual servoing and seam teaching and seam tracking concepts, is the starting point for designing and developing the SM System robotic cell. This topic will be covered in the next Chapter.

## 4 SM System S.r.l. Robotic Cell

This Chapter presents the details about the laser welding robotic cell developed at SM System S.r.l., from its initial conceiving to the final implementation. After a general introduction, the different subsystems of the cell are individually analyzed, providing also some modeling and simulation.

### 4.1 General Description

In November 2018, SM System S.r.l. received a job order for a laser welding robotic cell, intended for joining thin carbon steel components.

The development of the machine was carried out starting from the requirements defined by the client, that will be discussed in Section 4.2, from the study of the literature on automatic laser welding, previously analyzed in Section 3.2, and from the comparison with the cells proposed by the competitors, described in Section 3.3.

The following figures show the early concepts of the cell, which were initially proposed to the client. The cell is mainly composed of a 6-axis anthropomorphic robot, coupled with a frontal lathe and a rotating table. The robotic arm holds as end effector the laser welding head. The workpieces to be welded are mounted onto the lathe or are fixed to the rotating table, then the robot is in charge of welding. As shown in Figure 37 and Figure 38, the proposed cell is a box 4,30 m long, 2,90 m wide, and 2,80 m high.

The access to the cell is possible through manually operated doors, as shown in Figure 39. Two sliding panels open on the lathe side, and one in front of the rotating table. Moreover, if necessary, workpieces can be loaded on the lathe from above, using external lifting equipment.

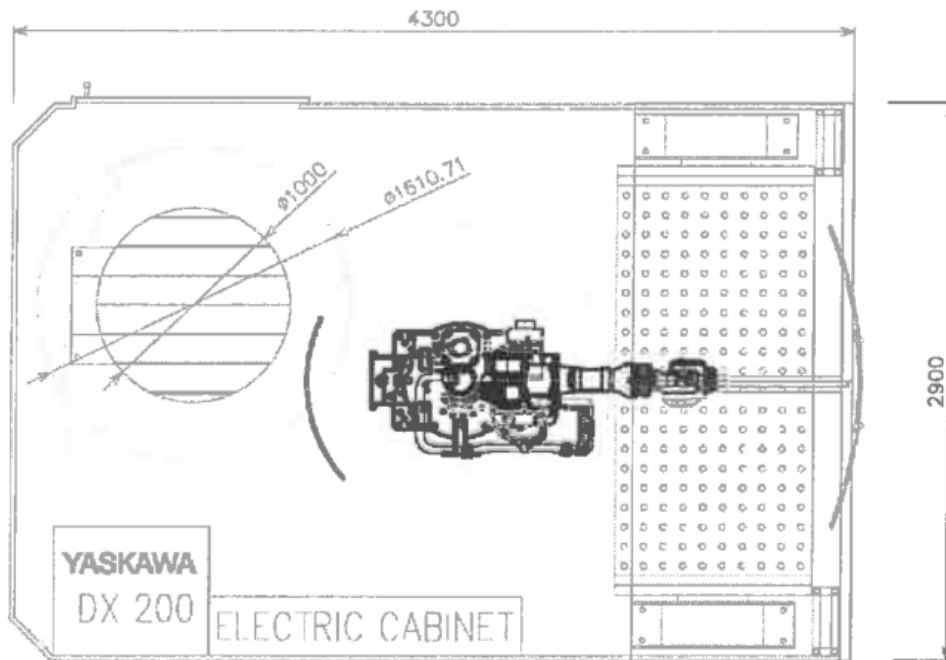


Figure 37 – Top view of the SM System robotic cell.

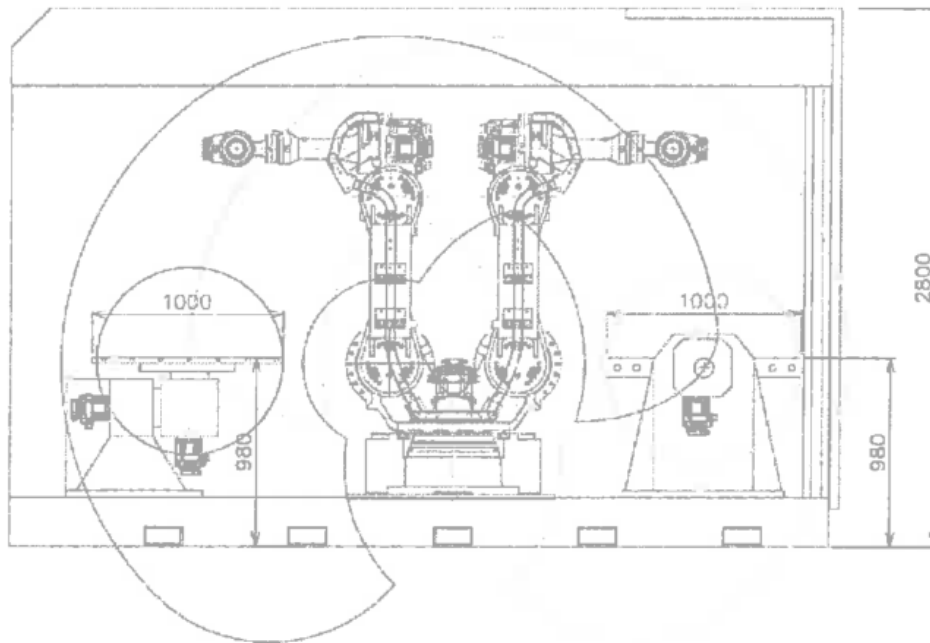


Figure 38 – Front view of the SM System S.r.l. robotic cell.

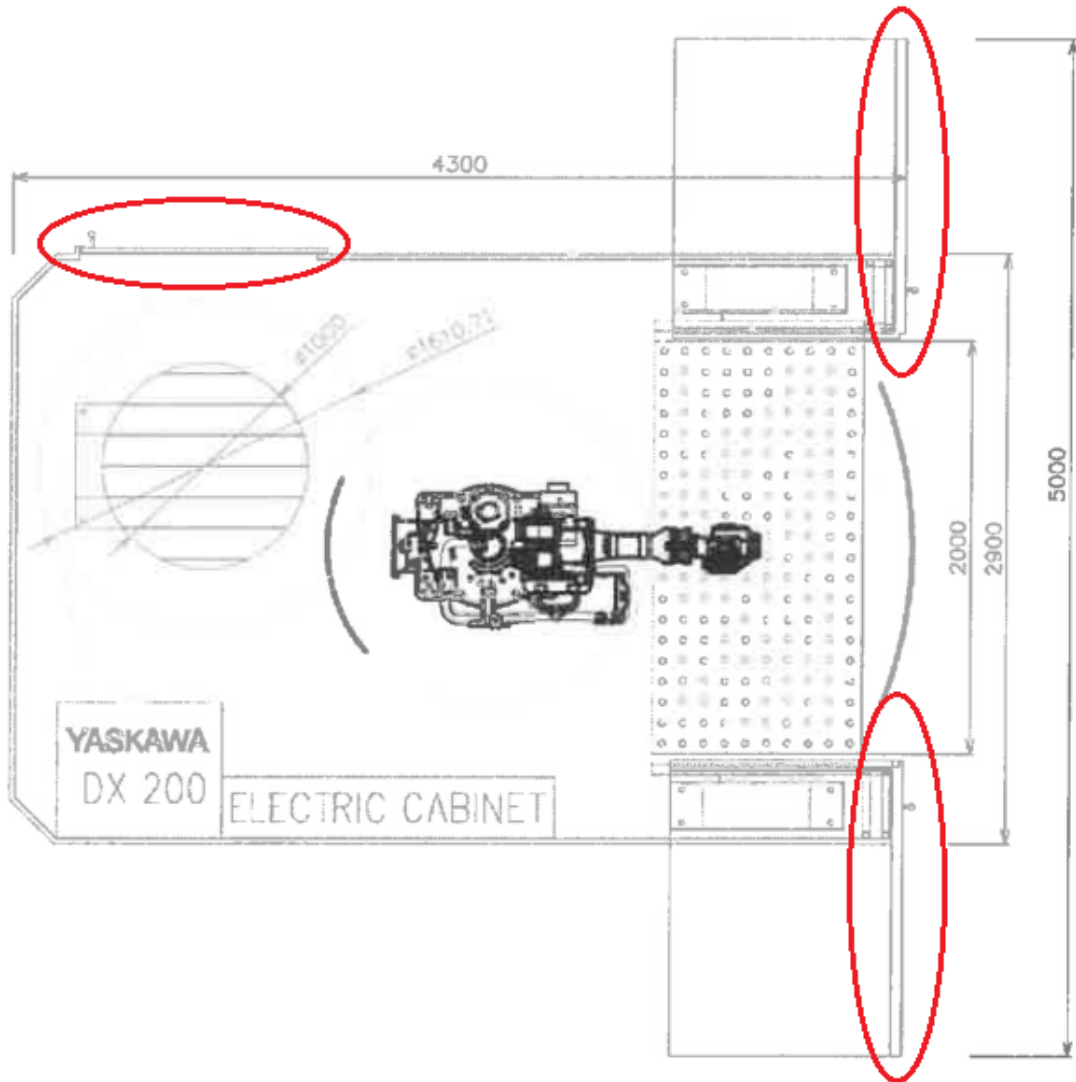


Figure 39 – Top view of the SM System S.r.l robotic cell, with highlighted doors.

In the following, the main parts of the cell are individually described:

- Basement and shell. The structural part of the cell is made of electrowelded carbon steel, while the shell and the doors are made of aluminum. The structure of the cell is conceived to damp and reduce the vibrations generated by the moving parts. In this way, it is possible to achieve high precision and accuracy during the laser welding operations.
- Robot. The core of the cell is the 6-axis anthropomorphic robot, in particular a

Yaskawa Motoman MC2000 II. It will be modeled and analyzed more in depth in Section 4.3.

- **Frontal lathe.** A rectangular table of size approximately  $2\text{ m} \times 1\text{ m}$  can be rotated about its longitudinal central axis by means of a Yaskawa SGMRV 20ANA-YR11 servomotor. The workpiece can be fixed to the table by means of a modular welding bed. The frontal lathe is well suited for welding large and bulky components. It will be analyzed more in depth in Section 4.4.
- **Rotating table.** A circular table of diameter  $1\text{ m}$  can be used in place of the frontal lathe for welding smaller and lighter components. The table has two degrees of freedom: it can rotate and it can tilt. The movements are obtained by means of two motors, both Yaskawa SGMRV 20ANA-YR11. The rotating table configuration will be described in Section 4.4.
- **Laser.** The welding laser is provided by IPG Photonics. The equipment consists of a laser cabinet, where the laser itself is generated, an optical fiber cable, through which the laser is transmitted into the cell, and a welding head, with specific functionalities. A more accurate description of the welding equipment is presented in the next Section.

## 4.2 Welding Requirements and Equipment

The client required a laser welding machine, capable of performing automatic welding in a small-to-medium production quantity context. The workpieces to be welded are small carbon steel components or bent metal sheets. The main requirement for the cell is flexibility: the machine has to be able to efficiently perform welding in different conditions, with very dissimilar components and with minimum human intervention. Flexibility is achieved, in first place, by providing the system with two different workstations: the frontal lathe and the rotating table; then, the anthropomorphic robot itself is a good choice for implementing complex welding trajectories; eventually, the vision system and the specifically designed control architecture further enhance the performances of the cell in every possible working scenario.

As regards more specifically the joints that the cell has to be able to recognize and to weld, they are the following:

- butt joint
- corner joint
- internal weld (tee joint)

and they are shown in the axonometric drawings in Figure 40, 41, and 42.

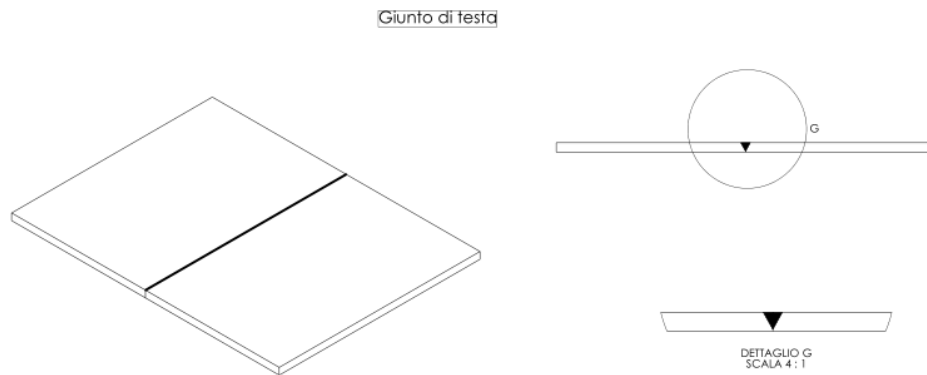


Figure 40 – *Butt joint model.*

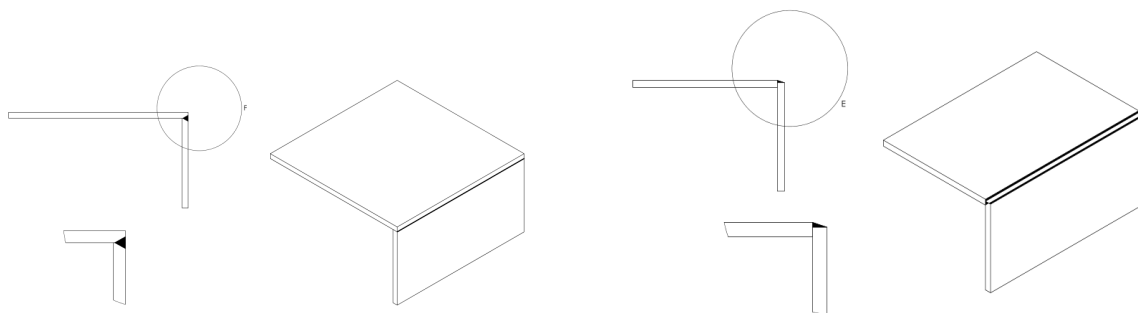


Figure 41 – *Corner joint model.*

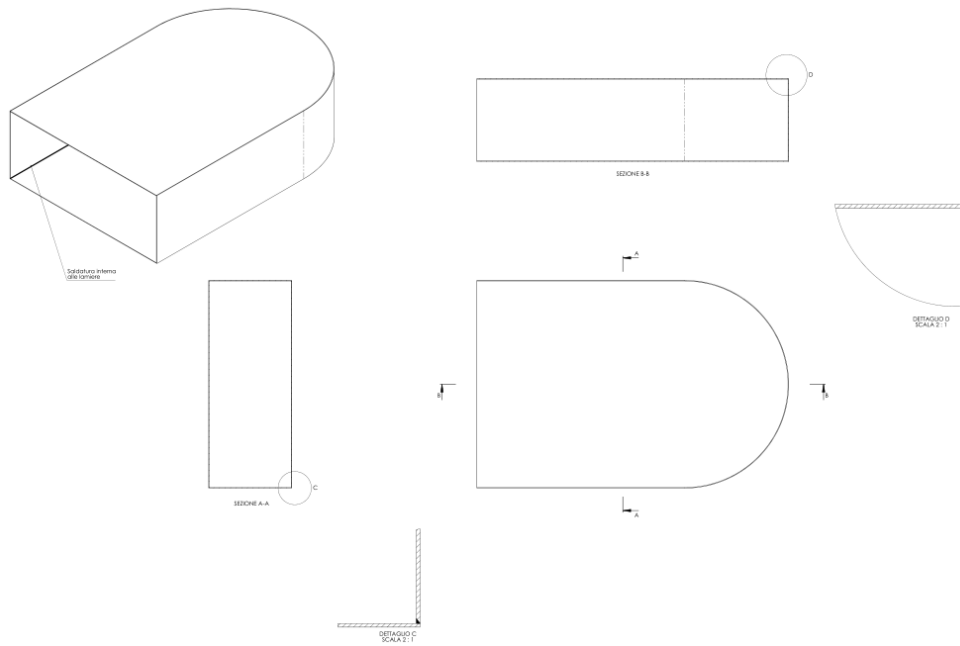


Figure 42 – *Internal joint model.*

For what concerns the laser equipment, on the basis of the discussion presented in Chapter 1, the following components were chosen:

- IPG Photonics YLS-3000-U industrial fiber laser [44], shown in Figure 43. According to its datasheet, it is a compact and reliable 3 kW fiber laser, suited for metal cutting and welding.
- Laser head: IPG Photonics FLW-D50-W laser welding head [45], shown in Figure 43 as well. It is an advanced module, specifically designed for high quality laser welding. The peculiarity of this welding head is the possibility of activating the wobbling mode.

Beam wobbling is the product of recent developments in the laser welding industry. It is realized by means of fast oscillations of the laser beam, superimposed to the linear motion of the welding head across the workpiece. The wobble effect is produced by high frequency rotations of the laser lens, moved by specific motors. Wetzig [46] describes the recent developments in beam scanning and shaping, including the wobbling strategy. As shown in Figure 44, the wobbling principle is very simple: a movable lens is able to



Figure 43 – SM System S.r.l. cell industrial laser (left) and welding head (right).

distract the beam during its feed motion; thanks to the dual oscillating mirror, several patterns can be adopted: circular, linear, ellipsoidal, eight shaped, infinity shaped, etc. Several other papers analyze this novel technique in all its aspects:

- Kuryntsev and Gilmutdinov [47] discuss the effects of a second welding pass, with wobbling enabled, for joining structural steels. They discover that wobbling produces lower cooling rates in the base metals and improves the ductility of the weld material.
- Vakili-Farahani et al. [48] investigate the influence of process parameters in wobbling laser welding of a  $Ti_6Al_4V$  alloy. They considered laser power, wobbling frequency, number of rotations and focus positions, developing several semi-empirical mathematical models based on their experimental results.
- Mrňa et al. [49] study the performance of the laser wobbling welding process through the radiation of plasma plume, pointing out that during the experiment there is a periodic change of depth and keyhole geometry, fluctuation that increases when increasing the wobbling frequency.
- Castellini and D'Andrea [50] propose the design of a brushless synchronous motor for moving the lens that provides the oscillations allowing the wobbling phe-

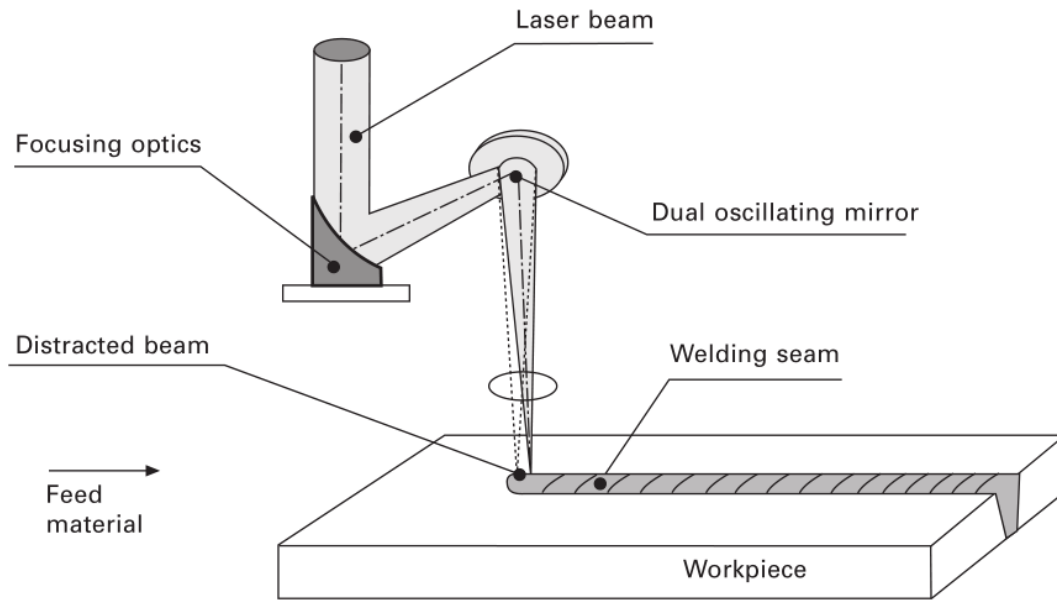


Figure 44 – *The wobbling principle. Picture from [46].*

nomenon.

- Kraetzsh et al. [51] develop a laser wobbling welding for joining different metallic materials. The high frequency beam oscillations produced crack-free welds.
- Shah et al. [52] provide a thorough analysis of beam wobbling and its effects. Their results are summarized in the following.

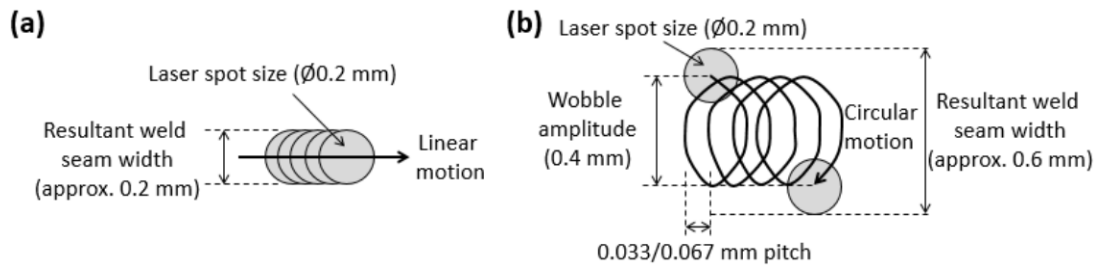


Figure 45 – *Typical wobbling path. Picture from [52].*

The laser wobbling technique has shown to be an effective means to improve joint strength by inhibiting fracture at the joints. Moreover, with respect to a traditional linear welding performed with the same setup and parameters, wobbling results in an increase in weld width but a decrease in weld penetration depth. This is logical, since the laser beam dissipates heat to a larger area per beam translational advancement. As shown in Figure 45, the wobbling technique covers a larger area compared to common linear welds, but shallower weld penetration has to be expected.

On the basis of the previous considerations, with regards to the SM System cell design, wobbling can provide the following three main advantages:

- it allows to weld components with larger gaps with small optical focus size and without the need of filler material;
- it enhances joint quality by mitigating brittle lower fusion zone formation in the weld region;
- it decreases required tracking accuracy by widening the bond area.

The IPG Photonics FLW-D50-W laser welding head, selected for the SM System cell, is able to perform beam wobbling at frequencies up to 700 Hz with different shapes, allowing to correctly weld gaps up to 450  $\mu\text{m}$ , with offsets up to 900  $\mu\text{m}$ , instead of 150  $\mu\text{m}$  and 300  $\mu\text{m}$ , respectively, without wobbling [53]. Table 2 shows the different wobbling modes that may be activated on the FLW-D50-W laser welding head.

### 4.3 Robot

In order to achieve the precision and accuracy required for laser welding, a Yaskawa Motoman MC2000 II [54] was chosen for carrying the laser head and for performing welding.

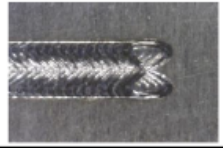
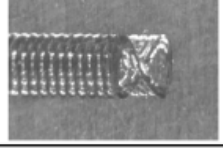
Wobble Mode	Schematic	Sample Weld
Circle (CW & CCW)		
Linear		
Eight		
Infinity		

Table 2 – *Wobbling modes provided by IPG Photonics FLW-D50-W laser welding head.*



Figure 46 – *The Yaskawa Motoman MC2000 II robot.*

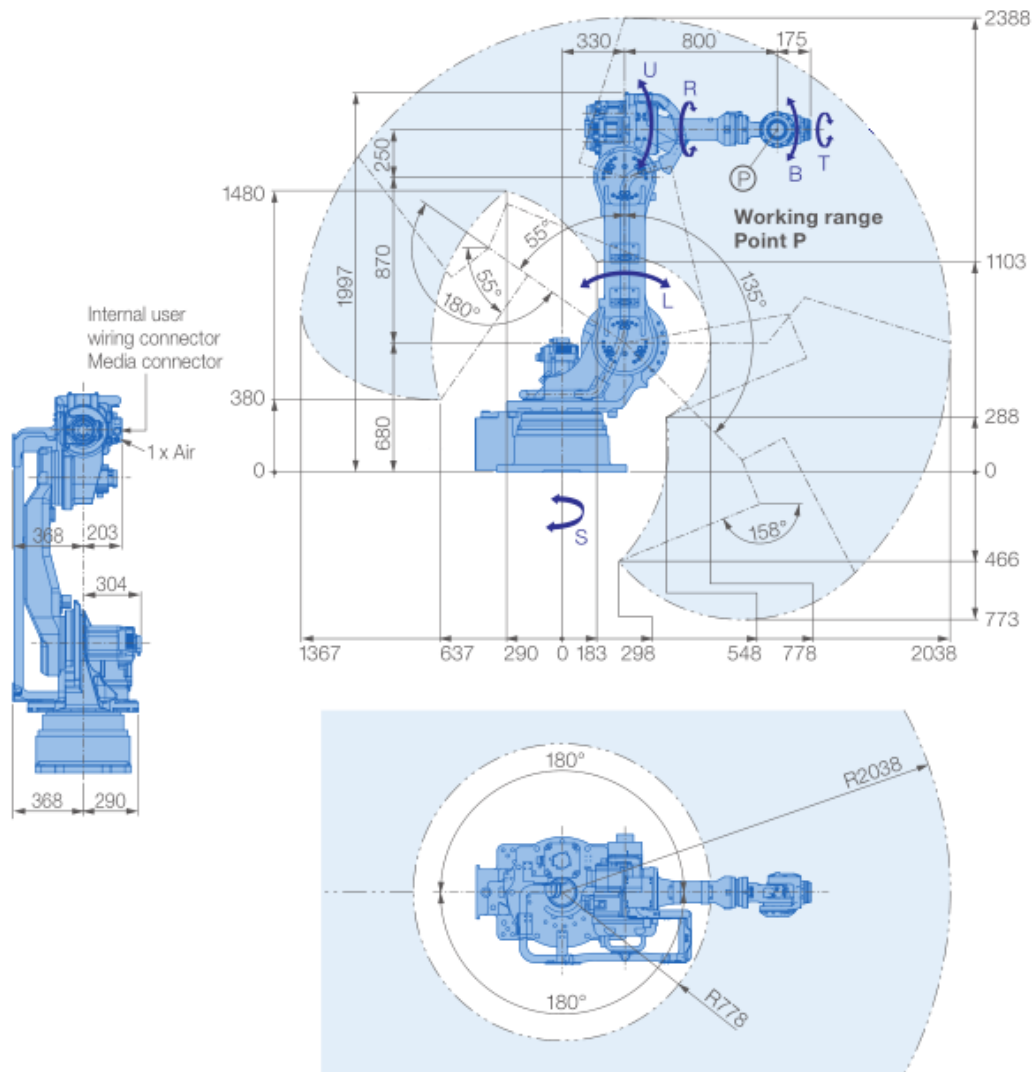


Figure 47 – Dimensions of the Yaskawa Motoman MC2000 II robot.

As it is possible to see in Figure 46, the Motoman MC2000 II is a compact 6-axis anthropomorphic robot, with a slim base waist and arm. The dimensions and the working range of the machine are shown in Figure 47. As the datasheet [55] points out, the robot is specifically designed for laser cutting and laser welding. Its versatility, precision and high rigidity are fundamental in achieving the performances required by the application.

The main benefits of using a Motoman MC2000 II are:

- compactness and versatility, with a maximum reach of 2038 mm
- high speed, up to 150 °/s for the shoulder and elbow joints, up to 250 °/s for the wrist joints
- path accuracy within 0.1 mm
- payload capacity of 50 kg, more than enough for carrying the welding head, that weights 2.5 kg

More detailed specifications of the robot can be found in Table 3. By convention, the six axes are sequentially named using the letters S, L, U, R, B, T, with S and L indicating the shoulder joint, U the elbow joint, and R, B and T the wrist joint.

Specifications MC2000 II						
Axes	Maximum motion range [°]	Maximum speed [°/sec.]	Allowable moment [Nm]	Allowable moment of inertia [kg · m <sup>2</sup> ]	Controlled axes	6
					Max. payload [kg]	50
S	±180	150	–	–	Repeatability [mm]	±0.07
L	+135/-90	150	–	–	Max. working range R [mm]	2038
U	+235/-158	150	–	–	Temperature [°C]	0 to +40
R	±360	250	110	7	Humidity [%]	20 – 80
B	±125	250	110	7	Weight [kg]	845
T	±360	250	55	1	Power supply, average [KVA]	3.5

Table 3 – *Main specifications of the Yaskawa Motoman MC2000 II 6-axis anthropomorphic robot.*

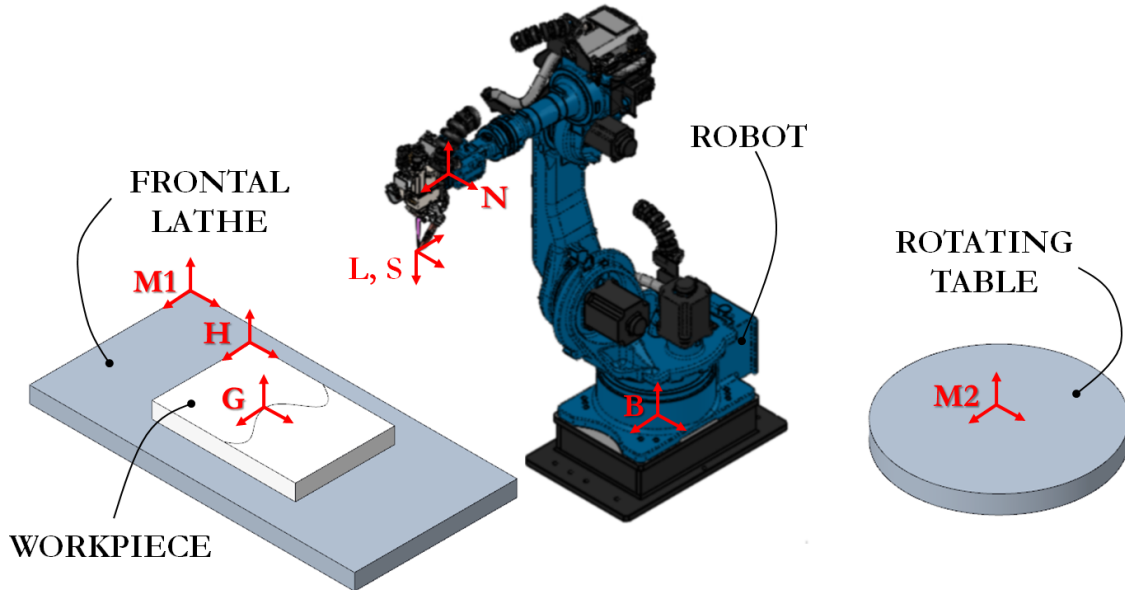


Figure 48 – *Detail of the robot reference frames.*

In order to characterize the motion of the robot within the cell, several different coordinate frames and transformations are defined. The frames are attached to specific points of the cell, of the robot, and of an hypothetical workpiece. The coordinate transformations allow to describe one reference frame with respect to another.

The following frames, suggested by De Graaf in [17] and reported in Figure 48, are defined:

- **B**: Base frame, World frame. It is attached to the robot base, it is an inertial reference frame, and it does not move with respect to the environment.
- **N**: Null frame. It is located at the robot end-effector, that is the end of the flange, at its center. It is possible to describe the Null frame with respect to the Base frame by means of transformation  $\mathbf{T}_N^B$ , that is a function of the present configuration of the robot  $\mathbf{q}(t)$ .
- **L**: Laser tool frame. It is located at the focal point of the laser beam. It is possible to describe the Laser frame with respect to the Null frame by means of transformation  $\mathbf{T}_L^N$ .

- **S**: Sensor tool frame. It is the frame with respect to which the vision sensor computes its measurements. It is possible to describe the Sensor frame with respect to the Null frame and to the Laser frame by means of the transformations  $\mathbf{T}_S^N$  and  $\mathbf{T}_S^L$ , respectively.
- **Mi**: Station frame. It is attached to the cell equipment that supports the workpiece. In this work, **Mi** can be **M1**, attached to the frontal lathe, or **M2**, attached to the rotating table. The transformations  $\mathbf{T}_{M1}^B$  and  $\mathbf{T}_{M2}^B$  describe the Station frames with respect to the Base frame and are function of the present configuration of the external axes. Please refer to section 4.4 for further details.
- **H**: Product frame. It is attached to the current workpiece. It can be described with respect to the relative Station frame by means of transformation  $\mathbf{T}_H^{M_i}$ . Usually this transformation is constant in time, since the workpiece is clamped to the worktable.
- **G**: Seam frame. Every discrete point on a seam can be characterized by means of a Seam reference frame. It is possible to build the transformation  $\mathbf{T}_G^H$  to describe each Seam frame with respect to the Product frame.

Given the previous considerations, it is clear that the Tool Center Point for this application has to be defined coincident with the laser tool frame origin, i.e. the focal point of the laser beam. From the CAD model of the laser head, shown in Figure 49, it is possible to obtain the distance between the center of the robot flange and the laser focal point; with respect to the Null reference frame, located at the center of the flange, the measures are:

- $\Delta x = 82.50\text{mm}$
- $\Delta y = 0.00\text{mm}$
- $\Delta z = 328.76\text{mm}$

These dimensions are hard-coded into the robot's memory, so that the control algorithms can work with the desired TCP position.

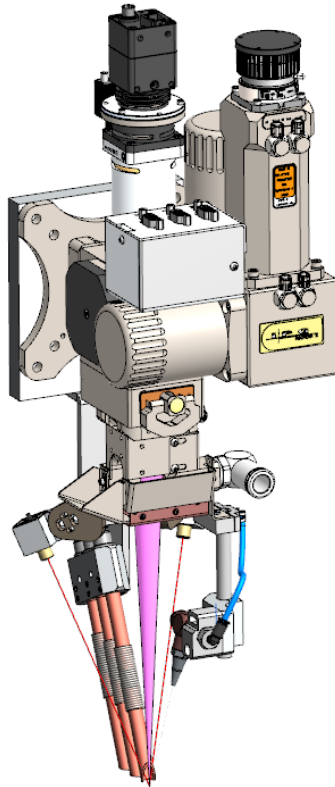


Figure 49 – CAD model of the IPG Photonics FLW-D50-W laser welding head.

The control of the robot is entrusted to the Yaskawa DX200 industrial robot controller, shown in Figure 50. The company states that it “features robust PC architecture and system-level control for robotic work cells” [56].

The DX200 is able to control the robotic arm by means of the Advanced Robot Motion (ARM) module, that provides high performance, state-of-the-art path planning, advanced collision avoidance, and teaching functionalities. To this purpose, a compact teach-pendant is also featured, providing increased flexibility and accessibility. Other specifications of the controller [57] are shown in Table 4.

As regards the fundamental algorithms and the main work patterns, the robot was programmed offline, by connecting a personal computer to the DX200 controller through the Ethernet line. At a higher level, a PLC controls the entire cell. The first step was to perform a mapping between the signals of the cell PLC and the signals of the robot.



Figure 50 – Image of the Yaskawa DX200 controller.

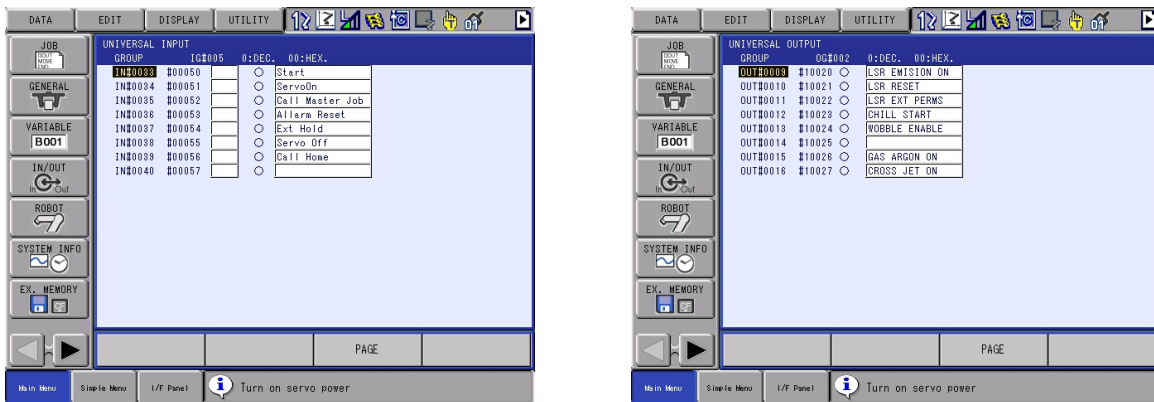


Figure 51 – Examples of signal mapping. Inputs on the left, outputs on the right.

Actually, outputs from the PLC are inputs to the robot, and outputs from the robot are inputs to the PLC. Examples of the first category are the signal to start a cycle or the signal to return home; examples of the second category are the signal to activate the laser beam or the signal to stop shield gas emission. The mapping was performed by associating the addresses of the PLC inputs/outputs to specific bytes of the robot controller memory. Examples of inputs and outputs addresses with the corresponding meaning are shown in Figure 51. Then, the robot was programmed using a language proprietary to Yaskawa. Each work program is a *job*, saved in a file with extension *.jbi* and called by a Master program, that works as a *main* function. Other files are needed

Control cabinet	
<b>Dimensions</b>	800 (W) x 1000 (H) x 650 (D)
<b>Weight</b>	Approx. 180 kg
<b>Protection class</b>	IP54
<b>Cooling system</b>	Indirect cooling
<b>Ambient temperature</b>	0° to +45°C (operation) -10° to +60°C (transport and storage)
<b>Relative humidity</b>	Max. 90 % non-condensating
<b>Power supply</b>	3-phase 400/415/440 VAC at 50/60 Hz
<b>Digital I/O</b>	40 inputs/40 outputs (standard) (expandable to 4096 inputs/4096 outputs)
<b>Analogue in/outputs</b>	40 channels (optional)
<b>Positioning system</b>	Absolute encoder / serial interface
<b>Program memory</b>	200.000 steps, 10.000 instructions and 15.000 PLC steps
<b>Interface</b>	Ethernet
<b>Color</b>	Graphit gray: RAL 7024 Light grey: RAL 7035

Table 4 – *Main specifications of the Yaskawa DX200 robot controller.*

for the definition of the tool, of the home position and of several other parameters.

The top-left picture of Figure 52 shows the beginning of the Master program: as a first step, the robot and the external axes are brought back to home position, then the individual job is called. The remaining pictures of Figure 52 show an example of welding program, where the robot is moved to a working station, the operating mode is selected and specific movements are performed.

Different types of movement can be selected, for example:

- MOVJ: movement in the joint space. It is fast, but the user has no control on the actual trajectory followed by the TCP.
- MOVL: movement in the task space with linear interpolation.
- MOVC: movement in the task space with circular interpolation.

The PL parameter, instead, characterizes the precision with which the movement is performed: with  $PL = 0$ , the robot goes to the precise given coordinate; as PL moves

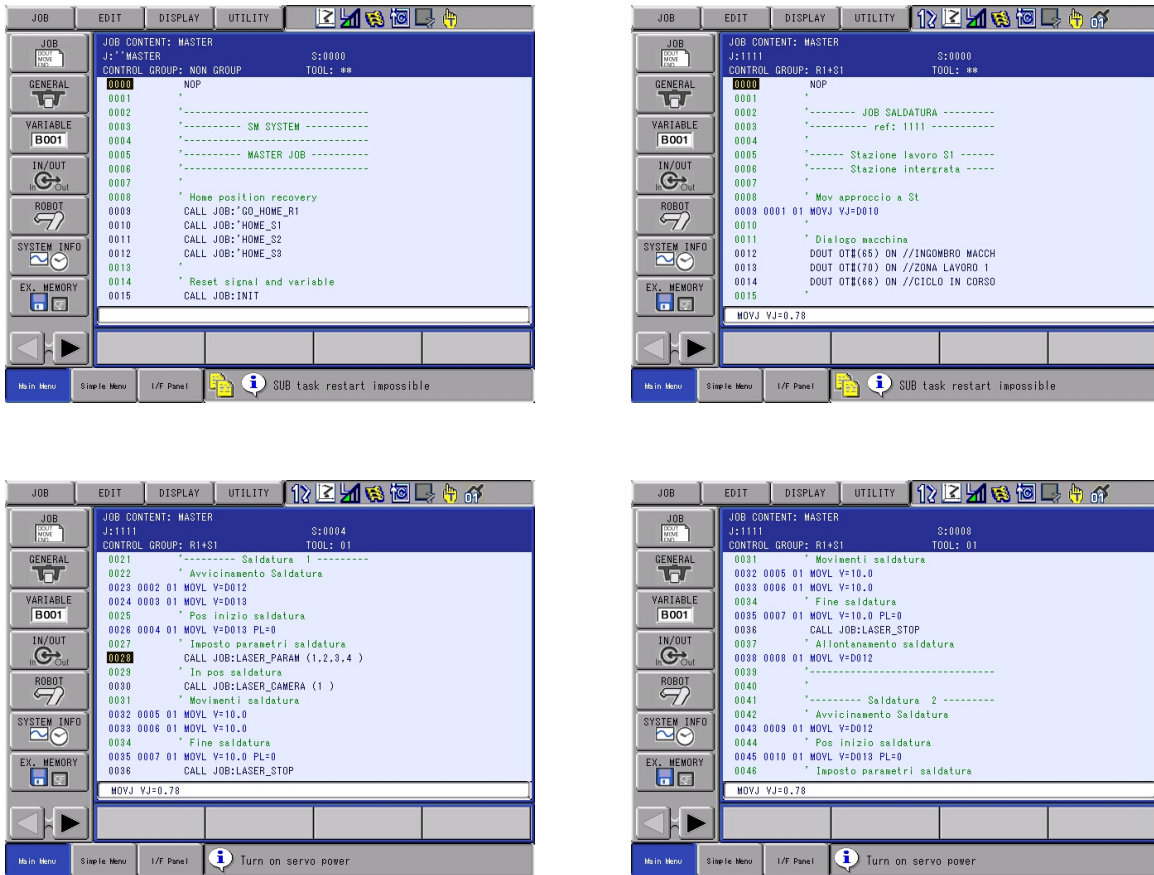


Figure 52 – Examples of the programs controlling the robot.

towards 8, the robot interpolates the points at a higher degree and trajectory becomes more rounded.

Obviously, all the movements can be manually programmed or can be derived from a CAD/CAM program.

For what concerns the various operating modes, please refer to Section 4.5, where more details will be given.

In any case, during operations, two important quantities have to be passed from the robot to the PLC for the high level control algorithms to be effective: the current TCP position and the current TCP velocity.

As regards the position, the robot controller has a built-in function to extract it in real time, as shown in Figure 53: the current x, y, z position and Rx, Ry, Rz orientation of

the TCP with respect to the Base reference frame are extracted and mapped to specific inputs of the PLC.

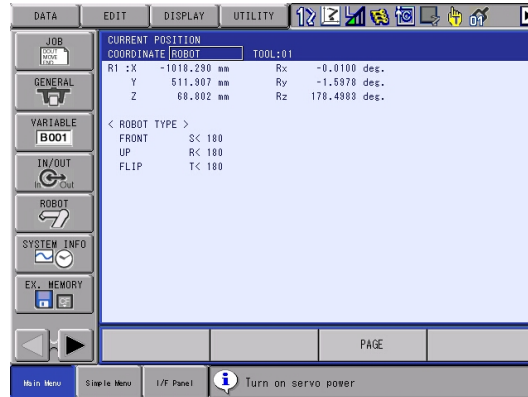


Figure 53 – Acquisition of the current position of the robot TCP.

A more challenging task was to acquire in real time the TCP current velocity. In [55] it is reported that a proportional analog system is capable of generating a control signal corresponding to the speed of the robot TCP. This signal is available as an analog voltage. The measurement is performed by the ARATI function, built-in in the Yaskawa environment. The robot returns a voltage between 0 V and 14 V on one of its analog channels. This quantity is converted into a digital number and saved into a *int16* variable  $n$  in the controller memory. *int16* is a type of variable that works on 16 bits, so it can store values between 0 and 32768.

In order to correctly acquire the velocity measure, it is possible to set the following parameters of the ARATI function:

- base speed BS: it is a reference TCP speed;
- base voltage BV: it is the voltage measured when the TCP speed is equal to the base speed;
- offset voltage OV: it is the voltage measured when the TCP speed is zero.

Then, it is required to build an equivalence between the volts and the number that appears on the teach-pendant. Under the hypothesis of perfect linearity, since  $V = 14V$

correspond to  $n = 32768$ ,  $V = 1V$  corresponds to  $n = \frac{32768}{14} = 2340,571$ . In general:

$$n = \frac{n_{max}}{V_{max}} V$$

And, given a certain number  $n$  on the teach-pendant, the corresponding voltage is:

$$V = \frac{V_{max}}{n_{max}} n \quad (13)$$

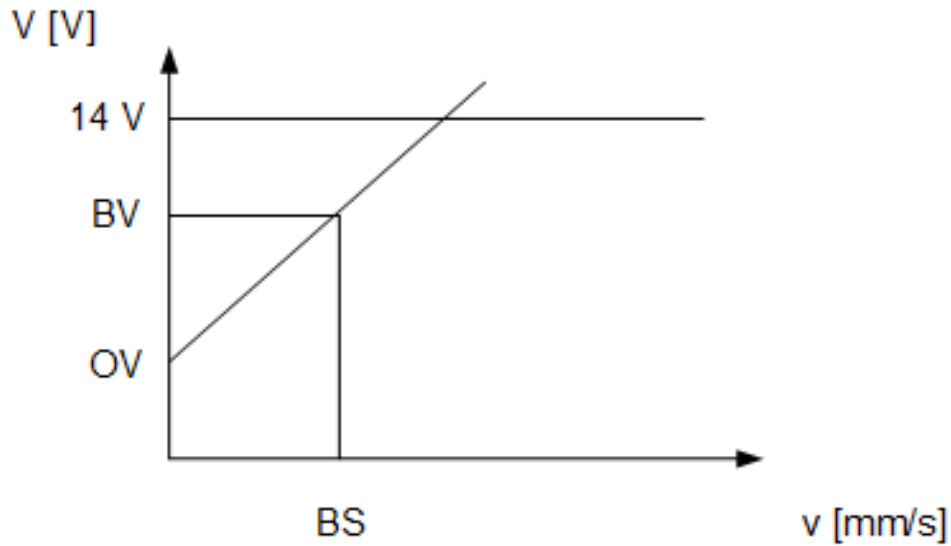


Figure 54 – Value mapping for the acquisition of the current TCP velocity.

In order to convert the voltage to the actual TCP speed, it is possible to use the line of figure 54:

$$m = \frac{BV - OV}{BS}$$

$$V = OV + m \cdot v$$

Therefore:

$$v = \frac{V - OV}{m}$$

That is:

$$v = \frac{BS}{BV - OV} (V - OV) \quad (14)$$

By combining Equation (13) and Equation (14), it is now possible to convert from the number on the teach-pendant to the actual speed of the TCP in mm/s, as shown in the following Equation (15):

$$v = \frac{BS}{BV - OV} \left( \frac{V_{max}}{n_{max}} n - OV \right) \quad [\text{mm/s}] \quad (15)$$

In the case under exam, the robot was set up with the following parameters:

- $BS = 100$  mm/s
- $BV = 10$  V
- $OV = 0$  V

Now that the robot is set up, it is required to configure the external axes. This will be the topic of the next Section.

## 4.4 External Axes

The robot can work at two different stations, that are mutually exclusive:

- Station S1: frontal lathe. It has a single motion axis, rotation.
- Station S2: rear table. It has two motion axes: rotation and tilt.

One external axis is defined for each independent movement, so we have:

- S1: frontal lathe rotation;
- S2.1: rear table rotation;
- S2.2: rear table tilt.

The movement of each axis is obtained by means of a 2 kW SGMRV 20ANA-YR11 electrical motor, whose specifications are presented in Table 5, taken from the Yaskawa datasheet [58].

Technical data	Models							
	SGMRV 05ANA-YR11	SGMRV 09ANA-YR11	SGMRV 13ANA-YR11	SGMRV 20ANA-YR11	SGMRV 30ANA-YR11	SGMRV 37ANA-YR11	SGMRV 44ANA-YR11	SGMRV 55ANA-YR11
Rated power [kW]	0.5	0.9	1.3	2.0	3.0	3.7	4.4	5.5
Nominal torque [Nm]	2.86	5.39	8.34	11.5	18.5	23.5	28.4	35
Continuous max torque [Nm]	2.94	5.68	8.83	12	19.8	27	30.1	36.1
Rated speed [min <sup>-1</sup> ]	1500	1500	1500	1500	1500	1500	1500	1500
Nominal current [A eff.]	5.2	5.7	9.5	16.7	22.7	23.6	28.7	28.3
Rated power [kW/s]	11.3	16.1	38.6	50.6	74.4	96.8	119.4	98
Nominal angle acceleration [Rad/s <sup>2</sup> ]	3950	2994	4633	4423	4022	4123	4207	2800
Peak torque [Nm]	8	13.5	18	32	48	67	71	96
Peak current [A eff.]	14	14	21	47	62.3	71	71	71
Max. speed [min <sup>-1</sup> ]	5000	3900	4500	4600	4600	4200	4000	3000
Moment of inertia [kg x m <sup>2</sup> x 10 <sup>-4</sup> ]	7.24	18	18	26	46	57	67.5	120
Torque constant [Nm/A eff.]	0.621	1.05	0.951	0.75	0.85	1.05	1.05	1.39
Temperature class	F	F	F	F	F	F	F	F
Input voltage [V]	200	200	200	200	200	200	200	200

Table 5 – Specifications of the SGMRV motor series. Picture from [58].

The stations are connected to the robot controller, Yaskawa DX200. In this way, the robot and each one of the stations can be operated in synchronous. The external axes, indeed, are comprised in the cell program for the different welding operations, allowing maximum flexibility. Each of them is equipped with an absolute encoder to provide feedback to the controller.

Some parameters are needed to setup for each axis:

- Zero position.

For the frontal lathe, a cylindrical plug with H7 tolerance was used to be certain that the table was in the mechanical-zero position, i.e. parallel to the floor; then, the software-zero position was registered using the teach-pendant. In this way, the mechanical-zero and the software-zero coincide and can be recovered even in the case of a failure of the motor, of the encoder, or of the controller.

A similar reasoning applies to the rear table axes. However, here there is not a mechanical plug that defines the mechanical-zero position. An external inductive sensor is used: it detects the passage of a metal nut, screwed onto the table.

- Motion range.

In order to obtain a high degree of flexibility, the motion range of the axes was set to values higher than the ones actually needed for general operation. In particular, the frontal lathe motion range was set to  $\pm 180^\circ$ , so that a full rotation is available. As regards the rear table, the tilt was limited to  $\pm 90^\circ$ , as defined by the mechanical constraints, while the rotation motion range was set to  $\pm 720^\circ$ , in order to have two full rotations from each side for potential particular welding trajectories.

- Reduction ratio

The robot controller needs to know the reduction ratio between the load speed and the motor speed. It is defined as:

$$r = \frac{\omega_M}{\omega_L} \tag{16}$$

- $r$  = reduction ratio, [–]
- $\omega_M$  = angular velocity of the motor, [rad/s]
- $\omega_L$  = angular velocity of the load, [rad/s]

For the frontal lathe, it comprises the reduction gears, directly mounted on the rotor shaft of the motor, and the cascaded belt-and-pulley transmission, as shown in Figure 55. The overall value is  $r_{S1} = 238$ .

As for the rear table, instead, the two motors are arranged as shown in Figure

56 and they are only equipped with reduction gears. Both the motors have a reduction rate of  $r_{S2.1} = r_{S2.2} = 119$ .

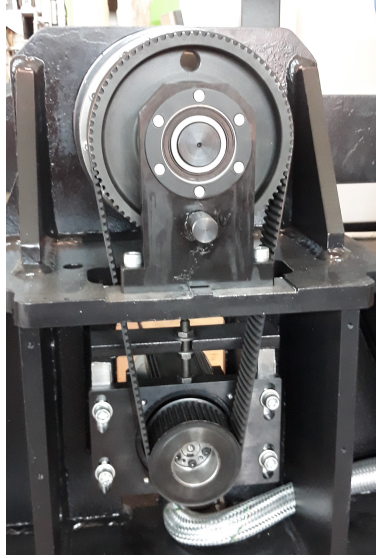


Figure 55 – *Detail of the belt transmission moving the axis of station S1.*

- Maximum angular velocity.

The maximum angular velocity of the motor that moves each axis was taken from the datasheet. Since all the motors are the same,

$$\omega_{M,max} = 1500 \text{ rpm} = 1500 \cdot \frac{2\pi}{60} \text{ rad/s} = 157.08 \text{ rad/s}$$

for all the axes.

- Acceleration time.

Since the external axes are configured and controlled by the robot controller, their motion follows the same rules that apply to the robot axes. In particular, the trajectory is generated using a trapezoidal velocity profile. Besides the maximum velocity, also the acceleration time is needed. From the requirements of the expected applications, this value was set to  $t_{acc} = 0.5 \text{ s}$  for all the axes.

It is worth making sure that, with these values of maximum angular velocity and acceleration time, the actual acceleration of the motor is less than the maximum



Figure 56 – Detail of the two motors that move the axes of station S2.

imposed by the datasheet, i.e.

$$\dot{\omega}_{M,max} = 500 \text{ rad/s}^2$$

Since the acceleration is constant and the starting velocity is null, it is possible to write:

$$\dot{\omega}_M = \frac{\omega_{M,max}}{t_{acc}} = \frac{157.08}{0.5} \text{ rad/s}^2 = 314.16 \text{ rad/s}^2 < 500 \text{ rad/s}^2$$

Therefore, the motion is compliant with the motor capabilities.

- Inertia ratio.

The inertia ratio is defined as the ratio between the moment of inertia of the load as seen by the motor and the moment of inertia of the motor itself:

$$\alpha = \frac{J_{L,m}}{J_M} \quad (17)$$

- $\alpha$  = inertia ratio, [–]
- $J_{L,m}$  = moment of inertia of the load, reported to the motor side, [kg · m<sup>2</sup>]
- $J_M$  = moment of inertia of the motor, [kg · m<sup>2</sup>]

According to the principles of transmission mechanics, in a system like the one

shown in Figure 57, the moment of inertia of the load can be reported to the motor side dividing by the square of the transmission ratio  $r$ :

$$J_{L,m} = \frac{J_L}{r^2} \tag{18}$$

The value of  $J_M$  is obtained from the datasheet of the motor; the value of  $J_L$  is calculated using the CAD software, assuming that the station is working at maximum load; the reduction ratio was analyzed above; eventually,  $J_{L,m}$  and  $\alpha$  are computed using equation 57 and 17, respectively. All the numerical values are summarized in Table 6.

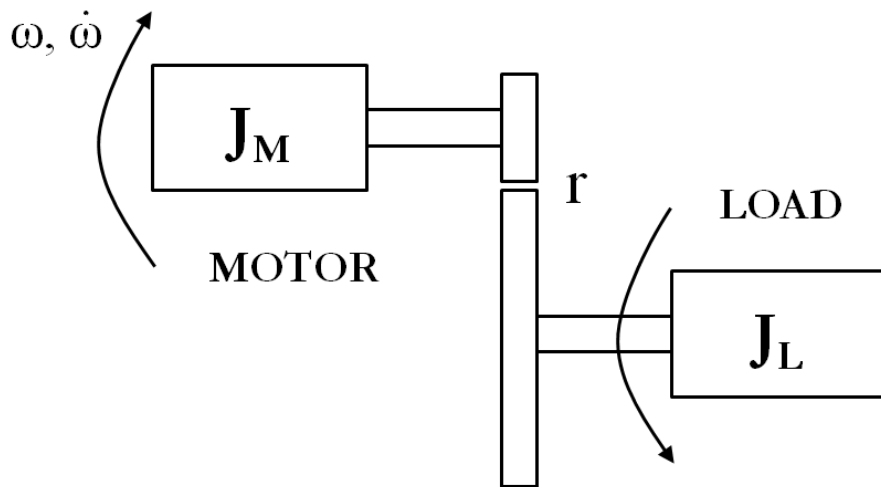


Figure 57 – Motor, transmission and load scheme.

	Frontal lathe	Rotating table
$J_M$ [kg m <sup>2</sup> ]	$26 \cdot 10^{-4}$	$26 \cdot 10^{-4}$
$J_L$ [kg m <sup>2</sup> ]	345	127
$r$ [-]	238	119
$J_{L,m}$ [kg m <sup>2</sup> ]	$6,09 \cdot 10^{-3}$	$8,97 \cdot 10^{-3}$
$\alpha$ [-]	2,34	3,45
$\alpha$ % [-]	234 %	345 %

Table 6 – Inertia ratio calculation for the external axes.

Figure 58 and 59 show the actual configuration of all the previous parameters, are shown on the teach-pendant screen.

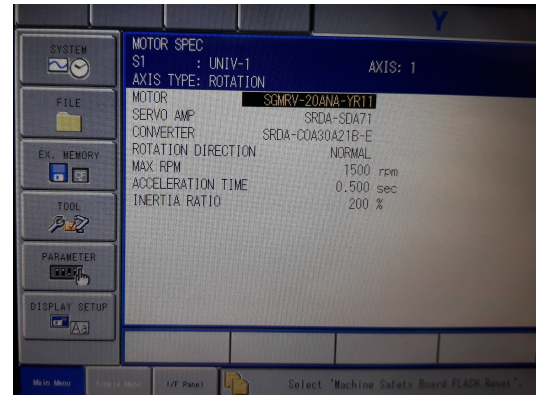
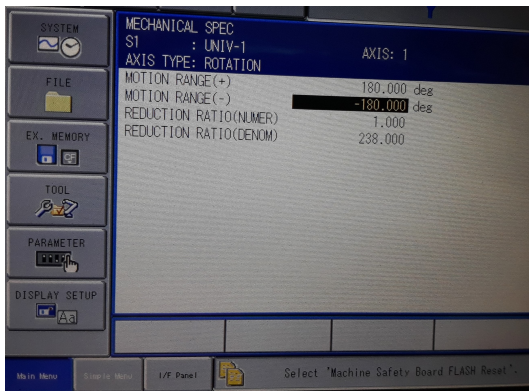


Figure 58 – Configuration parameters for the single axis of workstation S1.

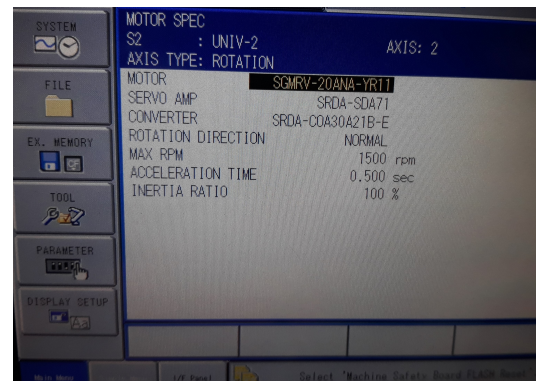
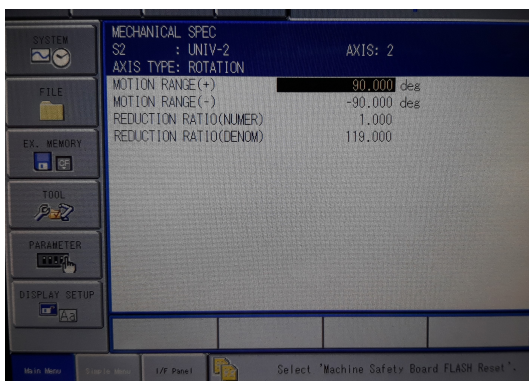
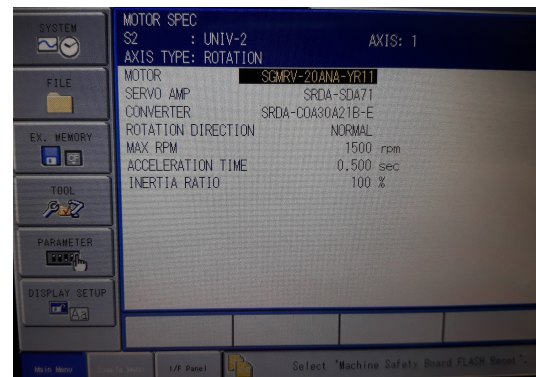
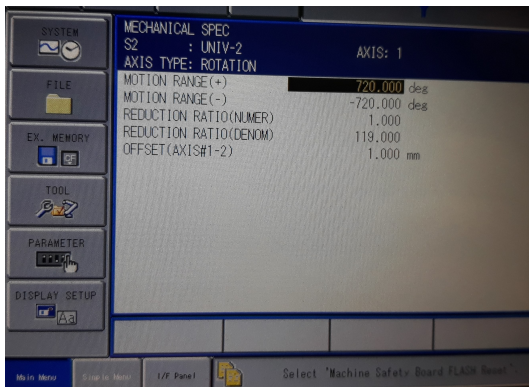


Figure 59 – Configuration parameters for the two axes of workstation S2.

## 4.5 Vision and Algorithms

The last core part of the SM System laser welding robotic cell is the vision system. Implemented in the eye-in-hand configuration, where the robot holds the camera as the end effector, the vision system is designed to be able to extract the seam position in all the different working conditions.

For this purpose, it is composed of several different components:

- Coaxial camera. The center of the image corresponds to the focus of the welding laser.
- Laser pointers.
- Led lighting source.
- Laser line.

The architecture is based on different papers analyzed in Section 3.2: the coaxial camera setup is present in the work of Regaard [31], as previously shown in Figure 30; the use of both a laser line and ambient light can be found, for example, in the article by Fan [40]; eventually, the working principles of the systems are derived from the publications of De Graaf, in particular [17].

Back to the vision system, the coaxial camera is in charge of taking pictures when requested. It can work in live mode or it can be activated by means of a trigger, sent by the external PLC.

The laser pointers are mounted on the welding head so that their low power light rays converge at the exact point where the welding laser is focused. In this way, the operator can see in advance where the welding spot is placed.

The led lighting source and the laser line are used by the seam teaching algorithm to detect the position of the seam, as suggested by several papers analyzed in Section 3.2. The main features of the vision system were studied and tested on their own in a test station, as shown in Figure 60, where it is possible to see the welding head, comprising the camera, attached to a test bench, a laser line source and a PC connected to the camera. The first experiments were performed on the test workpiece shown in Figure 61, composed of two thin metal sheets with a thin gap between them. The images from

the camera were transmitted to the PC and seam detection algorithms were run. Two different illumination methods were analyzed: in a first case, the seam was crossed by a laser line, whose deformation could be used to detect the joint; in a second case, the seam was lighted by a white led source. The test showed that each solution works with different kinds of joints to be welded: butt joints are too thin to generate a substantial deformation to the laser line, but the sharp separation between the two plates is clearly visible when illuminated by the led source. On the contrary, angular joints, like corner and tee joints, generate unwanted reflections when the led light source is present, so that the corresponding image is unusable; instead, when hit by the laser line, the joints are easily detectable.

For this reason, in order to achieve maximum flexibility, both the active and the passive illumination methods were added to the laser welding robotic cell. Unfortunately, since the camera is coaxial with the welding laser, it works with a very high level of zoom: in these conditions it is very difficult for a vision algorithm to understand whether the seam in the image plane is a butt joint or an angular joint. The information about the type of joint should be provided by the operator for each segment of the seam or, more conveniently, from the CAM software that generates the welding trajectory.

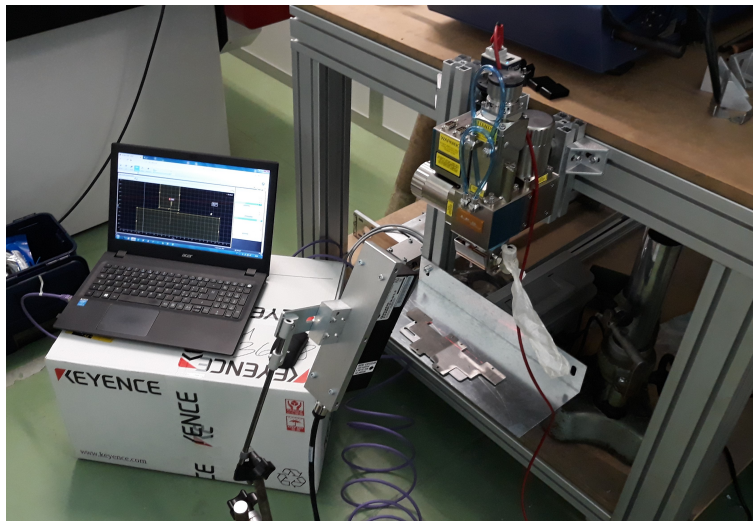


Figure 60 – *Experimental setup for the vision system tests.*

In any case, the vision equipment is switched on and off by a high-level algorithm,

---



Figure 61 – *Test workpiece for the vision system tests.*

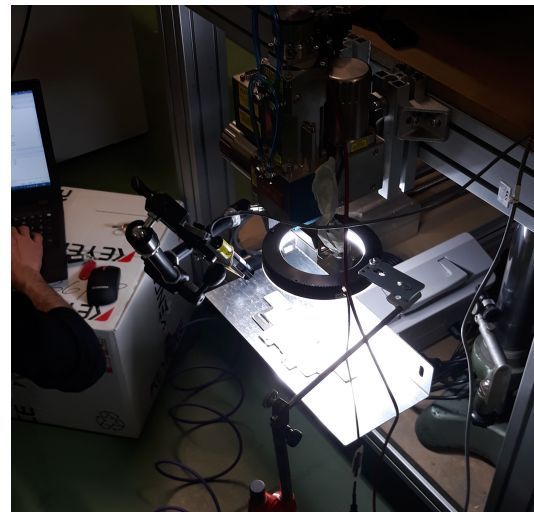
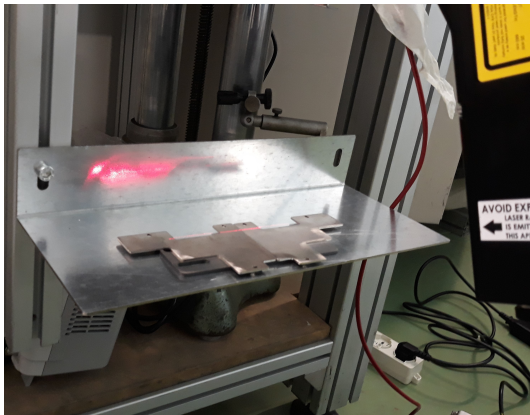


Figure 62 – *Illumination methods tests. Active on the left, passive on the right.*

that is in charge of controlling the robotic cell as a whole. Four modes of operation were implemented:

- Manual teaching. The operator takes control of the robot using the teach pendant and manually defines the points of the trajectory to be followed.
- Testing. The robot follows at low speed the trajectory defined by the operator through manual teaching or imported by the CAM software. The camera is activated in live mode, so that the operator can see where the laser will be actually focused during welding.

	Manual teaching	Testing (live)	Automatic reteaching	Automatic welding
Welding laser	off	off	off	CAM on/off
Camera	manual on/off	on	CAM on/off	off
Laser line	manual on/off	CAM on/off	CAM on/off	off
Illuminator	manual on/off	CAM on/off	CAM on/off	off
Laser pointers	manual on/off	manual on/off	off	off

Table 7 – *Activation and deactivation of the various cell equipment on the basis of the working mode.*

- Automatic reteaching. The robot automatically follows the taught trajectory, but the welding laser is not activated. The vision system captures images of the seam and an algorithm checks if the path corresponds to the seam to be welded.
- Automatic welding. The robot automatically follows the taught trajectory and performs the welding operations, according to the parameters specified in the work program.

On the basis of the current working mode, the various components of the cell are switched on or off. For example, the welding laser is activated only when the cell is performing the automatic loop, situation in which all the other equipment is turned off; in manual teaching mode the different light sources (laser line, led and laser pointers) are all manually controlled by the operator, that can also trigger the camera to have a clear indication of where the welding laser will be focused; in testing mode the most suitable light source is activated on the basis of the type of joint, while the laser pointers can still be manually turned on; in the automatic reteaching mode, eventually, the laser pointers are not needed, while the laser line and the led light source are once again managed by the software. Table 7 sums up when the different cell equipment should be switched on and off.

The most critical working mode is automatic reteaching, so a simulation of its working principle was implemented using Matlab/Simulink. The simulation employs Peter Corke's Robotics Toolbox [59] and only deals with the kinematic aspects of the problem. Despite this, it was a useful instrument to test and visualize the overall behavior

of the reteaching algorithm. The robot was modeled according to the explanation given in Section 4.3, then four different phases were implemented:

- Given a nominal trajectory, represented by the black line in the top left picture of Figure 63, the robot follows it at a given speed.
- In the meanwhile, at a constant rate, the camera is triggered. If the workpiece is exactly in the expected position, the seam is at the center of the image. In the top right picture of Figure 63 the red circles represent the points where the camera was activated.
- For each point in which the camera was triggered, a vision algorithm retrieves the actual position of the seam and calculates how much it is far from the center of the image. In the bottom left picture of Figure 63, the real positions of the seam points are represented by the blue circles. The correct seam trajectory is generated by interpolating between these points. Obviously, the trigger rate and the interpolation level have to be carefully selected for each specific application.
- The reconstructed trajectory is sent to the CAM software, where the operator can check it and decide whether to use it for actual welding, or to perform additional tests. In the bottom right picture of Figure 63 the robot has successfully followed the new trajectory, represented by the solid red line.

Figure 64 shows the Simulink scheme behind the simulation, where the tracking errors of the robot were modeled using random number sources.

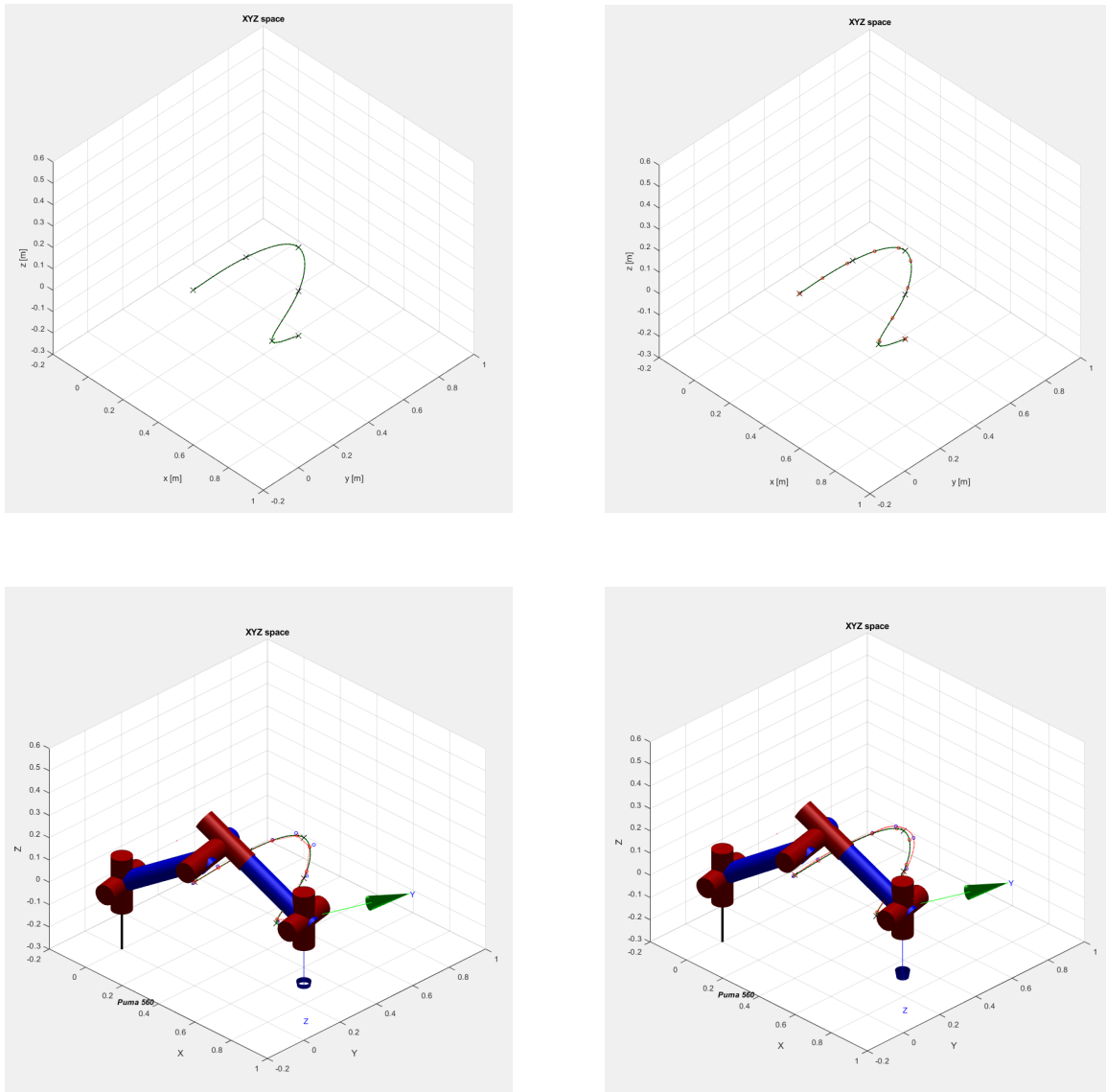


Figure 63 – Matlab simulation results of the automatic reteaching algorithm.

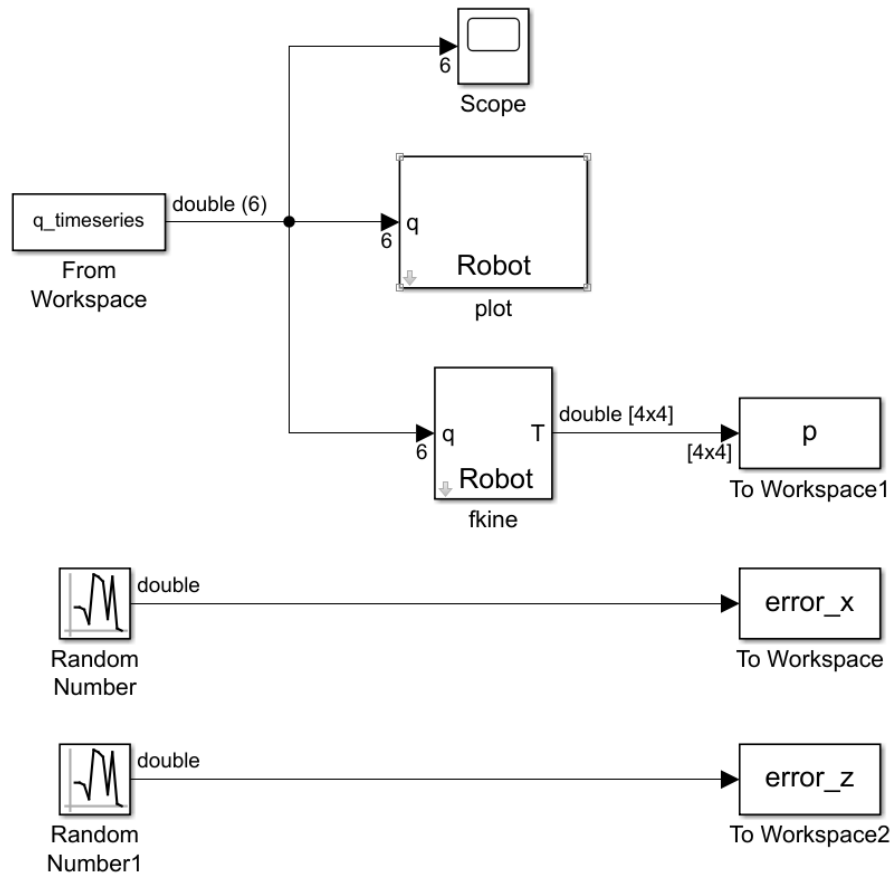


Figure 64 – *Simulink scheme employed in the automatic reteaching simulation.*

The actual reteaching algorithm was implemented in a similar way and stored in the robot controller. The operator can select the working mode from the main screen of the teach-pendant control panel, shown in the left picture of Figure 65. Then, if the manual teaching mode was selected, he has full control over the robot movements and the light sources to define the welding trajectory. An alternative is to load the CAD file of the workpiece to be welded by means of the CAM software integrated into the cell. By means of the human-machine-interface shown in the right picture of Figure 65, the operator has access to SprutCam [60], a CAM program that runs on Microsoft Windows and provides offline programming for CNC machines and articulated robots.

At this point, the operator can inspect the welding path in testing mode or he can let the system correct the trajectory through automatic reteaching. In this case, the

new corrected trajectory will be presented him in the CAM software, and he can choose whether to accept it or discard it. Eventually, when his approval is received, the cell can be set in automatic cycle mode, the laser is enabled, and the robot can start welding.

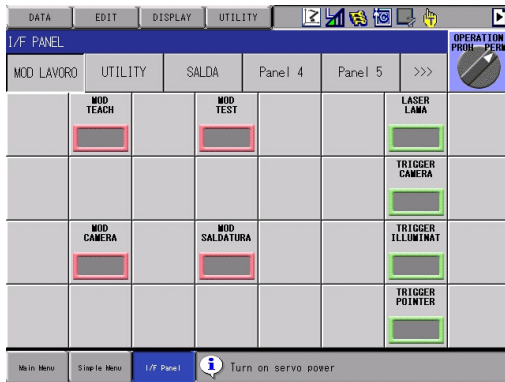


Figure 65 – Control panels of the cell. On the left, the main tab of the menu available on the teach pendant; on the right, the HMI with buttons and Windows environment.

## Conclusions

The SM System S.r.l. laser welding robotic cell was successfully completed in September 2019. It is capable of autonomously joining metal sheets with good flexibility and robustness, as required by the client. The different subsystems - the robot, the external axes, the vision equipment, and the high-level control algorithms - comply with the expected performances and are part of a unique comprehensive environment.

This Master Thesis explored all the different fields of knowledge involved in the design of the robotic cell, providing the theoretical basis on which the different design choices were made. The welding laser was selected starting from the study of the available laser welding technologies; the vision system was assembled on the basis of the visual servoing state of the art; the high-level control algorithms were developed accordingly to the thorough study conducted on the scientific literature about seam-teaching and seam-tracking; eventually, the robot was modeled and simulated using Matlab to test the applicability of the high-level control algorithms. Most importantly, all the subsystems were actually implemented on the real laser welding cell.

Despite the fact that the system is fully functional for the operations it is required to perform, it would be interesting to further investigate the feasibility issues of actual real-time seam-tracking, feature that was not implemented due to time and cost constraints. Moreover, new efforts should be put into eliminating the need of human intervention during the re-teaching phase, that was still necessary in the commercial release of the cell, mainly for safety reasons.

Working on this Thesis, I had the possibility to oversee a complex project from its conceptual design to its final implementation, dealing with the different obstacles that arose during the development. Furthermore, it was a chance to explore both the academic world and the industrial world: the research-oriented first part of the dissertation was complemented by the more practical second part, where the theoretical concepts were applied to a real-world application.

## Acknowledgments

First of all, I would like to thank my Academic Supervisor, Prof. Alessandro Rizzo of Politecnico di Torino. He consistently allowed this paper to be my own work, but gave me precious suggestions whenever I needed them. His support and feedback were fundamental for the development of this Thesis.

I would also like to thank all the people I met at SM System S.r.l., that allowed me to conduct studies on their laser welding robotic cell. In particular, I would like to acknowledge Eng. Stefano Garino, that accepted the role of Company Supervisor and actively helped me during these months.

Eventually, I would like to express my sincere gratitude to my parents, my girlfriend and my friends for providing me with precious support and continuous encouragement throughout my years of study and through the process of writing this Thesis. Thank you.

## References

- [1] “Sm System S.r.l.” [Online]. Available: <http://www.sm-system.it/>
- [2] M. P. Groover, *Fundamentals of modern manufacturing: materials processes, and systems*. John Wiley & Sons, 2007.
- [3] A. W. Society, *Welding Handbook*, 9th ed. American Welding Society, 2007, vol. 1.
- [4] H. B. Cary and S. C. Helzer, “Modern welding technology,” 1979.
- [5] T. Hong, M. Ghobakhloo, and W. Khaksar, “Robotic welding technology,” *Comprehensive Materials Processing*, vol. 6, pp. 77–99, 05 2014.
- [6] Ifr, “International federation of robotics.” [Online]. Available: <https://ifr.org/>
- [7] K. F. Renk, *Basics of laser physics*. Springer, 2012.
- [8] W. M. Steen and J. Mazumder, *Laser material processing*. springer science & business media, 2010.
- [9] C. Dawes, *Laser welding: a practical guide*. Woodhead Publishing, 1992.
- [10] B. Siciliano, L. Sciavicco, L. Villani, and G. Oriolo, *Robotics: modelling, planning and control*. Springer Science & Business Media, 2010.
- [11] A. Sanderson, “Image based visual servo control using relational graph error signal,” in *Proc. Int. Conf. Cybernetics and Society, Cambridge, 1980*, 1980.
- [12] S. Hutchinson, G. D. Hager, and P. I. Corke, “A tutorial on visual servo control,” *IEEE transactions on robotics and automation*, vol. 12, no. 5, pp. 651–670, 1996.
- [13] P. Corke, *Robotics, vision and control: fundamental algorithms in MATLAB® second, completely revised*. Springer, 2017, vol. 118.
- [14] B. Bona, *Dynamic modelling of mechatronic systems*. Celid, 2013.
- [15] S. Hans, “A brief comparative study of visual servoing system,” *International Journal for Scientific Research and Development*, vol. 6, pp. 145–155, 2018.

- [16] P. I. Corke, "High-performance visual closed-loop robot control," Ph.D. dissertation, 1994.
- [17] M. De Graaf, "Sensor-guided robotic laser welding," *University of Twente*, 2007.
- [18] Y. Xu, H. Yu, J. Zhong, T. Lin, and S. Chen, "Real-time seam tracking control technology during welding robot gta process based on passive vision sensor," *Journal of Materials Processing Technology*, vol. 212, no. 8, pp. 1654–1662, 2012.
- [19] W. Clocksin, J. Bromley, P. Davey, A. Vidler, and C. Morgan, "An implementation of model-based visual feedback for robot arc welding of thin sheet steel," *The International Journal of Robotics Research*, vol. 4, no. 1, pp. 13–26, 1985.
- [20] N. R. Nayak and A. Ray, *Intelligent seam tracking for robotic welding*. Springer Science & Business Media, 2013.
- [21] J. S. Kim, Y. T. Son, H. S. Cho, and K. I. Koh, "A robust visual seam tracking system for robotic arc welding," *Mechatronics*, vol. 6, no. 2, pp. 141–163, 1996.
- [22] P. Kim, S. Rhee, and C. H. Lee, "Automatic teaching of welding robot for free-formed seam using laser vision sensor," *Optics and Lasers in Engineering*, vol. 31, no. 3, pp. 173–182, 1999.
- [23] M. Fridenfalk and G. Bolmsjö, "Design and validation of a universal 6d seam tracking system in robotic welding based on laser scanning," *Industrial Robot: An International Journal*, vol. 30, no. 5, pp. 437–448, 2003.
- [24] D. Xu, M. Tan, X. Zhao, and Z. Tu, "Seam tracking and visual control for robotic arc welding based on structured light stereovision," *International Journal of Automation and Computing*, vol. 1, no. 1, pp. 63–75, 2004.
- [25] D. Xu, M. Tan, and Y. Li, *Visual Control System for Robotic Welding*, 12 2006.
- [26] M. De Graaf, R. Aarts, B. Jonker, and J. Meijer, "Real-time seam tracking for robotic laser welding," in *25th Benelux Meeting on Systems and Control 2006*, 2006.

- [27] M. De Graaf, R. Aarts, J. Meijer, and J. B. Jonker, "Robot-sensor synchronization for real-time seam-tracking in robotic laser welding," *Proc. 23rd Int. Cong. On Applications of Lasers and Electro-Optics*, vol. 1301, 2004.
- [28] —, "Modeling the seam teaching process for robotic laser welding," in *Proceedings of the Mechatronics & Robotics 2004 conference. APS-European Centre for Mechatronics*, 2004.
- [29] M. De Graaf, R. Aarts, B. Jonker, and J. Meijer, "Real-time seam tracking for robotic laser welding using trajectory-based control," *Control engineering practice*, vol. 18, no. 8, pp. 944–953, 2010.
- [30] M. De Graaf and R. Aarts, "Applications of robotics in laser welding," in *Handbook of laser welding technologies*. Elsevier, 2013, pp. 401–421.
- [31] B. Regaard, S. Kaielerle, and R. Poprawe, "Seam-tracking for high precision laser welding applications—methods, restrictions and enhanced concepts," *Journal of Laser Applications*, vol. 21, no. 4, p. 183, 2009.
- [32] K. Sung, H. Lee, Y. Choi, and S. Rhee, "Development of a multiline laser vision sensor for joint tracking in welding," *Weld J*, vol. 88, no. 4, pp. 79–85, 2009.
- [33] X. Shen and W. Teng, "A rapid image processing algorithm for structured light stripe welding seam tracking in laser welding," in *International Congress on Applications of Lasers & Electro-Optics*, vol. 2011, no. 1. LIA, 2011, pp. 118–124.
- [34] Y. Xu, G. Fang, N. Lv, S. Chen, and J. J. Zou, "Computer vision technology for seam tracking in robotic gtaw and gmaw," *Robotics and computer-integrated manufacturing*, vol. 32, pp. 25–36, 2015.
- [35] Y. Xu, N. Lv, G. Fang, S. Du, W. Zhao, Z. Ye, and S. Chen, "Welding seam tracking in robotic gas metal arc welding," *Journal of Materials Processing Technology*, vol. 248, pp. 18–30, 2017.
- [36] M. Dinham and G. Fang, "Detection of fillet weld joints using an adaptive line growing algorithm for robotic arc welding," *Robotics and Computer-Integrated Manufacturing*, vol. 30, no. 3, pp. 229–243, 2014.

- [37] O. Lahdenoja, T. Säntti, M. Laiho, A. Paasio, and J. K. Poikonen, "Seam tracking with adaptive image capture for fine-tuning of a high power laser welding process," in *Seventh international conference on machine vision (ICMV 2014)*, vol. 9445. International Society for Optics and Photonics, 2015, p. 94451V.
- [38] Y. Ding, W. Huang, and R. Kovacevic, "An on-line shape-matching weld seam tracking system," *Robotics and Computer-Integrated Manufacturing*, vol. 42, pp. 103–112, 2016.
- [39] W. J. Shao, Y. Huang, and Y. Zhang, "A novel weld seam detection method for space weld seam of narrow butt joint in laser welding," *Optics & Laser Technology*, vol. 99, pp. 39–51, 2018.
- [40] J. Fan, F. Jing, L. Yang, T. Long, and M. Tan, "A precise seam tracking method for narrow butt seams based on structured light vision sensor," *Optics & Laser Technology*, vol. 109, pp. 616–626, 2019.
- [41] "Flw welder series." [Online]. Available: <http://www.amada.co.uk/product/details/40/flw-welder-series>
- [42] "Trulaser weld 5000." [Online]. Available: [https://www.trumpf.com/en\\_US/products/machines-systems/laser-welding-systems/trulaser-weld-5000/](https://www.trumpf.com/en_US/products/machines-systems/laser-welding-systems/trulaser-weld-5000/)
- [43] "Robotic laser welding systems." [Online]. Available: <https://www.ipgphotonics.com/en/products/laser-systems/welding-and-brazing/laser-welding-systems/laser-welding-cells>
- [44] *YLS-3000-U*, IPG Photonics, 11- 2018, v. 1.1.6.
- [45] "FLW D50 Welding Head." [Online]. Available: <https://www.ipgphotonics.com/en/products/beam-delivery/process-heads/welding/flw-d50-welding-head>
- [46] A. Wetzig, "Developments in beam scanning (remote) technologies and smart beam processing," in *Handbook of Laser Welding Technologies*. Elsevier, 2013, pp. 422–433.

- [47] S. V. Kuryntsev and A. K. Gilmutdinov, “The effect of laser beam wobbling mode in welding process for structural steels,” *The International Journal of Advanced Manufacturing Technology*, vol. 81, no. 9-12, pp. 1683–1691, 2015.
- [48] F. Vakili-Farahani, J. Lungershausen, and K. Wasmer, “Process parameter optimization for wobbling laser spot welding of ti6al4v alloy,” *Physics Procedia*, vol. 83, pp. 483–493, 09 2016.
- [49] L. Mrňa, P. Horník, P. Jedlička, and J. Pavelka, “Study of laser wobbling welding process through the radiation of plasma plume.”
- [50] L. Castellini and M. D’Andrea, “High speed surface pm synchronous machine for wobble laser welding,” in *2015 IEEE International Electric Machines & Drives Conference (IEMDC)*. IEEE, 2015, pp. 1600–1606.
- [51] M. Kraetzsch, J. Standfuss, A. Klotzbach, J. Kaspar, B. Brenner, and E. Beyer, “Laser beam welding with high-frequency beam oscillation: welding of dissimilar materials with brilliant fiber lasers,” *Physics Procedia*, vol. 12, pp. 142–149, 2011.
- [52] L. Shah, F. Khodabakhshi, and A. Gerlich, “Effect of beam wobbling on laser welding of aluminum and magnesium alloy with nickel interlayer,” *Journal of Manufacturing Processes*, vol. 37, pp. 212–219, 2019.
- [53] *Wobble Heads*, IPG Photonics, 06- 2019, rev. 13.
- [54] “MC2000 II.” [Online]. Available: <https://www.motoman.com/en-us/products/robots/industrial/welding-cutting/mc-series/mc2000-ii>
- [55] *Motoman-MC2000II*, Yaskawa, 03- 2018, rev. 1.
- [56] “DX200.” [Online]. Available: <https://www.motoman.com/en-us/products/controllers/dx200>
- [57] *DX200*, Yaskawa, 09- 2019, rev. 18.
- [58] “Yaskawa Motors.” [Online]. Available: <https://www.yaskawa.it/en/products/robotics/accessories/>

- [59] P. I. Corke, *Robotics, Vision & Control: Fundamental Algorithms in MATLAB*, 2nd ed. Springer, 2017, ISBN 978-3-319-54412-0.
- [60] “CAM Software Solution for Your Manufacturing Needs.” [Online]. Available: <https://www.sprutcam.com/>

## List of Figures

1	<i>The heat transfer mechanism in fusion welding. Picture from [2]. . . . .</i>	6
2	<i>The main types of joints. Form left to right: butt, corner, lap, tee, edge. Picture from [2]. . . . .</i>	7
3	<i>Typical cross-section of a fusion-welded joint. Picture from [2]. . . . .</i>	8
4	<i>Application area of industrial robots in welding. Picture from [5]. . . . .</i>	10
5	<i>Radiations emitted by a light bulb versus radiations emitted by a laser. . . . .</i>	11
6	<i>Generic scheme of a laser. Picture from [7]. . . . .</i>	12
7	<i>Scheme of a Nd:YAG laser. Picture from [9]. . . . .</i>	15
8	<i>Scheme of a CO<sub>2</sub> laser. Picture from [9]. . . . .</i>	16
9	<i>Scheme of a fiber laser. Picture from [7]. . . . .</i>	16
10	<i>Micrograph of a joint obtained through laser welding. Picture from [8]. . . . .</i>	18
11	<i>Laser beam focused by means of a lens. Picture from [9]. . . . .</i>	19
12	<i>Example of penetration vs speed graph for a CO<sub>2</sub> laser. Picture from [8]. . . . .</i>	20
13	<i>Example of side tube gas shielding device. Picture from [9]. . . . .</i>	22
14	<i>Joint space control general scheme. . . . .</i>	24
15	<i>Task space control general scheme. . . . .</i>	24
16	<i>PBVS control scheme. Picture from [12]. . . . .</i>	27
17	<i>IBVS control scheme. Picture from [12]. . . . .</i>	27
18	<i>Direct PBVS control scheme. Picture from [12]. . . . .</i>	28
19	<i>Direct IBVS control scheme. Picture from [12]. . . . .</i>	28
20	<i>Position based visual servoing control general concept. . . . .</i>	29
21	<i>Implementation example of a position based visual servoing controller. . . . .</i>	31
22	<i>Position based visual servoing control general concept. . . . .</i>	31
23	<i>Sensing techniques. Active, on the left, and passive, on the right. Pictures from [17] and [18]. . . . .</i>	36
24	<i>Flow chart of the algorithm proposed by Kim et al. Picture from [21] . . . . .</i>	40
25	<i>Flow chart of the algorithm proposed by P. Kim et al. Picture from [22] . . . . .</i>	41
26	<i>Hybrid visual servoing control scheme proposed by Xu et al. Picture from [24] . . . . .</i>	43
27	<i>Teaching control scheme proposed by De Graaf. Picture from [17] . . . . .</i>	45
28	<i>Re-teaching control scheme proposed by De Graaf. Picture from [17] . . . . .</i>	46

29	<i>Trajectory-based control scheme proposed by De Graaf. Picture from [17]</i>	47
30	<i>Optical setup of the coaxial vision sensor proposed by Regaard et al. Picture from [31]</i>	48
31	<i>Image processing procedure proposed by Xu Y. et al. Picture from [18]</i>	50
32	<i>Stereo images and seam identification using Dinham's algorithm. Picture from [36]</i>	51
33	<i>Seam identification in Lahdenoja's work. Picture from [37]</i>	51
34	<i>Shape matching algorithm proposed by Ding et al. Picture from [38]</i>	52
35	<i>Image of the seam as detected by the algorithm proposed by Shao et al. Picture from [39]</i>	53
36	<i>Images of the seam under different illumination conditions, as analyzed by Fan et al. Picture from [40]</i>	54
37	<i>Top view of the SM System robotic cell.</i>	58
38	<i>Front view of the SM System S.r.l. robotic cell.</i>	58
39	<i>Top view of the SM System S.r.l. robotic cell, with highlighted doors.</i>	59
40	<i>Butt joint model.</i>	61
41	<i>Corner joint model.</i>	61
42	<i>Internal joint model.</i>	62
43	<i>SM System S.r.l. cell industrial laser (left) and welding head (right).</i>	63
44	<i>The wobbling principle. Picture from [46].</i>	64
45	<i>Typical wobbling path. Picture from [52].</i>	64
46	<i>The Yaskawa Motoman MC2000 II robot.</i>	66
47	<i>Dimensions of the Yaskawa Motoman MC2000 II robot.</i>	67
48	<i>Detail of the robot reference frames.</i>	69
49	<i>CAD model of the IPG Photonics FLW-D50-W laser welding head.</i>	71
50	<i>Image of the Yaskawa DX200 controller.</i>	72
51	<i>Examples of signal mapping. Inputs on the left, outputs on the right.</i>	72
52	<i>Examples of the programs controlling the robot.</i>	74
53	<i>Acquisition of the current position of the robot TCP.</i>	75
54	<i>Value mapping for the acquisition of the current TCP velocity.</i>	76
55	<i>Detail of the belt transmission moving the axis of station S1.</i>	80
56	<i>Detail of the two motors that move the axes of station S2.</i>	81

57	<i>Motor, transmission and load scheme. . . . .</i>	82
58	<i>Configuration parameters for the single axis of workstation S1. . . . .</i>	83
59	<i>Configuration parameters for the two axes of workstation S2. . . . .</i>	83
60	<i>Experimental setup for the vision system tests. . . . .</i>	85
61	<i>Test workpiece for the vision system tests. . . . .</i>	86
62	<i>Illumination methods tests. Active on the left, passive on the right. . . .</i>	86
63	<i>Matlab simulation results of the automatic reteaching algorithm. . . . .</i>	89
64	<i>Simulink scheme employed in the automatic reteaching simulation. . . .</i>	90
65	<i>Control panels of the cell. On the left, the main tab of the menu available on the teach pendant; on the right, the HMI with buttons and Windows environment. . . . .</i>	91

## List of Tables

1	<i>Laser welding performance for different alloys. Table from [8]. . . . .</i>	22
2	<i>Wobbling modes provided by IPG Photonics FLW-D50-W laser welding head. . . . .</i>	66
3	<i>Main specifications of the Yaskawa Motoman MC2000 II 6-axis anthropomorphic robot. . . . .</i>	68
4	<i>Main specifications of the Yaskawa DX200 robot controller. . . . .</i>	73
5	<i>Specifications of the SGMRV motor series. Picture from [58]. . . . .</i>	78
6	<i>Inertia ratio calculation for the external axes. . . . .</i>	82
7	<i>Activation and deactivation of the various cell equipment on the basis of the working mode. . . . .</i>	87